

PERMIAN TO CRETACEOUS EVOLUTION OF THE PIEDMONT ALONG THE
ALABAMA – GEORGIA COASTAL PLAIN UNCONFORMITY

Except where reference is made to the work of others, the work described in this thesis is my own or was done in collaboration with my advisory committee. This thesis does not include proprietary or classified information.

Nathaniel Timothy Layfield

Certificate of Approval:

Mark G. Steltenpohl
Professor
Geology and Geography

Willis E. Hames, Chair
Professor
Geology and Geography

Lorraine W. Wolf
Professor
Geology and Geography

George T. Flowers
Dean
Graduate School

PERMIAN TO CRETACEOUS EVOLUTION OF THE PIEDMONT ALONG THE
ALABAMA – GEORGIA COASTAL PLAIN UNCONFORMITY

Nathaniel Timothy Layfield

A Thesis
Submitted to
the Graduate Faculty of
Auburn University
in Partial Fulfillment of the
Requirements for the
Degree of
Master of Science

Auburn, Alabama
August 10, 2009

PERMIAN TO CRETACEOUS EVOLUTION OF THE PIEDMONT ALONG THE
ALABAMA – GEORGIA COASTAL PLAIN UNCONFORMITY

Nathaniel Timothy Layfield

Permission is granted to Auburn University to make copies of this thesis at its discretion,
upon request of individuals or institutions and at their expense. The author reserves all
publication rights.

Signature of Author

Date of Graduation

VITAE

Nathaniel Timothy Layfield, son of James and Nancy Layfield, was born on October 2, 1984, in Birmingham, Alabama. He graduated from Hewitt-Trussville High School in Trussville, Alabama in 2003. He attended Auburn University and graduated summa cum laude with a Bachelor of Science degree in Geology in August 2007. After graduation, he immediately entered graduate school at Auburn University in August 2007, where he studied geochronologic relationships of the southernmost Piedmont of Alabama and Georgia under the guidance and direction of Dr. Willis E. Hames.

THESIS ABSTRACT

PERMIAN TO CRETACEOUS EVOLUTION OF THE PIEDMONT ALONG THE ALABAMA – GEORGIA COASTAL PLAIN UNCONFORMITY

Nathaniel Timothy Layfield

Master of Science, August 10, 2009
(B.S., Auburn University, 2007)

145 Typed Pages

Directed by Willis E. Hames

The Piedmont of Alabama and Georgia contains the southernmost exposure of crystalline rocks related to the culmination of accreted terranes associated with the formation of the Appalachian Mountain system. This area is critical for tectonic interpretation of Alleghanian metamorphic timing and exhumational history due to being overlain by Cretaceous Coastal Plain sedimentary rocks and it being composed of demonstrably exotic terranes.

Samples were collected along a ~190 km segment along the Coastal Plain onlap from Notasulga, Alabama, to Macon, Georgia, in the Piedmont and Uchee terrane of Alabama and Georgia. $^{40}\text{Ar}/^{39}\text{Ar}$ analyses of hornblende, muscovite, and biotite from

exposure of a migmatite in north Columbus (Barin Quarry), Georgia, are dated at 292 ± 0.5 Ma, 276 ± 3.1 Ma, and 284.8 ± 1.0 Ma, respectively. (U-Th)/He analyses date zircon and apatite at 231.3 – 162.7 and 175.3 – 118.5 Ma, respectively, across the transect. Thermobarometry techniques based on microprobe analyses were used to characterize peak metamorphic temperature and pressure conditions at the Barin quarry study area of ~ 686 °C and ~ 5.4 kb, inferring middle to upper amphibolite-facies conditions.

A pressure-temperature-time model is constructed for the Barin quarry area based on thermochronometers and peak-metamorphic conditions. The model demonstrates peak metamorphic conditions following the Alleghanian orogeny at ~ 310 Ma with a subsequent period of rapid cooling and erosional uplift ($25^\circ/\text{m.y.}$ cooling with uplift at 0.85 mm/yr). Timing of this rapid unroofing corresponds well to the Pottsville Formation and sediment accumulation in the Black Warrior, Cahaba, and Coosa foreland basins in west and central Alabama. Depressurization, evident in the model from rapid uplift, correlates well to the onset of Late Carboniferous - Permian plutonism in the Piedmont of central Georgia. Apatite ages that young to the east are interpreted as evidence of increased heat flow due to crustal rifting associated with the breakup of Pangea along the eastern margin of Laurentia.

ACKNOWLEDGMENTS

The author would like to thank all individuals who supported this project. Financial support was provided through the Geological Society of America student research grant program, the Alabama Geological Society, the Gulf Coast Association of Geological Societies, and partial costs of $^{40}\text{Ar}/^{39}\text{Ar}$ analyses were supported by a National Science Foundation grant. Special thanks are extended to Dr. Willis E. Hames, my advisor, for guidance and direction for the duration of the project. Appreciation is also given to my committee members, Dr. Steltenpohl and Dr. Wolf, for continued guidance and support. Thanks to Dr. Zeki Billor for assistance with Ar/Ar preparation work and analyses, and thanks to the entire ANIMAL facility at Auburn University. Thanks to Dr. Daniel Stockli at the University of Kansas for facilitating (U-Th)/He analyses. Thanks to Vulcan Materials Company and Martin-Marietta Aggregates for access to facilities for sample collection. Also, thanks to the University of Alabama Central Analytical Facility and Rob Holler for electron microprobe use, guidance, and direction. Thanks to my family, friends, and especially my parents for their unconditional support in all my endeavors. Truly special thanks go to Emily for her support, guidance, patience, and continuous prayer. I could not have made it without her support. Finally, utmost thanks go to my Lord and Savior, Jesus Christ, for blessing me with His saving-grace and God-given abilities without which this project would not have been possible. "I can do all things through Christ who strengthens me." -Philippians 4:13

Style manual used: Geological Society of America Bulletin

Computer software used:

Microsoft Word

Microsoft Excel

Microsoft Powerpoint

Corel Designer

Adobe Photoshop 7

Golden Software Grapher 5.0

Isoplot

1DT

TABLE OF CONTENTS

LIST OF FIGURES	xii
LIST OF TABLES	xvii
CHAPTER 1: INTRODUCTION.....	1
1.1 INTRODUCTION	1
1.2 SIGNIFICANCE AND GOALS OF PROJECT.....	2
1.3 THE PIEDMONT	4
1.4 THE APPALACHIANS	5
1.4.1 THE TACONIC OROGENY	5
1.4.2 THE ACADIAN OROGENY	7
1.4.3 THE ALLEGHANIAN OROGENY	8
1.4.4 OROGENIC SEDIMENTATION	10
1.5 LATE PALEOZOIC TO MESOZOIC	10
1.5.1 ALLEGHANIAN PIEDMONT PLUTONISM.....	11
1.5.2 POST-ALLEGHANIAN EVOLUTION	12
CHAPTER 2: REGIONAL GEOLOGY AND GEOLOGY OF THE STUDY AREA ...	14
2.1 APPALACHIAN TECTONIC PROVINCES	14
2.2 THE PIEDMONT OF ALABAMA AND GEORGIA	14
2.2.1 INNER PIEDMONT.....	14
2.2.2 PINE MOUNTAIN TERRANE	16

2.2.3 UCHEE TERRANE.....	17
2.2.4 CAROLINA ZONE	20
CHAPTER 3: PREVIOUS ISOTOPIC STUDY OF POST-ALLEGHANIAN COOLING IN THE SOUTHERN PIEDMONT.....	21
3.1 PREVIOUS WORK.....	21
3.2 PURPOSE OF THE PRESENT STUDY	28
CHAPTER 4: $^{40}\text{Ar}/^{39}\text{Ar}$ AND (U-Th)/He AGE DATING TECHNIQUES.....	29
4.1 $^{40}\text{Ar}/^{39}\text{Ar}$ DATING	29
4.2 (U-Th)/He DATING	32
CHAPTER 5: METHODOLOGY AND TECHNIQUES	35
5.1 SAMPLE COLLECTION SITES.....	35
5.1.1 BARIN QUARRY, NORTH COLUMBUS, GEORGIA	35
5.1.2 JUNCTION CITY QUARRY, JUNCTION CITY, GEORGIA.....	36
5.1.3 MACON QUARRY, MACON, GEORGIA.....	36
5.1.4 NOTASULGA QUARRY, NOTASULGA, ALABAMA.....	38
5.1.5 MOFFITT'S MILL, ALABAMA.....	38
5.2 MINERAL SEPARATION	38
5.3 $^{40}\text{Ar}/^{39}\text{Ar}$ ANALYSIS.....	40
5.4 (U-Th)/He ANALYSIS.....	41
5.5 MICROPROBE ANALYSIS.....	41
5.6 THERMAL MODELING.....	42
CHAPTER 6: PETROGRAPHY	44
6.1 BARIN QUARRY	44

6.2 JUNCTION CITY QUARRY.....	49
6.3 MACON QUARRY	52
6.4 NOTASULGA QUARRY	55
CHAPTER 7: PETROLOGY	58
7.1 INTRODUCTION	58
7.1.1 HORNBLLENDE AND BIOTITE	61
7.1.2 PLAGIOCLASE AND ALKALI-FELDSPAR	62
7.2 ALUMINUM-IN-HORNBLLENDE GEOBAROMETER	65
7.3 HORNBLLENDE – PLAGIOCLASE GEOTHERMOMETER	67
7.4 TWO-FELDSPAR GEOTHERMOMETER	71
CHAPTER 8: GEOCHRONOLOGY	74
8.1 (U-Th)/He ANALYSES.....	74
8.2 ⁴⁰ Ar/ ³⁹ Ar ANALYSES.....	78
8.2.1 HORNBLLENDE	79
8.2.2 BIOTITE.....	81
8.2.3 MUSCOVITE	83
CHAPTER 9: DISCUSSION AND CONCLUSIONS	86
9.1 INTRODUCTION	86
9.2 GEOCHRONOLOGY AND PETROLOGY	86
9.3 THERMAL MODELING.....	90
9.4 CONCLUSIONS.....	99
REFERENCES	101
APPENDICES	111

LIST OF FIGURES

Figure 1. A portion of the geologic time scale of Gradstein et al., (2004) with the timing of selected, relevant events in the southernmost Piedmont indicated: Taconic orogeny (*light blue*, ~480 – 435 Ma; Glover et al., 1983, Stewart and Miller, 2001); Acadian orogeny (*light yellow*, ~410-330 Ma; Rodger, 1997; Hatcher, 2007); and Alleghanian orogeny (*light green*, ~330-250 Ma; Glover et al., 1983; Hatcher, 1989; Hatcher, 2005). Light brown box represents time interval for potential passage of the Bermuda hotspot across the southern United States from approximately 100 – 50 Ma (Baksi, 1997; Cox and Van Arsdale, 2002). Timing for coastal plain sediment accumulation of the uppermost Tuscaloosa Formation of Alabama is shown at ~96 Ma. CAMP = Central Atlantic Magmatic Province.....6

Figure 2. Regional Appalachian tectonic provinces from Alabama to Pennsylvania. Carolina zone includes Charlotte, Kiokee, King’s Mountain, and other smaller terranes; PMW = Pine Mountain Window, GMW = Grandfather Mountain Window, SMW = Sauratown Mountain Window (modified after Hibbard et al., 2002).....15

Figure 3. Geologic map, including major faults, representing the Pine Mountain window and Uchee terrane of the southernmost Piedmont of Alabama and part of the Carolina zone of east-central Georgia. Fault kinematics are primarily dextral (modified after Steltenpohl et al., 2008).....18

Figure 4. Map illustrating areas of discussed previous works as related to tectonic province. Dallmeyer (1978) - incremental heating $^{40}\text{Ar}/^{39}\text{Ar}$ hbl and bt of the GA Inner Piedmont. Anderson (1981) - fission-track apa, zir, and sph of the Uchee and Pine Mountain Terranes and the Inner Piedmont. Dallmeyer et al. (1986) - U-Pb zir and $^{40}\text{Ar}/^{39}\text{Ar}$ hbl, bt, and whole-rock slate/phyllite. Steltenpohl and Kunk (1993) - $^{40}\text{Ar}/^{39}\text{Ar}$ incremental heating hbl, musc, k-spar, and total-fusion of bt. Steltenpohl et al., (2008) – U-Pb zir and whole-rock. (hbl = hornblende, bt = biotite, apa = apatite, zir = zircon, sph = sphene, musc = muscovite, k-spar = alkali-feldspar).....22

Figure 5. Red dots indicate hornblende, muscovite, and biotite ages and locations within the Uchee terrane and Inner Piedmont from Steltenpohl and Kunk (1993). Blue dots are apatite fission track ages and locations within the Uchee terrane and Inner Piedmont of Georgia from Anderson (1981). Base maps modified from Pickering et al. (1976), Szabo and Copeland (1988), Osborne et al. (1988).....26

Figure 6. Piedmont and Uchee terrane time-temperature cooling history curves:
 A) South Carolina Piedmont cooling curves of: ⁴Dallmeyer (1978), ⁴⁰Ar/³⁹Ar (hornblende and biotite); ⁵Dallmeyer et al. (1986), ⁴⁰Ar/³⁹Ar (hornblende and biotite);
 B) Uchee terrane in this study and vicinity of ¹Steltenpohl and Kunk (1993), ⁴⁰Ar/³⁹Ar (hornblende, muscovite, biotite); ²Anderson (1981), apatite fission track (red dot); ³Steltenpohl et al. (2008), U-Pb (zircon).....27

Figure 7. Geologic map of Alabama and Georgia displaying sample collection locations (red boxes). From west to east: Notasulga (NQ), Moffitt's Mill Schist (MMS), Barin Quarry (BQ), Junction City Quarry (JCQ), and Macon Quarry (MQ). Base maps modified from Pickering et al. (1976), Szabo and Copeland (1988), Osborne et al. (1988).....37

Figure 8. Representative hand samples of Barin quarry phases: A) BQ-1 hand sample representing general coarse-grained gneissic assemblage; B) BQ-3 hand sample with porphyroblastic hornblende; and C) Leucocratic pegmatitic phase (BQ-6) including muscovite.....46

Figure 9. Thin section photomicrographs of Barin quarry gneiss and pegmatite with pictures observed at the same scale and cross-polarized illumination: A) BQ-1 assemblage of quartz + alkali-feldspar + biotite + plagioclase + hornblende + epidote; B) BQ-1 perthitic exsolution lamellae and texture in alkali-feldspar; C) BQ-1 poikiloblastic texture in alkali-feldspar and undulatory extinction in quartz (arrow); D) BQ-1 myrmekitic texture in plagioclase feldspar (red arrow) and deformation twins in plagioclase (yellow arrow); E) BQ-6 medium-grained muscovite in pegmatitic phase; and F) BQ-3 porphyroblastic, euhedral hornblende and minor biotite alteration to chlorite (arrow).....47

Figure 10. Blocks on Barin quarry floor representing structural fold styles: A) A tight to isoclinal fold defined by foliation and compositional layering of leucocratic alkali-feldspar, plagioclase, and quartz with biotite and hornblende, with fold and axial surface highlighted; and B) An open style fold (~120°) truncated by a local-scale fault shown with red-dashed line.....48

Figure 11. Representative hand sample of Junction City quarry phases: A) JCQ-1 is a moderate to fine-grained quartz-plagioclase-biotite-hornblende gneiss; and B) JCQ-3 is a hornblende-rich gneiss.....50

Figure 12. Thin section photomicrographs of Junction City quarry gneiss in plane polarized illumination (A), and crossed polarized illumination (B-F): A) JCQ-1 is a quartz-biotite gneiss with strained quartz and biotite defining the foliation with a quartz + plagioclase + biotite + epidote gross assemblage; B) same view as 'A' in crossed-polarized light; C) JCQ-1 with undulose extinction quartz grains (arrow); D) JCQ-3 is a hornblende-rich gneiss; E) JCQ-1 poikiloblastic texture in plagioclase with inclusions of quartz, biotite, and zircon (highlighted with red arrow and seen in

picture F); and F) inclusions in plagioclase with centered quartz inclusion possessing zircon inclusion (arrow).....51

Figure 13. Representative hand sample view of Macon quarry phases: A) MQ-3 with gneissic foliation; B) MQ-4 with contact between granitic gneiss and coarse-grained, alkali-feldspar rich pegmatite; C) pegmatite veins cross-cutting gneissic foliation; and D) gneissic texture parallel to pegmatite at far left end of block.....53

Figure 14. Thin section photomicrographs of Macon quarry gneiss with pictures observed at the same scale: A) MQ-3 granitic gneiss with weakly-defined foliation attributed to biotite with quartz, alkali-feldspar, and plagioclase under plane polarized illumination; and (B) same view under cross polarized illumination.....54

Figure 15. Sample NQ-1 from the Notasulga quarry with weakly defined gneissosity (shown with arrow) defined by biotite and abundant quartz and alkali-feldspar (orthoclase).....56

Figure 16. Thin section photomicrographs of Notasulga quarry metagranite sample NQ-1 with pictures observed at the same scale: A) biotite (dark brown) and muscovite (pale yellow) under plane polarized illumination; and B) metamorphic assemblage of alkali-feldspar, quartz, plagioclase, biotite and muscovite under crossed polarized illumination.....57

Figure 17. Microprobe thin section with black circled areas indicating initial areas of interest and highlighted circles demonstrating actual grains analyzed. Thin section size is standard 4.5 x 2.5 cm. All pictures taken under cross-polarized light with 4x magnification (BT = biotite, HBL = hornblende, K-SPAR = alkali-feldspar, PLAG = plagioclase).....60

Figure 18. Chart demonstrating chemical variation of calcic amphiboles according to measured atomic proportion of Si and (Na + K) in the A site. End members shown include Ed = edenite, Pa = pargasite, Ts = tschermakite, Hb = hornblende, and Tr = tremolite. Points are based on twenty-two microprobe analyses of amphibole.....63

Figure 19. A) Hornblende line traverse analysis CaO; B) hornblende line traverse analysis FeO; C) hornblende line traverse analysis MgO; D) biotite point analyses FeO; and E) biotite point analyses MgO.....64

Figure 20. CaO, Na₂O, and K₂O ternary diagrams representing selected plagioclase and alkali-feldspar compositions from EMP. Plagioclase is of andesine variety.....66

Figure 21. A) Pressure-temperature graph of ~100 analyses of the hornblende-plagioclase geothermometer from the Barin locale (BQ-1). Temperatures range from 652 – 715 °C and pressures range from 5.0 – 6.0 Kb with a standard deviation of 14.7 implied by error bars. B) Pressure-temperature diagram of ~100 analyses from figure A with metamorphic facies distribution. All analyses fall within amphibolite metamorphic facies (modified from Blatt et al., 2006).....	70
Figure 22. Anorthite, albite, and orthoclase feldspar ternary diagram with feldspar solvus as determined by SOLV CALC with the maximum given metamorphic conditions of 686 °C and 5.4 Kb. A) Solvus with tie lines between average plagioclase and alkali-feldspar compositions for BQ-1; B) tie lines of 91 randomly calculated plagioclase and alkali-feldspar compositions.....	72
Figure 23. Hornblende incremental heating and single crystal total fusion ⁴⁰ Ar/ ³⁹ Ar analyses (plateau steps are magenta and rejected steps cyan, IH box heights are 1σ: A) SCTF (BQ-1) with mean of 298.5 ± 3.1 Ma; B) IH (BQ-1) with plateau age of 286.4 ± 0.4 Ma including ~66% of the ³⁹ Ar; C) IH (BQ-7) with plateau age of 292.2 ± 0.5 Ma including ~97% of ³⁹ Ar. The age of 292.2 Ma is the preferred age for hornblende of this locale due to the high percentage of argon included in the calculated plateau.....	80
Figure 24. Biotite incremental heating and single crystal total fusion ⁴⁰ Ar/ ³⁹ Ar analyses for sample BQ-1 (plateau steps are magenta and rejected steps cyan, IH box heights are 1σ: A) SCTF with mean of 284.1 ± 2.0 Ma; B) IH with plateau age of 283.1 ± 0.8 Ma including ~95% of the ³⁹ Ar; C) IH with plateau age of 284.8 ± 1.0 Ma including ~100% of ³⁹ Ar. The age of 284.8 Ma is the preferred age for biotite of this locale due to the high percentage of argon included in the calculated plateau.....	82
Figure 25. Muscovite single crystal total fusion ⁴⁰ Ar/ ³⁹ Ar analyses: A) Barin locale from pegmatite sample BQ-6 with mean age of 276 ± 3.1 Ma; B) Moffitt’s Mill Schist with mean age of 284.7 ± 2.6 Ma.....	84
Figure 26. Map with sample locales (red boxes) and chart with ages of minerals dated from each locale. All ages are in Ma.....	87
Figure 27. Time-temperature thermal history of the Barin locale. Age constraints are provided by ⁴⁰ Ar/ ³⁹ Ar and (U-Th)/He geochronometers. See text and table 2 for model setup and parameters.....	93
Figure 28. Depth (pressure) – temperature history of the Barin locale. Maximum depth achieved attributed to thrust sheet burial is approximately 29.5 km and peak metamorphic conditions achieved are approximately 686 °C and 5.7 Kb (indicated by red dot). Assumed depth pressure relationship is 3.5 km/Kb. Aluminum silicate triple point indicated at 4 Kb and 500 °C and wet-granite melting curve (Blatt et al., 2006)...	94

Figure 29. Depth – time history as for the Alleghanian orogeny as demonstrated in the model developed for the Barin locale (see discussion in section 9.2). Major post-Alleghanian events depicted include Pennsylvanian Pottsville Formation sediment accumulation (~315 – 300 Ma), Piedmont plutonism (~300 – 250 Ma), and the rift-to-drift transition due to development of a passive margin along the eastern Laurentian margin (~200 Ma for rifting).....95

LIST OF TABLES

Table 1. (U-Th)/He ages for apatite (left) and zircon (right); BQ = Barin locale, MQ = Macon locale, NQ = Notasulga locale, JCQ = Junction City locale. Asterisk (*) represents sample with anomalous age not considered for statistical average. See appendix for analytical results.....	75
Table 2. Modeling parameters, including time and uplift velocity utilized; negative value for velocity indicates velocity toward surface.....	92

CHAPTER 1: INTRODUCTION

1.1 INTRODUCTION

The Piedmont tectonic province lies at a critical position on the southeastern flank of the Appalachian Mountains with respect to developing an increased understanding of the post-orogenic pressure-temperature-time exhumational history and relationships to sediments accumulated in the foreland basins and Gulf and Atlantic Coastal Plains. From central Alabama to Newfoundland, Canada, the Appalachian Mountains extend over 3,000 km, and are arguably the most prominent, continental-scale geologic and topographic feature in eastern North America (Rast, 1989; Rodger, 1997). The culmination of three Paleozoic orogenic events, the Ordovician-Silurian Taconic, the Devonian Acadian, and the Pennsylvanian-Permian Alleghanian, the Appalachian Mountains record approximately 200 million years of contractional collisions and accretion of island arc and exotic terranes. Rocks of the southern Appalachians were variably influenced by each of these orogenic events, as metamorphic grade varies from sub-chlorite to eclogite facies (Hatcher, 1989; Adams et al., 1995).

The timing of Late Paleozoic to Mesozoic post-Alleghanian uplift and denudation of the southernmost terminus of the Appalachian Mountains is relatively well constrained by geochronologic techniques. This project addresses the post-Alleghanian metamorphic, exhumationally related, moderate to late-stage thermal cooling history of amphibolite-facies rocks within the southernmost Piedmont of Alabama and Georgia. Several studies

have documented Late Pennsylvanian metamorphic cooling ages as recorded by hornblende, muscovite, and biotite. This study further develops the database of geochronologic information by testing intercrystalline age distribution and the closure temperature concept for $^{40}\text{Ar}/^{39}\text{Ar}$ cooling ages on hornblende, biotite, and muscovite. A low-temperature thermochronologic database utilizing (U-Th)/He techniques on apatite and zircon is underdeveloped in the southern Appalachians, and this study will contribute such data to the existing set of apatite fission-track ages. Mineral chemistry of hornblende, biotite, plagioclase, and alkali-feldspar is applied to modern thermobarometry techniques to derive peak metamorphic pressure and temperature conditions and constrain achievement of equilibrium. Geochronologic analyses are synthesized to constrain and develop thermal models to interpret post-Alleghanian exhumation paths and further understand Mesozoic history of the southern Piedmont of Alabama and Georgia. These integrated approaches allow this study to draw conclusions regarding several key questions regarding Post-Alleghanian events in Alabama and Georgia. These questions include the Alleghanian influence on Late Carboniferous to Permian plutonism in central Georgia, the sedimentological response attributed to orogenic unroofing, thermal evidence for possible passage of the Bermuda hotspot, and indicators of passive margin development along eastern Laurentia.

1.2 SIGNIFICANCE AND GOALS OF PROJECT

Metamorphic events occur in response to temperature and pressure changes (Spear, 1995). Orogenesis is directly related to tectonic collisions of accreted terranes or other continental plates. Collisional events cause stacking of terranes due to thrust faulting resulting from contraction. Crustal thickening directly relates regional

metamorphism to orogenic development (Thompson and Ridley, 1987). Pressure in the footwall increases at a rate determined by tectonic movements, whereas conductive temperature increases with heat flow. Heat flow can be described by the equation

$$\frac{dT}{dt} = k \frac{\partial^2 T}{\partial z^2} + \frac{A}{\rho c} - U_z \frac{dT}{dz}$$

where T = temperature, t = time, k = thermal diffusivity (m²/s), z = depth, A = radioactive heat production (μW/m³), ρ = density (kg/m³), c = specific heat (J/kgK), and U_z = vertical velocity (m/s) (England and Thompson, 1984; Spear, 1995). Crustal thickening through tectonic processes, such as thrusting or large-scale folding, increase the temperature and pressure on a short time scale that generally produce transient (non-equilibrium) geotherms (Spear, 1995). Maximum pressure and temperature (P-T) conditions experienced by a rock are a result of tectonic burial and thermal heat-transfer associated with exhumation (Spear, 1995).

Exhumation involves bringing buried, subsurface rock to the Earth's surface. Erosion is the process of removing material from the surface through chemical and mechanical processes and depositing it elsewhere. Exhumation is erosional or tectonically related. Unroofing is the transfer of rock at depth to the surface involving the process of exhumation occurring through erosional mechanisms. These mechanisms provide the primary means for uncovering tectonically buried rock and define uplift. The post-orogenic history of orogenic belts is largely governed by erosion as sharp topographic relief increases erosional unroofing.

This project delineates the post-Alleghanian thermal history of the southernmost Piedmont by utilizing multiple geochronologic techniques in order to ascertain the timing

of post-metamorphic thermal history and uplift of rocks related to the Appalachian (Alleghanian) orogenic belt across an approximately 190 km transect across the southern Piedmont of Alabama and Georgia. Thermochronology is a useful source for time-temperature data to uncover exhumational history. $^{40}\text{Ar}/^{39}\text{Ar}$ analyses yield ages of closure for retention of argon within certain minerals, and can quantify time-temperature information for rocks from ~500 °C to 300 °C utilizing hornblende, muscovite, and biotite. Low-temperature (U-Th)/He thermochronology can yield time-temperature information from ~200 °C to 70 °C utilizing apatite and zircon which can be particularly useful to uncover the most recent, near-surface time-temperature history. The combination of these methods results in the production of a time-temperature-pressure post-Alleghanian cooling curve revealing the assumed post-peak metamorphic path experienced for the southernmost Piedmont of Alabama and Georgia.

1.3 THE PIEDMONT

The Piedmont represents the southernmost exposures of metamorphic and intrusive crystalline Appalachian rock. Farther south, these lithologies are covered beneath Mesozoic sediments of the Coastal Plain (Steltenpohl and Kunk, 1993). The southern Appalachians and Piedmont serve as a reasonable and likely provenance for much of this detritus. These sediments unconformably pare exposure of Appalachian rocks and structures in Georgia and Alabama, including possible sutures or interfaces between Laurentian rocks and those of other accreted Gondwanan (Suwanee terrane) or peri-Gondwanan terranes (Uchee terrane) (Hatcher, 1989; Steltenpohl and Kunk, 1993; Steltenpohl et al., 2008). Cambrian to Devonian rocks of the Suwanee terrane beneath Coastal Plain sediments yield fossils, plutons, and volcanics documenting Gondwanan

origin (Chowns and Williams, 1983). This Gondwanan terrane extends beneath the Coastal Plain of south Alabama, Georgia, and Florida (Chowns and Williams, 1983; Dallmeyer, 1989).

1.4 THE APPALACHIANS

The Appalachians provide evidence of a complete Wilson Cycle that began with rifting of the supercontinent Rodinia followed by three orogenic collisions and subsequent Mesozoic rifting of eastern proto-North America, forming the opening of the modern Atlantic Ocean (Hatcher, 2005). The present-day southern Appalachians were strongly affected by the most-recent Late Paleozoic Alleghanian orogeny. Since that time, exhumation and erosional processes have continued to govern and shape the Appalachians. The Appalachian mountain system consists of several regional tectonic provinces, which are as follows: from west to east, the Appalachian Plateau, Valley and Ridge, Blue Ridge, and Piedmont (e.g., Rast, 1989; Hatcher, 2005).

1.4.1 THE TACONIC OROGENY

The Taconic orogeny has been primarily described as a series of back arc accretions due to subduction and obduction of adjacent magmatic arc and microcontinent terranes (Glover et al., 1983; Hatcher, 1987, 2007; Rodger, 1997). Timing constraints on the Taconic orogeny are interpreted as Middle through Late Ordovician to Early Silurian (~480 – 435 Ma) with peak metamorphism approximately 460 - 450 Ma (Glover et al., 1983; Stewart and Miller, 2001) (Fig. 1). In Tennessee, North Carolina, and Alabama the Valley and Ridge tectonic province is dominated by clastic sedimentary units associated with the Taconic event (Glover et al., 1983).

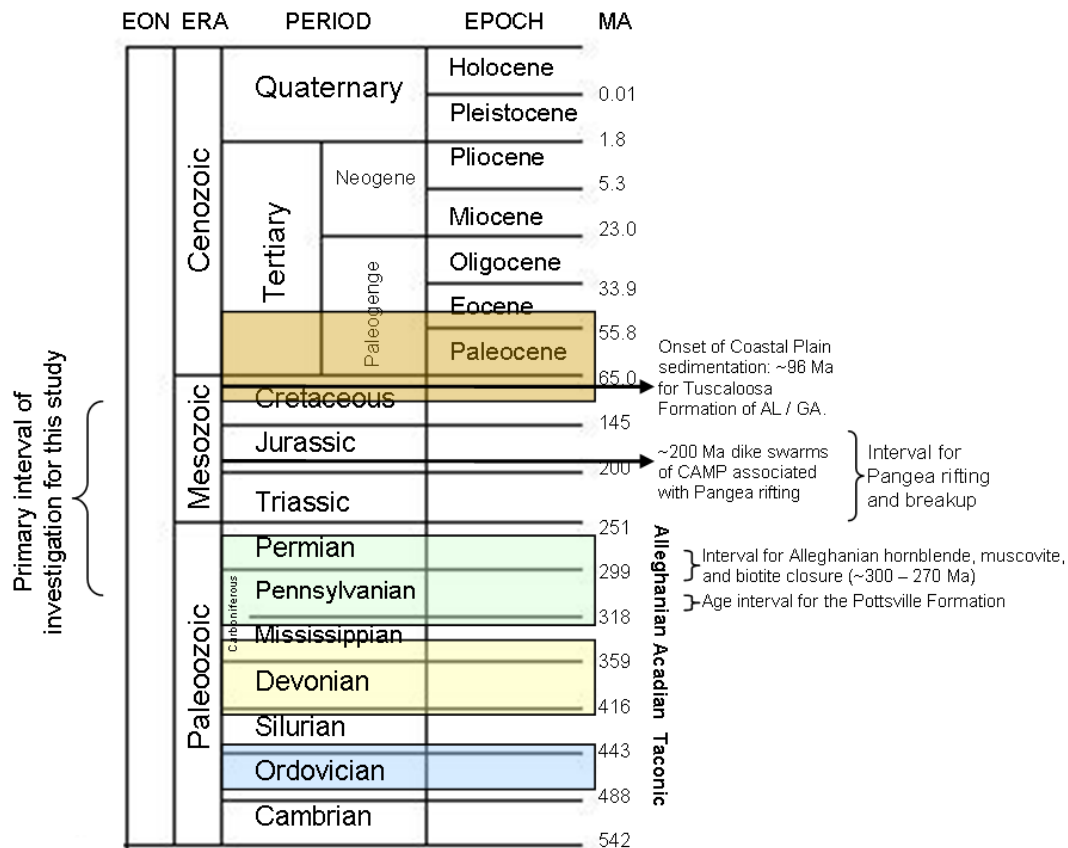


Figure 1. A portion of the geologic time scale of Gradstein et al., (2004) with the timing of selected, relevant events in the southernmost Piedmont indicated: Taconic orogeny (*light blue*, ~480 – 435 Ma; Glover et al., 1983, Stewart and Miller, 2001); Acadian orogeny (*light yellow*, ~410-330 Ma; Rodger, 1997; Hatcher, 2007); and Alleghanian orogeny (*light green*, ~330-250 Ma; Glover et al., 1983; Hatcher, 1989; Hatcher, 2005). Light brown box represents time interval for potential passage of the Bermuda hotspot across the southern United States from approximately 100 – 50 Ma (Baksi, 1997; Cox and Van Arsdale, 2002). Timing for coastal plain sediment accumulation of the uppermost Tuscaloosa Formation of Alabama is shown at ~96 Ma. CAMP = Central Atlantic Magmatic Province

The Taconic orogenic event is attributed to accretion of the Carolina (Avalon in the northern Appalachians) terrane and is thought to have had a prominent effect on the southern and central Appalachians resulting in regional metamorphism and ductile deformation (Glover et al., 1983). Metamorphic conditions during the Taconic are interpreted as moderate temperature and moderate to high pressure. There is compelling evidence for Taconic metamorphism of the Laurentian margin in the southern Appalachians. Eclogites dated at ~460 Ma in North Carolina have been attributed to an accretionary complex associated with the Taconic orogeny (Stewart and Miller, 2001). Some Cambrian-Ordovician granitoid plutons are observed in the southern Appalachians (Drake et al., 1989). U-Pb ages of metamorphic monazite in the western Blue Ridge have produced Taconic ages of 450 +/- 5 Ma (Corrie and Kohn, 2007).

1.4.2 THE ACADIAN OROGENY

The Acadian orogeny has been estimated as Late Silurian to Early Mississippian (~420-330 Ma) (Rodger, 1997; Hatcher, 2007) (Fig. 1). Dallmeyer and Van Breeman (1981) correlate Acadian Devonian metamorphism with the occurrence of 394-381 Ma plutons. Acadian metamorphism and polyphase deformation attributed to accretion of several small terranes is well documented in the northern Appalachians, but not readily observed within the Blue Ridge and Piedmont of Virginia and Maryland or in western North Carolina, Tennessee, Georgia, and Alabama; however, Alleghanian metamorphic overprinting associated with thrusting and folding may have muted evidence for Acadian relics in those areas (Glover et al., 1983; Rast, 1989; Osberg et al., 1989). Metamorphic effects due to the Acadian are not as widespread as the effects of the higher-grade Taconic, and in many places reflect only greenschist to lower amphibolite-facies

overprint of Taconic metamorphic fabrics and assemblages (Glover et al., 1983). The Talladega Slate belt of central Alabama and Georgia is a unique terrane thought to have experienced only Acadian metamorphism (Tull, 1980; Glover et al., 1983). Lithologies include the Talladega Group that is composed of weakly metamorphosed arkosic sandstones and graywackes, laminated siltstone, and diamictite. Acadian metamorphic conditions likely reached a maximum of kyanite and sillimanite grade in the westernmost Inner Piedmont of Alabama, Georgia, South Carolina and parts of North Carolina (Glover et al., 1983).

1.4.3 THE ALLEGHANIAN OROGENY

The Alleghanian orogeny, the final episode of a complete Wilson cycle by closing of the Iapetus ocean, represents the amalgamation of Laurentia and Gondwana and the formation of Pangea (Hatcher, 2005). The Alleghanian orogeny is attributed to continent-continent convergence of Laurentia and Gondwana in an oblique, north-to-south progressive collision (Secor et al., 1986; Rodger, 1997; Hatcher, 2005). This oblique, zipper-like collision reactivated strike-slip faults such as the Brevard, Modoc, Goat Rock, and Bartlett's Ferry in the southern Piedmont (Hatcher, 2005). Strike-slip fault reactivation is attributed to the north-to-south compressional movement of the Laurentia-Gondwana collision. Alleghanian peak metamorphic and subsequent cooling ages are generally between Late Mississippian to Permian (Glover et al., 1983; Hatcher, 1989; Hatcher, 2005) (Fig. 1).

In the southern Appalachians, head-on collision of the southeastern margin of Laurentia with Gondwana is responsible for thrust-related transport of the previously docked terranes of the Taconic and Acadian orogenies onto the Laurentian platform

(Hatcher, 2005). Studies demonstrate that the majority of the southern Appalachian orogen consists of pre-Alleghanian metamorphic, allochthonous rocks on a single master thrust (Cook et al., 1979; Harris and Bayer, 1979; Rast, 1989; Hatcher et al., 1989). In the foreland fold and thrust belt, thrusts emplaced Cambrian rocks above Pennsylvanian rocks with thrust faults extending hundreds of kilometers. It has been estimated that transport distances range up to 350 km (Hatcher, 2005) with more conservative minimal estimates on the order of ~175 km (Secor et al., 1986). In the southern Appalachians, the transport of the large Blue-Ridge/Piedmont thrust sheet is responsible for the fold and thrust-dominated character of deformation of the sedimentary rocks in the foreland (Hatcher et al., 1989; Hatcher, 2005).

Evidence for metamorphism associated with the Alleghanian orogenic event is generally best observed in the central and southern Appalachians, where the Alleghanian metamorphic effects are widespread and pervasive. However, Alleghanian metamorphic effects are less well-documented in the northern Appalachians (Rast, 1989, Hatcher et al., 1989). In the southern Appalachians, metamorphic conditions generally reached a maximum of upper amphibolite grade. Previously metamorphosed, low-grade, Taconic rocks in parts of the Carolina terrane achieved amphibolite-facies metamorphism during the Alleghanian event (Hatcher, 2005). In the Piedmont, evidence for Alleghanian regional metamorphism is well observed and is contemporaneous with the emplacement of Late Carboniferous to Permian granitoids (Rast, 1989). Peak metamorphism of the easternmost Piedmont is constrained at 315 – 295 Ma (Secor et al., 1986; Hatcher et al., 1989).

1.4.4 OROGENIC SEDIMENTATION

The ages of sedimentary units in foreland basins yield information regarding tectonic setting and primary sediment sources. These foreland basins are large-scale, cratonward propagating clastic wedges with sediments sourcing from the adjacent Appalachian highlands (Thomas, 1989). In the Appalachian foreland, the Taconic clastic wedge is defined by Middle Ordovician to Late Silurian siliciclastics (Thomas, 1989). The Alleghanian orogeny is recorded by sediments that accumulated in Mississippian to Permian depositional basins (Thomas, 1989). Large basins such as the Black Warrior and Cahaba basins in central Alabama provide valuable settings to examine sediments shed from the contiguous Appalachians. The Pennsylvanian Pottsville Formation (Fig. 1) provides information on Alleghanian sediment provenance. $^{40}\text{Ar}/^{39}\text{Ar}$ analysis on detrital muscovite for the Pottsville Formation is interpreted to provide evidence of the composite mega-thrust model for the Alleghanian by demonstrating Taconic, Acadian, and Alleghanian sources (Peavy, 2008).

1.5 LATE PALEOZOIC TO MESOZOIC

The Late Paleozoic to Mesozoic post-Alleghanian uplift history of the southernmost Appalachians is governed by isostatic exhumation and erosional processes typical of a thrust-constructed orogenic belt. Other Alleghanian to post-Alleghanian events include emplacement of large plutons, Mesozoic rifting and associated dike emplacement of the central Atlantic magmatic province, hypothesized passage of the Bermuda hotspot, and formation of the Gulf and Atlantic Coastal Plain.

1.5.1 ALLEGHANIAN PIEDMONT PLUTONISM

Large, syntectonic magmatic plutons occur along strike of the Piedmont and Carolina terrane from Georgia to southern Virginia. Radiometric dating of many of these plutons reveal ages reflecting Alleghanian plutonism from approximately 325 – 265 Ma (Speer et al., 1994). Speer et al. (1994) states that these plutons are either metaluminous biotite or amphibolite granitoids or peraluminous biotite + muscovite ± garnet or cordierite granitoids. A small percentage are also intermediate to gabbroic in composition. Evolution of these plutons begins with Alleghanian thrusting from the collision of Laurentia and Gondwana and thickening of continental crust. Magma generation may be the function of several melt mechanisms, but decompression melting may be the predominant mechanism due to the relatively rapid unroofing of the southern Appalachians, which is supported by $^{40}\text{Ar}/^{39}\text{Ar}$ geochronologic studies of the southern Piedmont (further discussed later, section 9.2). Occurrence of many of the Carboniferous plutons in Georgia and South Carolina coincide with major shear zones, which may have partially induced melting or provided a path of propagation (Speer et al., 1994).

The Elberton Batholith of east-central Georgia is a well-studied Alleghanian pluton that encompasses an area of over 500 km² (Dallmeyer et al., 2005). Crystallization of the Elberton Batholith occurred at approximately 320 ± 20 Ma as documented via U-Pb zircon analysis (Dallmeyer et al., 2005). $^{40}\text{Ar}/^{39}\text{Ar}$ incremental heating analysis of hornblende and biotite reveals ages of 274 – 256 ± 4 Ma and 241 – 235 ± 4 Ma, respectively (Dallmeyer et al., 2005). The Elberton pluton lacks chill zones or contact metamorphic effects, likely indicating that adjacent country rock was still sufficiently hot (Dallmeyer et al., 2005). The field and geochronologic evidence indicate emplacement of

the Elberton batholith during the Alleghanian event while surrounding host rocks were still approximately 600 – 650 °C, with subsequent cooling from ~500 to 300 °C at a rate of ~7.0 °C/m.y.

1.5.2 POST-ALLEGHANIAN EVOLUTION

Mesozoic rifting shaped the easternmost extent of the Appalachians with the breakup of Pangea and formation of Mesozoic rift basins along the eastern Laurentian margin. Also, the Bermuda hotspot migration path is estimated to have crossed the southeastern United States within the interval of 100 – 50 Ma (Baksi, 1997; Cox and Van Arsdale, 2002). Magmatic rocks formed during the migration of the hotspot occur from central Arkansas (near Magnet Cove) to central Mississippi (Jackson Dome). However, magmatic evidence for hotspot migration may be lacking to the east due to thickness of stacked Appalachian thrust sheets, as magmas do not easily penetrate through the thickened crust.

Dallmeyer (1978) estimates that the current erosion surface of the Piedmont was tectonically buried at depths of >25 km and 725 °C at approximately 365 Ma. The thermochronologic data of Dallmeyer (1978) also indicates geothermal gradients from 30 °C/km to 20 °C/km for the past ~220 Ma with an average temperature decrease of ~0.07 °C/km/m.y. coinciding with an average uplift rate of ~0.16 mm/yr (Dallmeyer, 1978). This would indicate rapid early erosion of the Piedmont followed by decreasing erosion rates in the Late Mesozoic to Cenozoic. Mesozoic to Cenozoic exhumation can potentially be further quantified utilizing low-temperature age-dating techniques such as (U-Th)/He which provide an indication of when lithologies cooled below 300 – 70 °C.

Evidence of the continental-scale central Atlantic magmatic province or CAMP is observed across eastern North America, northeastern South America, southwestern Europe, and northwestern Africa (Dallmeyer, 2005). This approximately 200 Ma event is associated with Mid-to-Early Triassic rifting of Pangea. The CAMP also affected and intruded central Georgia. Numerous basaltic dikes, sills, and flows occur in central Georgia within the Piedmont and beneath the Coastal Plain (Dallmeyer et al., 2005). Milla and Ragland (1992) further discuss the occurrence of Early Mesozoic diabase dikes in southwest Georgia near Talbotton. $^{40}\text{Ar}/^{39}\text{Ar}$ incremental heating analysis of plagioclase from three dikes from the South Carolina Piedmont yield ages of approximately 198.8, 199.5, and $199.7 \pm 1.5 - 2.2$ Ma, contemporaneous with Pangea rifting (Hames et al., 2000).

Cretaceous Coastal Plain sediments overlay crystalline Piedmont rocks across central Alabama and Georgia. The basal unconformity for the Cretaceous section is thought to have an age of ~96 Ma (King and Skotnicki, 1992). The adjacent Appalachian Mountains are a likely source for much of the Coastal Plain detritus.

CHAPTER 2: REGIONAL GEOLOGY AND GEOLOGY OF THE STUDY AREA

2.1 APPALACHIAN TECTONIC PROVINCES

The southernmost Appalachians experienced polyphase metamorphism and deformation in the Paleozoic, and are broadly delineated into four provinces. The provinces, with references provided for further insight, include from west to east the Cumberland Plateau (Wiltschko and Geiser, 1989), Valley and Ridge (Wiltschko, 1989; Wiltschko and Geiser, 1989), western and eastern Blue Ridge (Butler, 1972; Rankin, 1976; Hatcher, 1987; Wiltschko and Geiser, 1989; Steltenpohl, 2005), and the Piedmont (discussed in this text) (Fig. 2).

2.2 THE PIEDMONT OF ALABAMA AND GEORGIA

2.2.1 INNER PIEDMONT

The southernmost Appalachian Piedmont is divided into the Inner Piedmont, the Uchee terrane, and the Pine Mountain terrane. The most extensive terrane of the Piedmont province, the Inner Piedmont, is bordered to the northwest by the Brevard fault zone and fault associated cataclastics as well as accompanying low-grade metamorphics, and has been interpreted as a thin allochthonous thrust sheet originating along the Laurentian margin (Dallmeyer, 1978; Cook et al., 1979). The Inner Piedmont is characterized by a migmatitic assemblage of biotite gneiss, granitic gneiss, and amphibolite grade metamorphics (Dallmeyer, 1978). The Inner Piedmont regionally

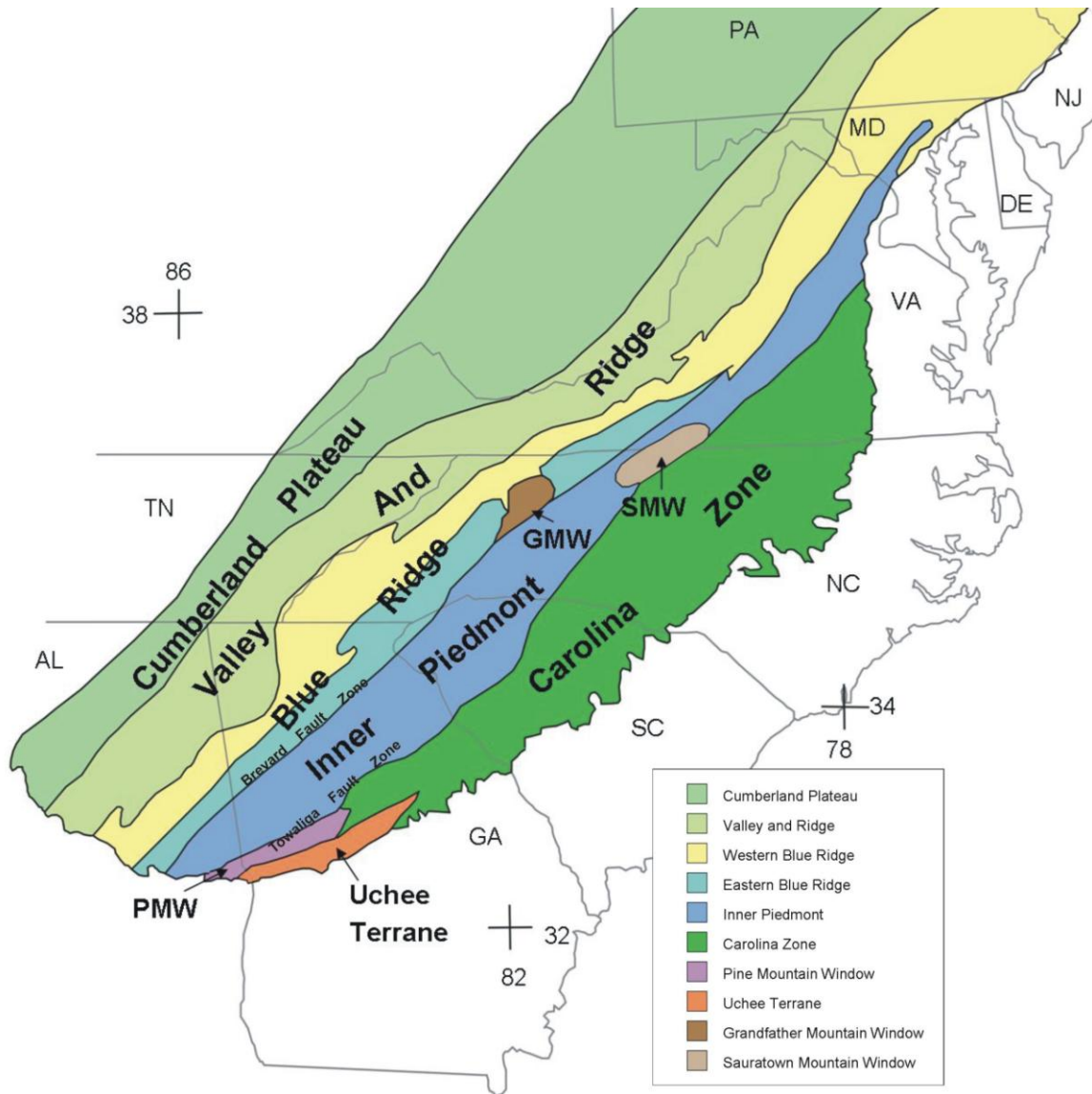


Figure 2. Regional Appalachian tectonic provinces from Alabama to Pennsylvania. Carolina zone includes Charlotte, Kiokee, King's Mountain, and other smaller terranes; PMW = Pine Mountain Window, GMW = Grandfather Mountain Window, SMW = Sauratown Mountain Window (modified after Hibbard et al., 2002).

experienced amphibolite-facies metamorphic conditions (Hanley et al., 1997). From South Carolina to Alabama, the Inner Piedmont's southern boundary is defined by the Towaliga fault zone (Hanley et al., 1997). This fault zone separates it from the metavolcanic, metasedimentary, and felsic plutons of the King's Mountain terrane in South Carolina and Georgia, and also marks the boundary between the Inner Piedmont and the high-grade gneisses and plutons of the Charlotte and Carolina terranes of the Carolina zone in east-central Georgia (Dallmeyer, 1978; Hibbard et al., 2002). The Ocmulgee and Dean Creek faults represent the eastward transition between the Piedmont and the Carolina terrane (Hanley et al., 1997). In Alabama, the Inner Piedmont has been subdivided into the metagneous and metavolcanic Dadeville Complex and the primarily metasedimentary Opelika Complex (Bentley and Neathery, 1970; Steltenpohl, 2005).

In Alabama and Georgia, the southern Piedmont province consists of the early Paleozoic arc or back-arc Inner Piedmont, Grenville basement gneiss and associated metasedimentary cover of the Pine Mountain terrane, and the Early Paleozoic arc or back-arc Uchee terrane that is part of the Carolina terrane in eastern Georgia (Steltenpohl and Kunk, 1993). All Piedmont terranes are bounded by major mylonitic, dextral, strike-slip fault zones (Hanley et al., 1997).

2.2.2 PINE MOUNTAIN TERRANE

The Pine Mountain terrane is a fault bounded Grenville basement massif that retains its miogeoclinal stratigraphic cover (Steltenpohl, 2005). The Towaliga fault also serves as the northern boundary for the Pine Mountain terrane in eastern Alabama and western Georgia. The Pine Mountain terrane is a Grenville basement massif (>1 Ga) covered by a metasedimentary cover sequence known as the Pine Mountain Group

consisting of the Hollis Quartzite, Chewacla Marble, and Manchester Schist (Steltenpohl, 2005) (Fig. 3). Metamorphism within the Pine Mountain Group was kyanite and sillimanite grade in Georgia and predominantly staurolite in Alabama (Steltenpohl, 2005). Timing of metamorphism within this group is not well constrained. Early metamorphism possibly occurred during the Devonian, but recent evidence suggests Alleghanian related amphibolite-facies overprint (Hanley et al, 1997; Steltenpohl, 2005). The Pine Mountain terrane is fault bounded defined to the north by the Towaliga fault zone and to the south by the Barlett's Ferry and Goat Rock fault zones. Speculation exists that these mylonite zones were once contiguous across the Pine Mountain anticline and current exposures now provide a window through the southern Appalachian decollement (Steltenpohl, 2005).

2.2.3 UCHEE TERRANE

The Uchee terrane represents the most southern and eastern extent of exposed crystalline Piedmont rocks in Alabama and Georgia and are covered by Cretaceous Coastal Plain sediments to the southeast. The Uchee terrane is suggested to be an accreted volcanic or back arc terrane of Gondwanan or peri-Gondwanan affinity (Steltenpohl, 2005; Steltenpohl et al., 2008). This terrane is characterized by polyphase deformation and metamorphism of amphibolite grade felsic and hornblende gneiss, amphibolite, and minor schist (Hobbs et al., 2004). Rocks within the Uchee terrane have been variably migmatized, and also include localized occurrences of quartzites, cataclastics, and mylonites (Hanley, 1986; Hanley et al., 1997). Peak regional metamorphic conditions within the Uchee terrane have been estimated by Chalokwu and Kuehner (1992) at 750 °C and up to 10 kb with evidence supporting retrograde

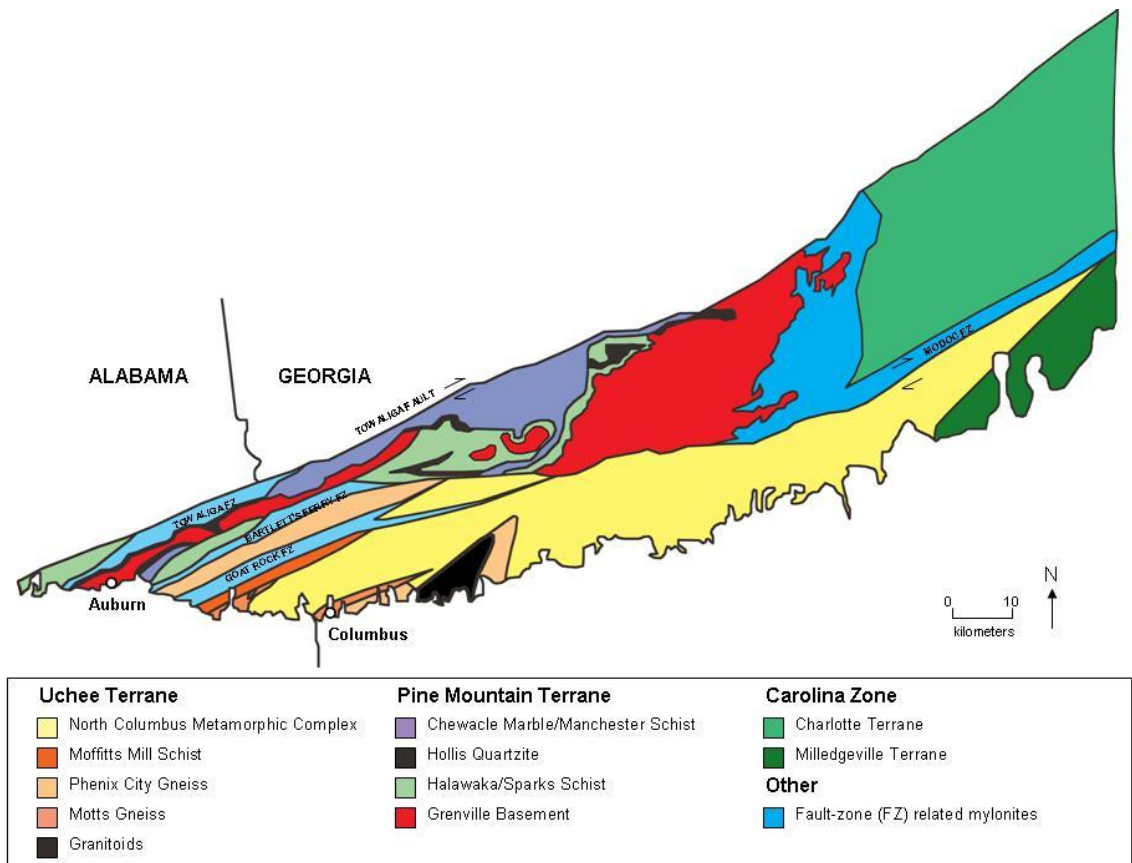


Figure 3. Geologic map, including major faults, representing the Pine Mountain window and Uchee terrane of the southernmost Piedmont of Alabama and part of the Carolina zone of east-central Georgia. Fault kinematics are primarily dextral (modified after Steltenpohl et al., 2008).

metamorphic effects at 524 °C and 6 kb. Broad structural characterization of the Uchee terrane consists of a gently plunging synform known as the Lake Oliver synform.

Lithologic distinction of the Uchee terrane is three-fold and defined by the Phenix City Gneiss, Moffitt's Mill Schist, and North Columbus Metamorphic Complex (Hanley et al., 1997) (Fig. 3). Each of the three units of the Uchee terrane is herein described.

The Phenix City Gneiss (PCG) is a hornblende-epidote gneiss with variable amphibolite bodies and compositionally consists of alkali-feldspar, quartz, hornblende, biotite, apatite and minor opaques (Hanley et al., 1997). Hornblende gneiss and amphibolite are diagnostic of the PCG (Bentley et al., 1985). Pressure-temperature conditions of the amphibolite occurrences reveal maximum conditions at the upper amphibolite-facies with retrogression to epidote-amphibolite-facies conditions (Chalokwu, 1989). Chalokwu (1989) estimates that amphibolite-facies metamorphism occurred at depths between 20 and 36 km. Pegmatitic occurrences are common throughout the PCG. Hanley et al. (1997) speculate that, based on composition and associated lithologies of amphibolites and calcium-silicate occurrences that the PCG is a regionally metamorphosed layering of intermediate to mafic volcanics attributed to possibly exotic accreted arc protolith. This unit's occurrence is associated with the outermost limbs of the Lake Oliver synform. Geochemical analysis of amphibolite within the PCG indicates tholeiitic to calc-alkaline affinities in the northern and southern limbs, respectively, supporting possible island arc protolith (Hanley et al., 2005).

The Moffitt's Mill Schist (MMS) is a strongly-foliated biotite-muscovite schist with components of plagioclase, alkali-feldspar, and local sillimanite and garnet (Hanley et al., 1997). Quality exposures of the MMS are rare due to the unit's high susceptibility

to weathering and Coastal Plain cover, but exposure is available at the type locality in Moffitt's Mill, Alabama. Structurally, the MMS occupies the space between the PCG and the core North Columbus Metamorphic Complex of the Lake Oliver synform (Hanley et al., 1997).

The North Columbus Metamorphic Complex (NCC) encompasses several lithologies that are variably migmatized, indicating high heat flow at depth causing partial melting. Rocks of this complex have also experienced varying degrees of deformation and associated intrusion (Hanley et al., 1997). Rock types of the NCC include quartz diorite gneiss and migmatized granitic gneiss primarily consisting of plagioclase, hornblende, biotite, quartz, alkali-feldspar, and apatite (Hanley et al., 1997). Calcium-silicate lenses are commonly associated with the NCC (Hanley et al., 1997).

2.2.4 CAROLINA ZONE

The Carolina zone, also known as Carolinia (Hibbard et al., 2007), is composed of an accreted assemblage of several Neoproterozoic to Early Paleozoic meta-igneous and volcanic terranes that have been interpreted to be peri-Gondwanan in origin (Hatcher, 1989; Hibbard et al., 2002). The Carolina zone extends from central Georgia near Macon, where it is in contact with the Uchee terrane, to Virginia. Terranes included within the Carolina zone include the suprastructural Carolina, Spring Hope, Roanoke Rapids, Augusta, and Milledgeville terranes, and the infrastructural Charlotte, Crabtree, Falls Lake, Raleigh, Triplet, and Savannah River terranes (Hibbard et al., 2002). The infrastructural terranes have generally experienced amphibolite-facies metamorphic conditions and deformation.

CHAPTER 3: PREVIOUS ISOTOPIC STUDY OF POST- ALLEGHANIAN COOLING IN THE SOUTHERN PIEDMONT

3.1 PREVIOUS WORK

Accurate isotopic age constraints are important in developing a more complete understanding of the timing of metamorphism, deformation, and post-metamorphic cooling in rocks of the southernmost Appalachian Piedmont. Previous studies utilizing $^{40}\text{Ar}/^{39}\text{Ar}$, U-Pb, K-Ar, Rb-Sr, and fission track geochronology have been conducted within the Piedmont of Alabama and Georgia. The present study provides additional data to construct a more complete understanding of post-Alleghanian Piedmont thermal and exhumation history, including low-temperature ($\sim 70^\circ\text{C}$) thermochronology data.

Dallmeyer (1978) (Fig. 4) reports $^{40}\text{Ar}/^{39}\text{Ar}$ cooling dates of hornblende and biotite from the Georgia Inner Piedmont. Analyses of biotite separates from selected amphibolites and biotite-rich gneisses yield concordant incremental-release spectra defining Carboniferous to Permian cooling ages. These results are consistent with a younging trend for cooling through hornblende and biotite closure temperatures from northwest to southeast across the Inner Piedmont transect. Hornblende incremental-release analyses from six amphibolite samples yield plateau ages of 355 – 300 Ma. Dallmeyer (1978) reports that samples with coexisting biotite and hornblende, hornblende closure pre-dates biotite by approximately 20 Ma. This result is consistent with the comparison of the higher closure temperature of hornblende versus biotite (see

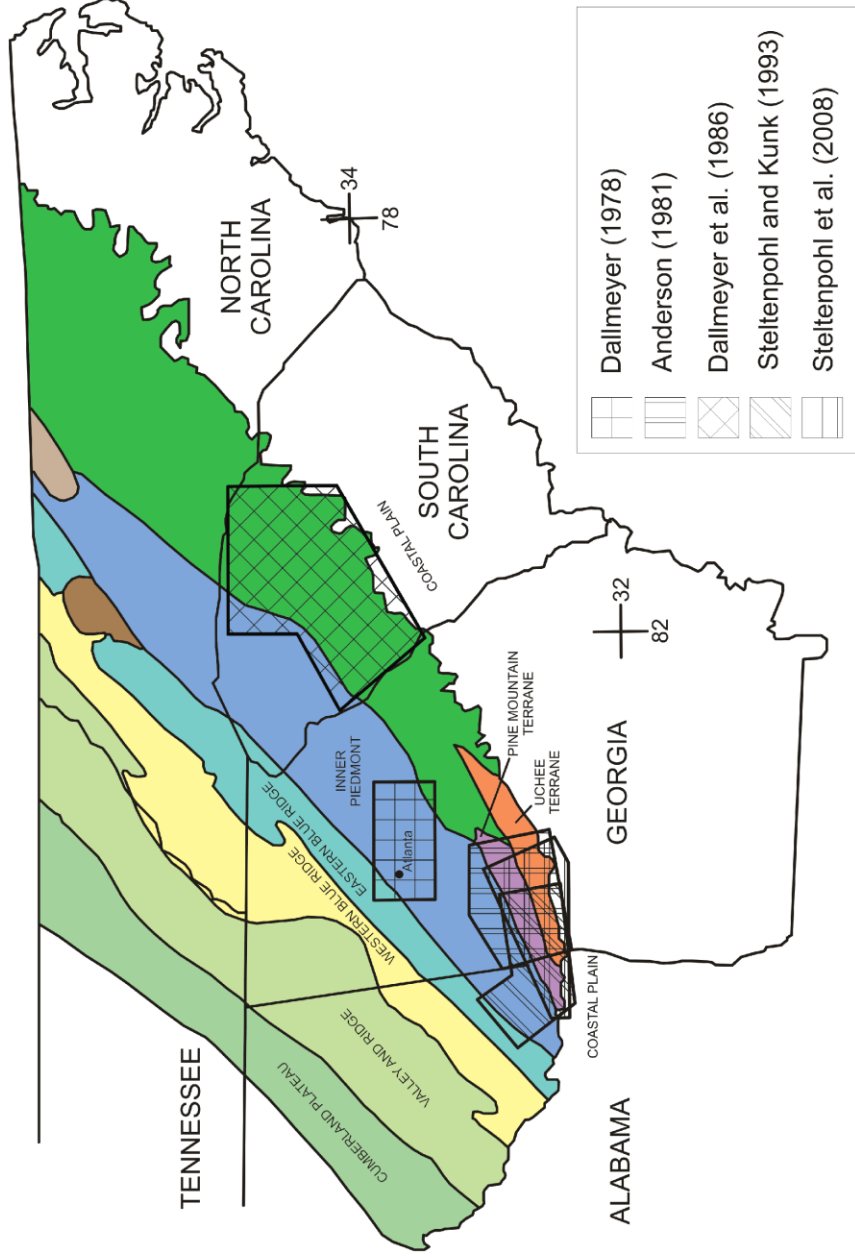


Figure 4. Map illustrating areas of discussed previous works as related to tectonic province. Dallmeyer (1978) - incremental heating $^{40}\text{Ar}/^{39}\text{Ar}$ hbl and bt of the GA Inner Piedmont. Anderson (1981) - fission-track apa, zir, and sph of the Uchee and Pine Mountain Terranes and the Inner Piedmont. Dallmeyer et al. (1986) - U-Pb zir and $^{40}\text{Ar}/^{39}\text{Ar}$ hbl, bt, and whole-rock slate/phyllite. Steltenpohl and Kunk (1993) - $^{40}\text{Ar}/^{39}\text{Ar}$ incremental heating hbl, musc, k-spar, and total-fusion of bt. Steltenpohl et al., (2008) - U-Pb zir and whole-rock. (hbl = hornblende, bt = biotite, apa = apatite, zir = zircon, sph = sphene, musc = muscovite, k-spar = alkali-feldspar)

discussion on $^{40}\text{Ar}/^{39}\text{Ar}$ and closure temperature for selected minerals) for K-Ar and $^{40}\text{Ar}/^{39}\text{Ar}$ dating (Hart, 1965). Dallmeyer (1978) attributes this northwest to southeast younging trend to variations in peak metamorphic conditions and depth of exhumation. The northwestern Inner Piedmont, west of Atlanta, Georgia, experienced lower-grade metamorphic conditions and was less exhumed in comparison to the southern and eastern Inner Piedmont. Dallmeyer (1978) estimates a 10 – 15 m.y. period for cooling from maximum metamorphic temperature to effective retention of argon in hornblende suggesting moderate to quick post-peak metamorphic uplift. Peak metamorphic conditions are estimated for the northwest Inner Piedmont near Stone Mountain, Georgia, at approximately 700 – 750 °C at pressures of 7 – 9 kb (Dallmeyer, 1978).

The work of Dallmeyer et al. (1986) (Fig. 4) evaluates post-Alleghanian $^{40}\text{Ar}/^{39}\text{Ar}$ cooling dates on hornblende and biotite of the eastern Piedmont of South Carolina as well as U-Pb crystallization ages of zircons within the Charlotte and Kiokee terranes of the southern Carolina Zone. U-Pb dates yield crystallization ages of tonalitic plutons associated with an accreted meta-volcanic arc setting around 550 Ma (Dallmeyer et al., 1986). A U-Pb date of ~317 Ma determined for the Edgefield granite documents Alleghanian intrusion into the Kiokee terrane which is supported by $^{40}\text{Ar}/^{39}\text{Ar}$ cooling ages that range from 288 – 278 m.y. (Dallmeyer et al., 1986). Regional $^{40}\text{Ar}/^{39}\text{Ar}$ analysis on hornblende, biotite, and whole-rock phyllite (Dallmeyer et al., 1986) are utilized in order to further develop the metamorphic extent, intensity, and timing of Alleghanian events in the Piedmont of South Carolina. Hornblende and biotite from Kiokee terrane incremental heating analyses yields average dates of ~302 and ~282 Ma, respectively,

while incremental heating analyses of hornblende and biotite from the Charlotte and King's Mountain terranes and the Inner Piedmont yield average age plateaus of ~308 and ~275, respectively (Dallmeyer et al., 1986). Dallmeyer et al. (1986) estimated peak amphibolite-facies metamorphic conditions at approximately 310 Ma with subsequent cooling from 500 – 300 °C occurring predominantly from 295 – 285 Ma. This estimate is consistent with estimates for peak-Alleghanian metamorphic conditions in the South Carolina Piedmont between 315 – 295 Ma (Secor et al., 1986). Whole-rock, incremental-heating $^{40}\text{Ar}/^{39}\text{Ar}$ analysis on Carolina Slate belt phyllites from central South Carolina yield release spectra with a plateau age of 291 - 280 Ma. These release spectra are primarily attributed to the relatively high content of white mica in the phyllite and are seemingly consistent with the expected closure temperature of muscovite ca. 350 °C (Dallmeyer et al., 1986).

Moderately rapid cooling of 20 °C/m.y. is maintained by erosion and tectonic unroofing within the South Carolina Piedmont to achieve cooling temperatures. Dallmeyer et al. (1986) estimate average initial uplift rates due to erosion at approximately 0.6 mm/yr, which is consistent with uplift rates for younger mountain chains such as the Alps and Himalayas.

Steltenpohl and Kunk (1993) conducted $^{40}\text{Ar}/^{39}\text{Ar}$ analyses on hornblende, muscovite, biotite, and alkali-feldspar from the Alabama and Georgia Piedmont (Fig. 4). Sample collection included the Inner Piedmont, Pine Mountain terrane, and parts of the southernmost Uchee terrane. Incremental heating analysis of hornblende, muscovite, and alkali-feldspar, and total fusion ages of biotite from the Inner Piedmont were determined at 320, 296, 267-234, and 293 Ma, respectively (Steltenpohl and Kunk, 1993). Uchee

terrane plateau ages were determined at 297 – 288 Ma for hornblende, 285 Ma for muscovite, 276 Ma for biotite (single crystal fusion), and a release range for alkali-feldspar from 261 – 230 Ma (Fig. 5). These ages indicate thermal conditions of >500 °C (amphibolite-facies) until 288 Ma resulting from Alleghanian thrusting (Fig. 6).

Steltenpohl and Kunk (1993) demonstrate that the southern Piedmont of Alabama and Georgia experienced peak metamorphic regional amphibolite-facies conditions around 320 – 292 Ma, and relates the Alabama-Georgia Piedmont to the similar post-Alleghanian thermal history of the South Carolina Piedmont (see Secor et al., 1986).

Steltenpohl and Kunk (1993) conclude that the Uchee terrane units experienced minimum burial of 15 km based on $^{40}\text{Ar}/^{39}\text{Ar}$ dates and an estimated rate of uplift of 0.36 mm/yr for the Uchee terrane.

Few low-temperature thermochronologic constraints exist for the southern Piedmont of Alabama and Georgia. Anderson (1981) reports fission-track ages for six apatite, six zircon, and three sphene samples for the southern Georgia Piedmont (Fig. 4). Apatite fission-track dates reflect a low-closure temperature of approximately 100 – 120 °C, while fission-track closure temperature for zircon is ~175 °C and ~300 °C for sphene (Hodges, 1991). Apatite closure temperature typically corresponds to the upper ~3 km of crust. Fission-track analysis of apatite reveal average closure around 118 Ma for the southern Georgia Piedmont (Anderson, 1981) (Fig. 5). Three fission-track sphene ages are 582, 372, and 359 Ma, while six zircon fission-track ages are 449, 345, 302, 510, 505, and 512 Ma. The zircon and sphene ages therefore, generally do not fit Alleghanian timing. Anderson (1981) attributes this large variation to only partial resetting of fission tracks due to the Alleghanian event. This potentially explains why one zircon age (302)

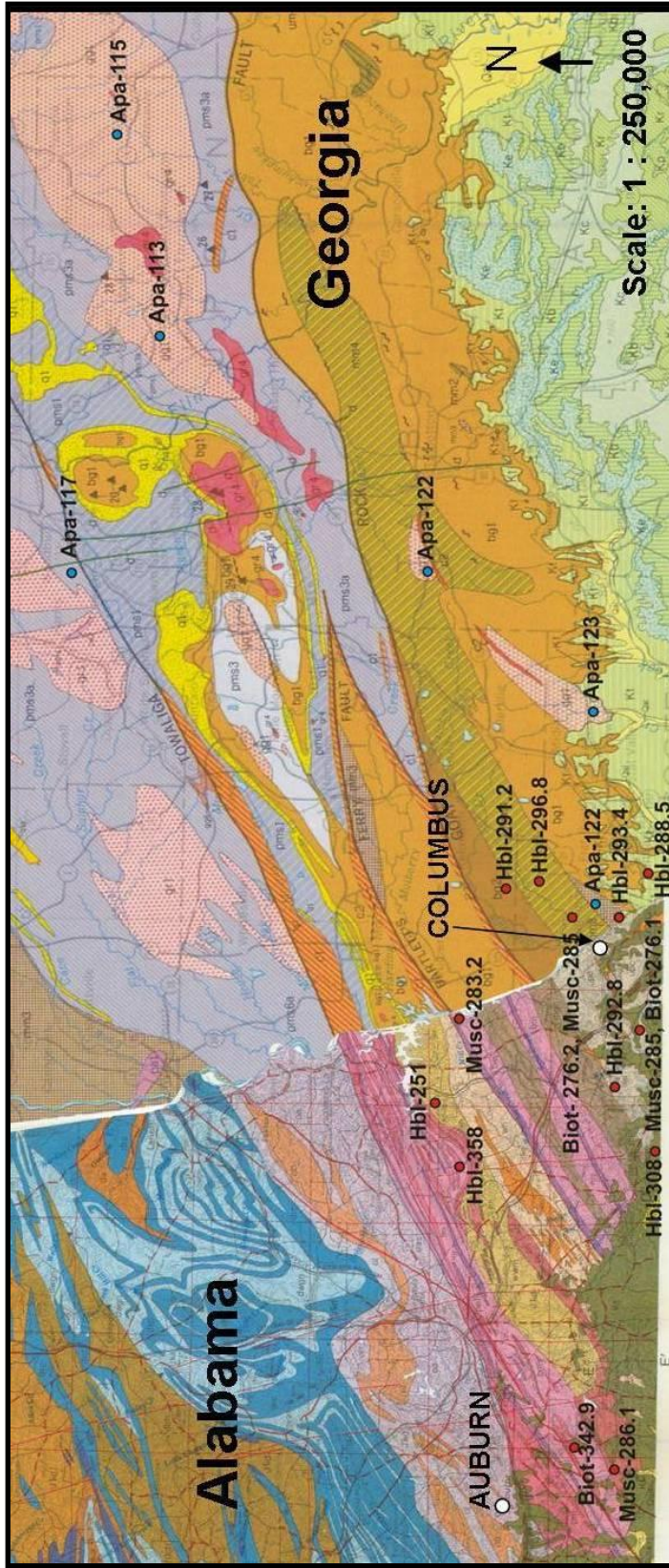


Figure 5. Red dots indicate hornblende, muscovite, and biotite ages and locations within the Uchee terrane and Inner Piedmont from Steltenpohl and Kunk (1993). Blue dots are apatite fission track ages and locations within the Uchee terrane and Inner Piedmont of Georgia from Anderson (1981). Base maps modified from Pickering et al. (1976), Szabo and Copeland (1988), Osborne et al. (1988).

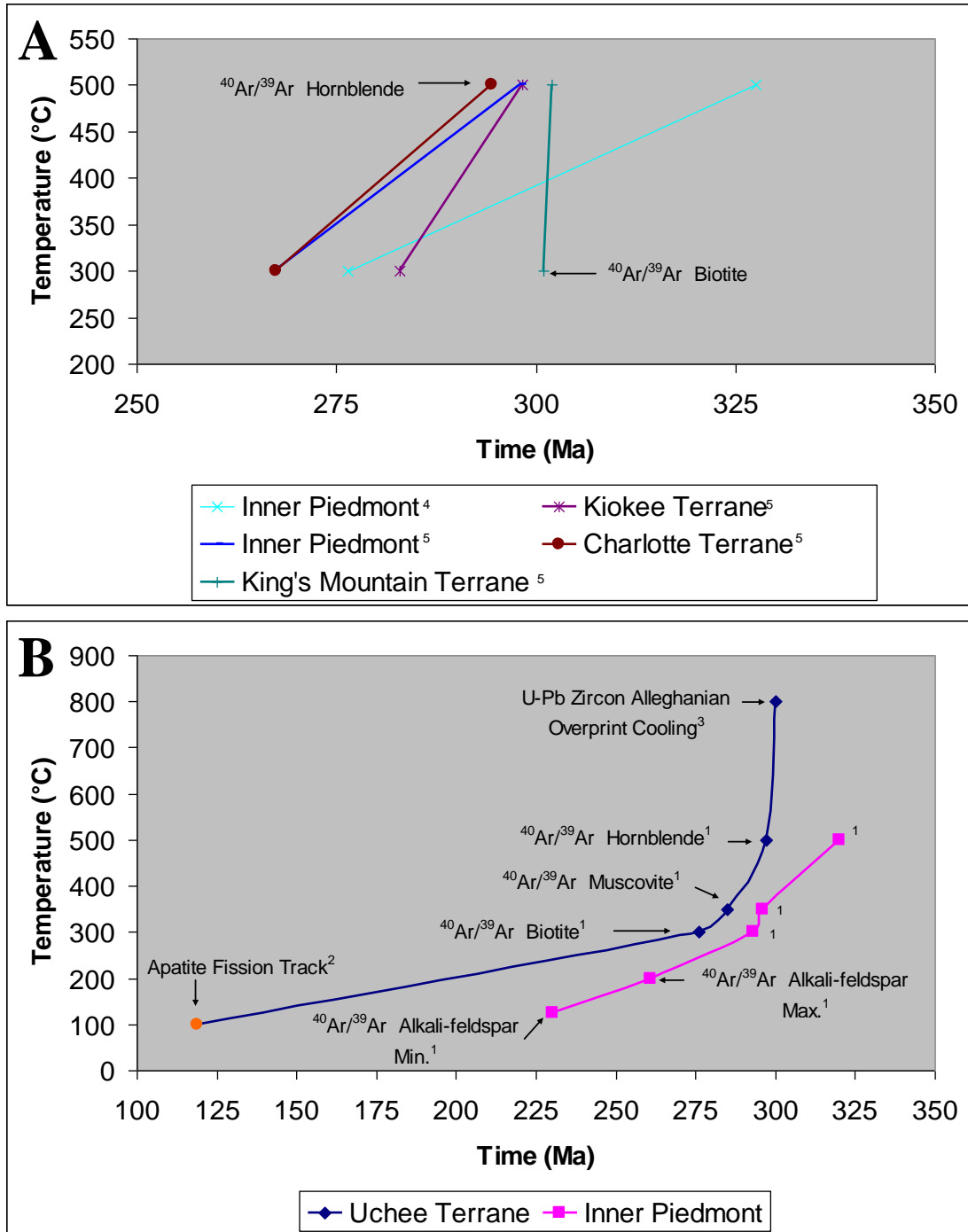


Figure 6. Piedmont and Uchee terrane time-temperature cooling history curves: A) South Carolina Piedmont cooling curves of: ⁴Dallmeyer (1978), ⁴⁰Ar/³⁹Ar (hornblende and biotite); ⁵Dallmeyer et al. (1986), ⁴⁰Ar/³⁹Ar (hornblende and biotite); B) Uchee terrane in this study and vicinity of ¹Steltenpohl and Kunk (1993), ⁴⁰Ar/³⁹Ar (hornblende, muscovite, biotite); ²Anderson (1981), apatite fission track (red dot); ³Steltenpohl et al. (2008), U-Pb (zircon).

could correspond to Alleghanian cooling, while others are up to 200+ Ma older. Apatite fission-track ages provide documentation of post-Alleghanian, near-surface cooling while sphene and zircon do not indicate resetting of ages from the Alleghanian event.

3.2 PURPOSE OF THE PRESENT STUDY

Clarity is still needed for several questions such as (1) What influence did the Alleghanian orogenic event have on Piedmont plutonism, (2) What was the sedimentological response to rapid orogenic unroofing, (3) Does thermal (geochronologic) evidence exist from possible passage of the Bermuda hotspot, and (4) What relationships can be deduced between post-Alleghanian cooling and the formation of a passive margin? The present study will address these questions through four integrated approaches: (1) accurately quantify $^{40}\text{Ar}/^{39}\text{Ar}$ age dates on hornblende, muscovite, and biotite in the southernmost exposures of the crystalline Piedmont adjacent to the Coastal Plain unconformity; (2) contribute to the development of a low-temperature thermochronologic database with (U-Th)/He analyses on apatite and zircon in order to understand and further constrain near-surface cooling history; (3) quantify mineral chemistry in order to utilize thermobarometric techniques to simulate peak-metamorphic temperatures and pressures; and (4) develop a thermal model of pressure-temperature-time relationships depicting a likely post-Alleghanian metamorphic cooling and exhumational history path. The interpreted history for the study area will be compared to previous studies of areas affected by Alleghanian amphibolite-facies metamorphism in the southern and central Appalachians for congruency of post-peak metamorphic cooling history.

CHAPTER 4: $^{40}\text{Ar}/^{39}\text{Ar}$ AND (U-Th)/He AGE DATING TECHNIQUES

4.1 $^{40}\text{Ar}/^{39}\text{Ar}$ DATING

The Ar/Ar age dating technique utilizes the decay of natural radioactive isotopes of potassium and is a useful method to quantify the thermally-governed retention of decay products. The diffusion of radiogenically produced ^{40}Ar is governed by thermally-activated diffusion such that retention is effective below a closure temperature (T_c) for each mineral (see Dodson, 1973). This daughter to parent isotopic ratio is measured to determine age utilizing the age equation:

$$t_{\text{age in years}} = 1/\lambda * \ln (D/P + 1)$$

where λ is the decay constant in years⁻¹ and D/P is the measured ratio of daughter to parent isotopes. Several basic assumptions must be made when utilizing the above age equation: (1) λ is known, (2) λ is constant, (3) the D/P ratio can accurately be measured, (4) no daughter atoms exist at $t = 0$, and (5) there has been no loss or gain of daughter or parent isotopes since the system closed at $t = \text{age}$ (e.g., McDougall and Harrison, 1999).

Diffusion is a natural, thermally-regulated (see following discussion on the closure temperature concept) transport mechanism for radiogenically produced daughter isotopes. Atoms may utilize one of several mechanical movements such as atom exchange or interstitial exchange when thermal energy is sufficiently high to enable such movements (e.g., McDougall and Harrison, 1999).

Volume diffusion is governed by the following Arrhenius relationship:

$$D = D_0 * e^{(-E/RT)}$$

where D = diffusion coefficient at absolute temperature T, D₀ = frequency factor, E = activation energy for diffusion, and R = gas constant in kcal/mol-K (Dodson, 1973; e.g. Harrison et al., 2009). A determined ⁴⁰Ar/³⁹Ar age corresponds to a particular point in time at which radiogenic ⁴⁰Ar atoms were retained within the boundaries of a particular crystal system. Diffusion occurring along grain boundaries or crystal defects can enhance diffusive loss of ⁴⁰Ar.

The closure temperature (T_c) of a cooling geochronologic system is the temperature of the system at the time given by its apparent age (Dodson, 1973), as defined by:

$$T_C = (E / R) / \ln [(A * R * T_C^2 * D_0 / a^2) / (E * dT/dt)]$$

where E = activation energy, R = gas constant, A = a numerical constant depending on geometry, D₀ = diffusion coefficient, a = a characteristic diffusion dimension, and dT/dt = cooling rate. Gross crystal geometry (grain size, shape, radius, etc) also determines fractional loss due to diffusion which is incorporated into cylinder, sphere, or sheet geometries governing single atom diffusion and accommodation (e.g., McDougall and Harrison, 1999). Isotopic closure in volcanic rocks generally occurs during eruption and ⁴⁰Ar/³⁹Ar ages for potassic minerals typically correspond to the timing of eruption. For samples which have experienced prolonged thermal effects due to intrusion, burial, and metamorphism, T_c does not correspond to crystallization, but rather to typical monotonic passage of a particular sample through crustal isotherms during exhumation related to faulting, rifting, or erosion (McDougall and Harrison, 1999). Widely accepted T_c for minerals applied in this study with respect to the ⁴⁰Ar/³⁹Ar method are hornblende ~500

°C, muscovite ~350 °C, and biotite ~300 °C, but greater accuracy is achieved through T_C calculation according to the above equation for each locale (see discussion in section 8.2) (Hodges, 1991).

The retention of ^{40}Ar relative to the parent ^{40}K and ^{39}Ar can be measured and quantified in selected potassium-bearing minerals such as hornblende, muscovite, biotite, and alkali-feldspar. ^{40}K undergoes dual radioactive decay to ^{40}Ca and ^{40}Ar in a ratio of approximately 9:1 (Hamilton, 1965; e.g., McDougall and Harrison, 1999). ^{40}Ar is a stable daughter isotope. ^{39}Ar is derived from ^{39}K during the irradiation process via the reaction $^{39}\text{K} (n,p) ^{39}\text{Ar}$ through fast neutron bombardment in a nuclear reactor. A monitor sample with a known, widely-accepted K-Ar age must be irradiated with unknown samples as a monitor of the $^{39}\text{K} (n,p) ^{39}\text{Ar}$ reaction. This enables calculation of an irradiation parameter known as J which is applied to the unknown samples. J is determined by rearranging the age equation as follows:

$$J = \frac{(e^{\lambda t}) - 1}{^{40}\text{Ar}/^{39}\text{Ar}_K}$$

where t is the age of the known standard, and the ratio of ($^{40}\text{Ar}/^{39}\text{Ar}$) is measured (e.g., McDougall and Harrison, 1999). The determined value of J is then to be applied to calculate the ages for the unknown samples as follows:

$$t_{\text{age in years}} = 1/\lambda * \ln (^{40}\text{Ar}/^{39}\text{Ar} * J + 1)$$

^{40}Ar also occurs as nonradiogenic argon found in small quantities (~1%) in the atmosphere and is corrected by measuring ^{36}Ar which maintains a relative constant ratio of 295.5 with ^{40}Ar in nature (Nier, 1950; Steiger and Jäger, 1977). After a sample has been irradiated, the sample is fused in a vacuum system to extract argon isotopes.

Abundances of ^{40}Ar , ^{39}Ar , ^{37}Ar , and ^{36}Ar are measured using a mass spectrometer. An advantage of the $^{40}\text{Ar}/^{39}\text{Ar}$ method includes the ability to produce ages from single grain fusion as well as incremental heating (Merrihue and Turner, 1966). These more sophisticated analytical approaches give greater ability to the $^{40}\text{Ar}/^{39}\text{Ar}$ age dating method to evaluate samples with mixed age populations or extraneous non-atmospheric argon.

4.2 (U-Th)/He DATING

The (U-Th)/He system is a low-temperature geochronologic tool that uses the natural decay of uranium and thorium and production of alpha particle emissions at a steady, known rate. The natural decay of uranium and thorium to produce helium and its feasibility for geochronologic applications was initially recognized in 1905 by Rutherford (Zeitler et al., 1987; Lippolt et al., 1994; Wolf et al., 1996). Alpha particles are chemically identical to a ^4He atom which includes two protons and two neutrons. Apatite, zircon, and to a lesser extent, sphene, are particularly adapted for (U-Th)/He analyses due to sufficient uranium and thorium content to produce measurable radiogenic helium. This method possesses some of the lowest closure temperatures available, $\sim 70 - 75\text{ }^\circ\text{C}$ in apatite, and $\sim 180\text{ }^\circ\text{C}$ in zircon corresponding to the uppermost 1-3 km of crust (Wolf et al., 1996; Farley, 2000; Soderlund et al., 2005; Dunkl et al., 2006). This unique ability has applications including landform evolution and erosion, structural geology and neotectonics, near-surface tectonic activity, and geodynamics related to exhumation (Warnock et al., 1997; Reiners et al., 2002; Ehlers and Farley, 2003).

(U-Th)/He age dates are determined by measurement of the ratio of parent (uranium and thorium) to daughter (radiogenic helium) isotopes since closure assuming

no extraneous source of helium is available to the system (Ehlers and Farley, 2003). In order to determine the age of a system, selected crystals must be degassed in a heated vacuum oven or by laser (Ehlers and Farley, 2003; Dunkl et al., 2006). The sample is heated to temperatures up to 1400 °C in order to activate a thermal mechanism for diffusion and gas extraction of all retained helium for analysis utilizing a mass spectrometer (Zeitler et al., 1987; Warnock et al., 1997). After degassing, crystals are dissolved and analyzed for uranium and thorium parent isotope content by inductively coupled plasma mass spectrometry (ICP-MS) (Ehlers and Farley, 2003).

The three primary isotopes involved in production of alpha particles by radiogenic decay are ^{238}U , ^{235}U , and ^{232}Th , producing 8, 7, and 6 alpha particles per decay, respectively (Lippolt et al., 1994). The quantity of alpha ejections for each isotope is directly related to the age equation (Ehlers and Farley, 2003) for the uranium-thorium helium system in apatite as follows:

$$^4\text{He} = 8 [^{238}\text{U}] (e^{\lambda_{238}t-1}) + 7 [^{235}\text{U}](e^{\lambda_{235}t-1}) + 6 [^{232}\text{Th}](e^{\lambda_{232}t-1}).$$

In this equation, ^4He , ^{238}U , ^{235}U , and ^{232}Th are measured concentrations of each isotope; λ represents the alpha decay constants for each isotope that have been previously determined; and t represents the time over which alpha particles have accumulated. Once all other variable have been measured then the time, t , can be mathematically derived.

The lack of uniformity of gross crystal size and shape and the effect of alpha particle stopping distance necessitate the need for applied corrections. During active decay, ejected alpha particles can travel between 11 μm to 34 μm as observed by Farley et al. (1996). This distance is referred to as the alpha particle stopping distance and can be thought of as the distance necessary for an alpha particle to come to rest within or beyond

the geometric boundaries of an individual crystal. Alpha particle stopping distance is a function of the isotope, crystal system geometry, and crystal density (Farley et al., 1996). Grains that possess a large crystal-surface to crystal-volume ratio or a radius of 250 μm or less are subject to alpha particle loss of >5% or >50% for a grain radius less than 30 μm (Warnock et al., 1997; Farley et al., 1996). Alpha particle loss can be corrected for by employing the alpha emission correction of Farley et al. (1996) which quantifies the retention of alpha particles in ideal spherical geometries:

$$F_T = 1 - \left(\frac{3S}{4R}\right) + \left(\frac{3S}{16R^3}\right)$$

where S = the radius of a sphere for alpha stopping distance from imaginary center of a parent nuclide X_0 , and R = the radius of the ideal mineral sphere. However, few crystals are ideal spheres and corrections become further involved (see Farley et al., 1996). The alpha emission correction is directly tied to another correction to derive a corrected age:

$$\text{Corrected age} = \text{measured age} / F_T$$

This equation from Farley et al. (1996) accounts for lost alpha particles that diffuse beyond the crystal's physical boundaries. Inclusions should be avoided in minerals for (U-Th)/He analyses as inclusions of other minerals can yield extraneous sources of helium and produce inaccurate, elevated He ages (Ehlers and Farley, 2003).

CHAPTER 5: METHODOLOGY AND TECHNIQUES

5.1 SAMPLE COLLECTION SITES

Samples for this study were collected from five locales in west-central Alabama and east-central Georgia in the Southern Piedmont adjacent to the Coastal Plain onlap boundary (figure 7). Sample collection was typically conducted in aggregate quarries to obtain samples minimally influenced by surface erosional and weathering processes. Sample location selection was based on general lithology coinciding with availability of necessary minerals for $^{40}\text{Ar}/^{39}\text{Ar}$ age dating analysis (hornblende, muscovite, and biotite), minerals for (U-Th)/He analysis (apatite and zircon), and availability of quality exposures. Samples were collected from the Vulcan Materials Notasulga Quarry in Notasulga, Alabama, Barin Quarry in North Columbus, Georgia, and Macon Quarry in Macon, Georgia. Samples were also collected at the Martin-Marietta Junction City Quarry in Junction City, Georgia. Sample collection was also conducted of the Moffitt's Mill Schist at the type locality near Moffitt's Mill, Alabama, along Little Uchee Creek. Exposures of this unit are sparse and limited to stream and river erosion outcrops. Localized geology of outcrops and sample descriptions are herein briefly described.

5.1.1 BARIN QUARRY, NORTH COLUMBUS, GEORGIA

The Barin sample site is within the North Columbus Metamorphic Complex of the Uchee terrane, near the core of the Lake Oliver synform. The rock type at this locality is

defined as an alkali-feldspar-quartz-biotite migmatitic gneiss. Protolith for this location is likely an I-type granitoid associated with an accreted arc setting. Strong gneissic foliation is defined by leucocratic and melanocratic layers defined by quartz and potassium feldspar, and biotite and coarse hornblende, respectively. Epidote and sphene are apparent in hand sample though little to no muscovite is observed, likely due to the high temperature and depth of metamorphism and low-aluminum content of the protolith. Muscovite is observed in leucocratic pegmatites. Numerous small scale (~5 – 10 cm amplitude) and larger (>1 m) close to isoclinal and recumbent isoclinal folds are observed and are indicative of high ductile strains at depth.

5.1.2 JUNCTION CITY QUARRY, JUNCTION CITY, GEORGIA

The Junction City Quarry sample site is located within the Uchee terrane and is a fine-grained quartz-biotite gneiss. Gneissic foliation at this locale is on a millimeter scale and defined by an interlayering of leucocratic quartz and potassium feldspar and melanocratic biotite with lesser amounts of hornblende. Numerous folds are not observed at this locale; however, vertical jointing is prominent throughout the quarry. Sulfides are readily observed in hand sample.

5.1.3 MACON QUARRY, MACON, GEORGIA

The Macon Quarry site is located in north Macon, Georgia. This area lies intermediate near or within a disputed boundary between the largely amphibolite-facies Uchee terrane and generally lower-grade (greenschist facies) Carolina zone supracrustal block, but amphibolite grade characteristics of this specific locality lead the author to interpret it as a part of the Uchee terrane.

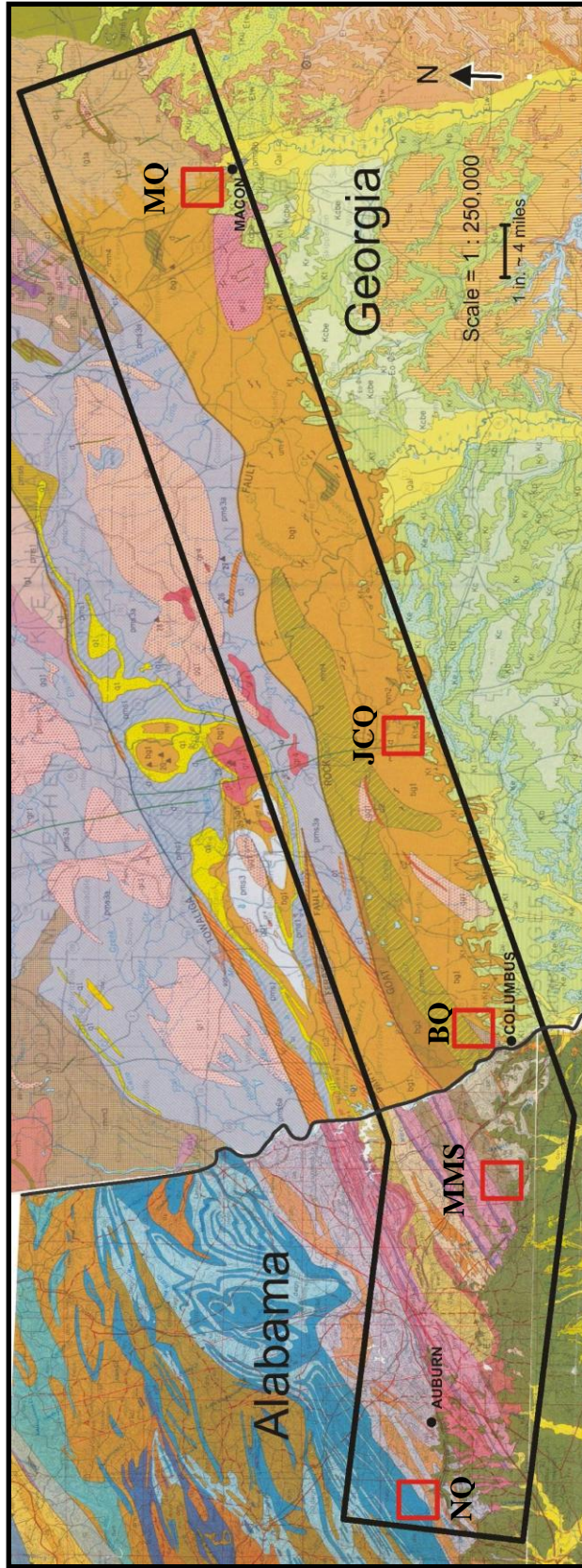


Figure 7. Geologic map of Alabama and Georgia displaying sample collection locations (red boxes). From west to east: Notattulga (NQ), Moffitt's Mill Schist (MMS), Barin Quarry (BQ), Junction City Quarry (JCQ), and Macon Quarry (MQ). Base maps modified from Pickering et al. (1976), Szabo and Copeland (1988), Osborne et al. (1988).

Rock type at this locality is generally granitic gneiss. Gneissic foliation is defined by leucocratic bands of quartz, plagioclase, and alkali-feldspar alternating with bands of melanocratic biotite and hornblende. Gneissic foliation is generally observed on a <10 mm scale. Minor migmatitic pods are observed indicating minor secondary melting. Several minor (<1 – 2 m thick) dikes are observed in the quarry walls. Large orthoclase grains yield pink hues to rocks with little gneissic foliation observed in hand sample.

5.1.4 NOTASULGA QUARRY, NOTASULGA, ALABAMA

The Notasulga Quarry is located within the Opelika Complex of the southern Inner Piedmont near Notasulga, Alabama. Sample collection at this locale was from the Farmville metagranite. Exposures of the Farmville at this locality include a medium to coarse-grained, weakly gneissic, pink (orthoclase) granite. Farmville crystallization has been dated at approximately 444 to 477 Ma via sensitive high-resolution ion microprobe (SHRIMP) analysis (Steltenpohl et al. 2005), which contrasts with a Goldberg and Burnell (1987) rubidium-strontium age of approximately 369 Ma.

5.1.5 MOFFITT'S MILL, ALABAMA

Sample collection for muscovite was conducted at Moffitt's Mill, Alabama, along Little Uchee Creek. This locale provides a rare stream-erosion exposure of the sparsely-exposed Moffitt's Mill Schist. The rock type observed at this locale is generally quartzofeldspathic schist dominantly consisting of quartz, biotite, and muscovite, which is particularly susceptible to weathering.

5.2 MINERAL SEPARATION

Hand samples from each locale were collected for thin section preparation. The samples were cut to chip size, perpendicular to foliation, by a rock saw and sent for

professionally made thin sections. Thin sections were analyzed for overall mineralogy and structural/deformation indicators along with relative abundance and characteristics of minerals necessary for $^{40}\text{Ar}/^{39}\text{Ar}$ and (U-Th)/He analyses. Thin sections were analyzed using a Nikon Eclipse 50iPol transmitted and reflected light microscope equipped with 2x, 4x, 10x, and 40x objectives. Thin section pictures were taken using a down-ocular Nikon DS-Fi1 digital camera.

Bulk hand samples were disaggregated for individual mineral separation. Samples were reduced to pebble to cobble size (~ 40 – 80 mm) by hand and further crushed by a steel jaw crusher. Small chips were further pulverized by a steel plate disk-mill grinder. All samples were subsequently sieved. Sieve fraction size necessary was dependant upon grain size of sample to avoid composite grains. All samples were sieved for 60/80 (0.250 – 0.177 mm), 80/100 (0.177 – 0.149 mm), and 100/120 (0.149 – 0.125 mm) fractions. The 100/120 sieve fraction was used only for the JCQ samples due to their fine-grained nature.

Mineral separation used heavy liquids, magnetic separation, and water column floatation techniques. Selected sieved fractions were broadly separated on relative mineral density by separation in filtered, reclaimed methylene iodide (CH_2I_2 , specific gravity adjusted to ~ 3.15). Heavy liquid separation effectively separates quartz, feldspars, muscovite, biotite etc. (density < 3.15) from hornblende, apatite, epidote, zircon, sulfides etc. (density > 3.15). Mineral separate concentrations were filtered, thoroughly washed with acetone to remove any remaining methylene iodide, and dried. Mineral concentrations were further separated by use of a Frantz magnetic separator. Muscovite was also separated by use of a water floatation column which takes advantage

of the sheet-like nature of muscovite in order to ‘float’ in a gently flowing, vertical column of water.

A Frantz magnetic separator makes use of the natural magnetic susceptibility of various minerals through an electromagnet with user ability to control the power (amps) of the magnet and ability to control forward and slide slope. Minerals such as hornblende, epidote, and biotite (typically magnetic at ~ 0.8 amps) possess a much higher natural susceptibility than that of muscovite, apatite, and zircon (typically magnetic at ~1.2 + amps) and thus will respond at a lower power setting. After magnetic separation procedures, mineral concentrates were hand picked in a petri dish under a binocular microscope in ethyl alcohol and stored in centrifuge vials. Grains were selected based on gross grain shape and scanned for inclusions and aggregate grains where applicable.

5.3 $^{40}\text{Ar}/^{39}\text{Ar}$ ANALYSIS

$^{40}\text{Ar}/^{39}\text{Ar}$ analyses of hornblende, muscovite, and biotite were conducted at Auburn University in the Auburn Noble Isotope Mass Analysis Laboratory (ANIMAL). Prior to analysis, samples were irradiated in individual aluminum foil packets in a reactor in Ontario Canada for 120 mWh. After irradiation, samples were hand loaded under a stereomicroscope into a copper planchet with one grain per hole for single crystal fusion or multiple grains for incremental heating analysis (~5 for biotite, ~20 for hornblende). Monitor minerals (FC-2, 28.02 Ma, and MMHB as a secondary standard) were also loaded for control and J calculation. Blanks were measured after every 5 – 7 unknowns. Routine measurements of air from a pipette indicate $^{40}\text{Ar}/^{36}\text{Ar}$ ratios of 293 ± 1.5 , and all data are corrected for mass discrimination. Sample heating was achieved through use of a CO_2 laser system sufficient for heating and total fusion.

The ANIMAL facility utilizes a 10 cm radius, 90° sector instrument mass spectrometer with a single electron multiplier detector and a volume of approximately 400 cc. The electromagnet analyzer consists of two coil pairs that are optimized to measure singly charged ions ranging from 36 to 40.

5.4 (U-Th)/He ANALYSIS

(U-Th)/He analysis of apatite and zircon was conducted at the University of Kansas. Mineral grains were handpicked, screened for inclusions, and photographed using a Nikon stereomicroscope. The (U-Th)/He laboratory utilizes an ultra-high vacuum noble gas purification and extraction line. Components of the system include a U.S. Laser continuous-mode Nd-YAG laser, all-metal extraction line equipped with Nupro valves, precise volume aliquot system for ³He and ⁴He, and a Blazers Prisma QMS-200 quadrupole mass spectrometer. Components are computer-controlled and fully automated with LabView Software. Following He extraction, content of uranium and thorium must be quantified utilizing a Fisions/VG Plasmaquad II Inductively Coupled Plasma Mass Spectrometer.

5.5 MICROPROBE ANALYSIS

Electron microprobe (EMP) analyses were conducted to examine elemental composition of hornblende, biotite, plagioclase, and alkali-feldspar. A microprobe thin-section was professionally-made and polished from the sample BQ-1 from the Barin locale. Microprobe analysis was conducted at the University of Alabama's Central Analytical Facility. The microprobe is a JEOL 8600 model Electron Probe Microanalyzer. The analyses were completed utilizing a 15 kV accelerating potential for the electron beam with a beam current of 20 nanoamps. Microprobe analysis utilizes a

stream of electrons focused in a beam from ~1 micron (hornblende and biotite) to ~5 microns (plagioclase and alkali-feldspar) in order to minimize Na loss due to large ion size. The EMP counts x-rays (in counts/second) using an argon-filled proportional counter with a beryllium window. Digital and Quantitative Analysis Tool, or dQant32, software was used for EMP results.

Positive grain identification was aided by the use of energy dispersive x-ray spectroscopy or EDS. EDS is an analytical tool that produces and measures x-ray emission peaks according to elemental composition of grains in response to high energy electron bombardment. Software for EDS analysis included PGT eXcalibur.

5.6 THERMAL MODELING

Modeling of pressure-temperature-time paths of terranes within orogenic belts is important in order to better understand timing of metamorphic conditions followed by exhumation. Orogenic events involve a rapid stacking of crust creating medium to high-pressure metamorphic terranes followed by erosion (Thompson and Ridley, 1987). Thermal modeling is conducted utilizing the program 1DT of Haugerud (1986) which allows user input control of up to a 4 layer scenario with 7 stages of user-defined uplift. Other user-defined parameters include thrust sheet thickness, crustal thermal properties, and up to 12 tracking points indicating pressure-temperature conditions for that point in the crust. The program has the ability to calculate and produce graphs for pressure-temperature, temperature-time, and pressure-time relationships. Thermal modeling for this project essentially creates a virtual, instantaneous thrust event contemporaneous to the Alleghanian event ~330 Ma and recording pressure-temperature-time relationships

utilizing $^{40}\text{Ar}/^{39}\text{Ar}$ and (U-Th)/He geochronologic constraints as check points for the model.

CHAPTER 6: PETROGRAPHY

6.1 BARIN QUARRY

Samples from the Barin Quarry in north Columbus, Georgia, are generally an alkali-feldspar-quartz-biotite migmatitic gneiss and a pegmatitic phase, which is also present in a small percentage of samples. Hand sample BQ-1 has characteristics of a migmatite with strongly folded and deformed gneissic texture with leucocratic layers dominated by quartz and feldspar and melanocratic layers with predominantly biotite and coarse porphyroblastic hornblende (Fig 8). The BQ-1 metamorphic assemblage is quartz + alkali-feldspar + biotite + plagioclase + hornblende + epidote. Prismatic hornblende porphyroblasts of 2 – 3 mm in length are particularly common and crystals are generally subhedral to euhedral. Locally, samples have minor retrogressive alteration of biotite to chlorite. Some samples are more massive, lacking pervasive gneissosity, and in hand sample and thin section have a granofelsic (seemingly igneous) texture. Myrmekitic texture is observed as vermicular growth and interaction of quartz and plagioclase feldspars, and some single alkali-feldspars have a perthitic texture with exsolution lamellae. Alkali-feldspars occur as subhedral porphyroblasts with grain diameters ranging from 2 – 4 mm with subhedral inclusions of quartz, biotite, hornblende, sphene, and apatite forming a poikiloblastic texture. Exsolution results from the difference in the ionic radius of Na and K and is exhibited as albite within alkali-feldspar. Exsolution occurs in less than 10% of feldspar grains. Plagioclase is mildly sericitized. Most quartz grains

have subgrain undulatory extinction indicating a degree of deformation on the crystal lattice with undulatory extinction angles averaging 8° . Deformation twinning is observed in some plagioclase grains.

Point counting was conducted on sample BQ-1 to quantify overall mineralogy. Three-hundred and eleven counts were made with 1 mm spacing. Relative abundances are as follows: alkali-feldspar (26.9%), quartz (26.6%), biotite (18.8%), plagioclase (17.8%), hornblende (7.4%), epidote (1.6%), apatite (tr.), sphene (tr.), and zircon (tr.) (Fig 9). Overall mineralogy appears indicative of a middle to upper amphibolite-facies assemblage of a dioritic protolith.

The pegmatitic phase assemblage (sample BQ-6) is quartz + alkali-feldspar + plagioclase + biotite + muscovite + epidote. In this phase, hornblende is not observed, biotite displays minor alteration to chlorite, and medium-grained muscovite is common which is not observed in other gneissic phases. Muscovite occurs as subhedral tabular shaped crystals (0.5 – 1.0 mm diameter) typically associated along grain boundaries or as small inclusions in alkali-feldspar and plagioclase.

Exposure of the North Columbus Metamorphic Complex and the local alkali-feldspar-quartz-biotite migmatitic gneiss at the Barin quarry reveal a structurally deformed and folded environment characteristic of a high temperature, plastic deformation setting (Fig. 10). In thin section, deformation twins are observed along with undulatory extinction. The steep walls of the Barin quarry expose magnificent and pervasive folds of gneissosity that appear dominantly isoclinal with gently dipping axial surfaces. No attempt was made to analyze the geometry of the folds in the context of this study, consistent with safety policies requiring avoidance of high walls. However,

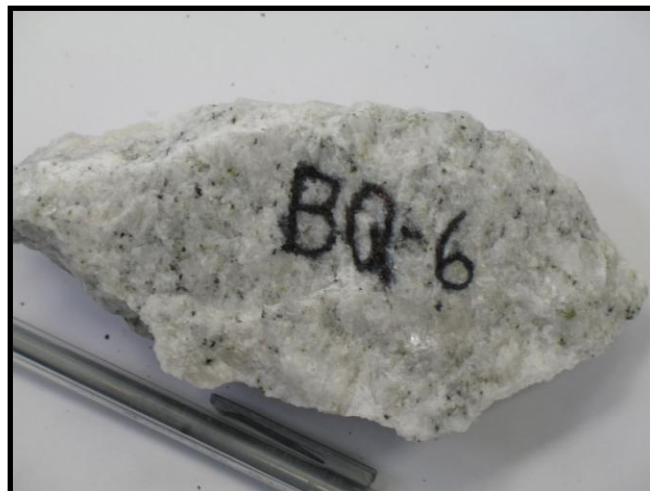
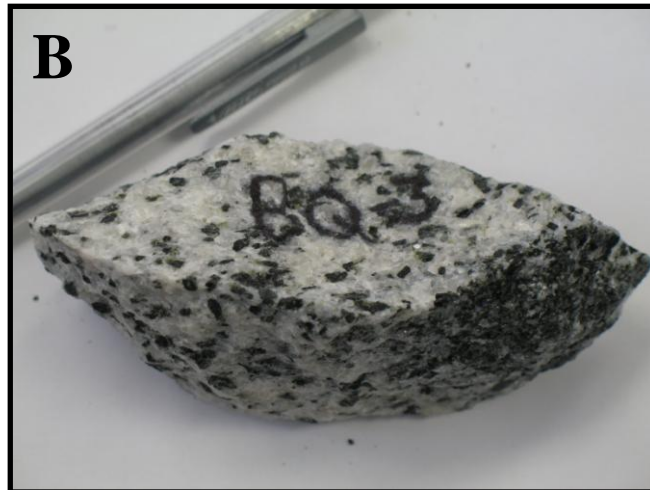
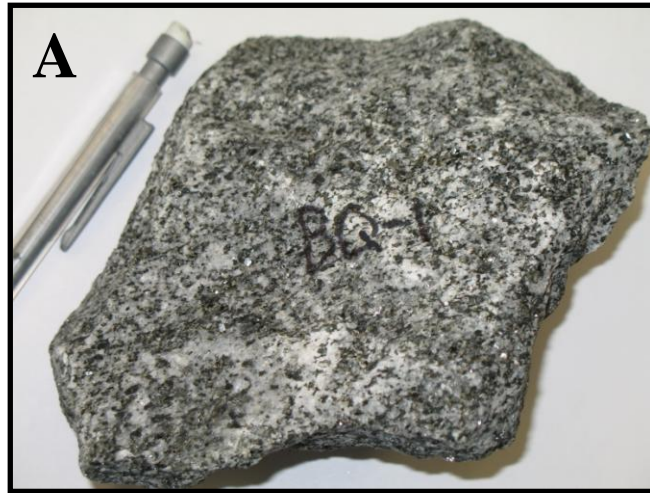


Figure 8. Representative hand samples of Barin quarry phases: A) BQ-1 hand sample representing general coarse-grained gneissic assemblage; B) BQ-3 hand sample with porphyroblastic hornblende; and C) Leucocratic pegmatitic phase (BQ-6) including muscovite.

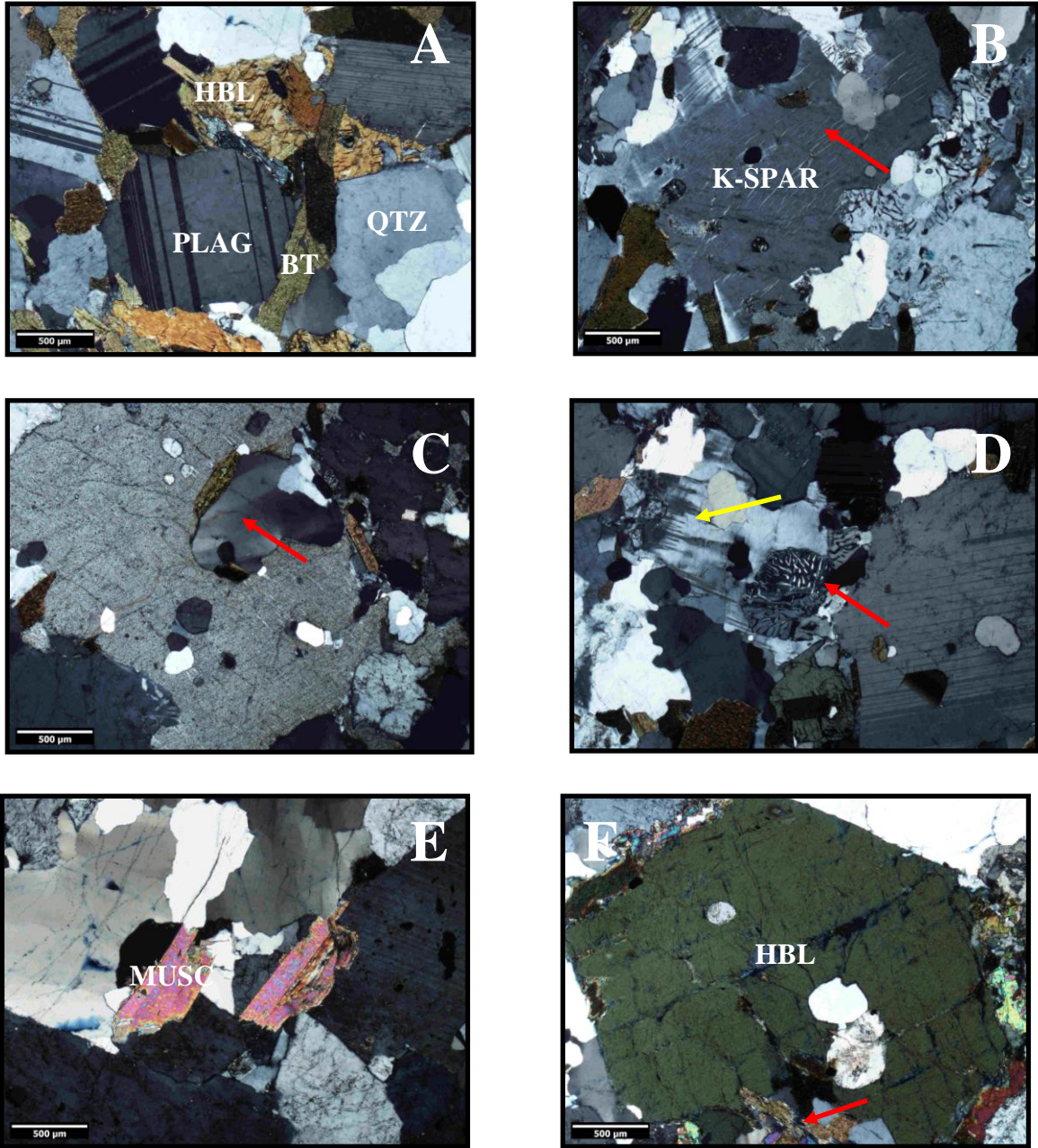


Figure 9. Thin section photomicrographs of Barin quarry gneiss and pegmatite with pictures observed at the same scale and cross-polarized illumination: A) BQ-1 assemblage of quartz + alkali-feldspar + biotite + plagioclase + hornblende + epidote; B) BQ-1 perthitic exsolution lamellae and texture in alkali-feldspar; C) BQ-1 poikiloblastic texture in alkali-feldspar and undulatory extinction in quartz (arrow); D) BQ-1 myrmekitic texture in plagioclase feldspar (red arrow) and deformation twins in plagioclase (yellow arrow); E) BQ-6 medium-grained muscovite in pegmatitic phase; and F) BQ-3 porphyroblastic, euhedral hornblende and minor biotite alteration to chlorite (arrow).



Figure 10. Blocks on Barin quarry floor representing structural fold styles: A) A tight to isoclinal fold defined by foliation and compositional layering of leucocratic alkali-feldspar, plagioclase, and quartz with biotite and hornblende, with fold and axial surface highlighted; and B) An open style fold (~120°) truncated by a local-scale fault shown with red-dashed line.

loose blocks have isoclinal folds (F_2) that contain refolded folds (F_1) and are overprinted by gentle folds (F_3). Fold geometries appear randomly oriented on a meter scale and adjacent folds and small faults locally truncate other folds.

6.2 JUNCTION CITY QUARRY

The Junction City quarry, located in Junction City, Georgia, (Fig. 7) generally contains quartz-plagioclase-biotite-hornblende gneiss. In hand sample view, a millimeter-scale, gneissic texture is defined by leucocratic quartz and plagioclase and melanocratic layers dominated by biotite, epidote, and hornblende. Gneissosity is pervasive in hand sample and thin section (Fig. 11). The metamorphic assemblage for this sample, JCQ-1, is quartz + plagioclase + biotite + epidote + hornblende (Fig. 12). Overall grain size is ~0.10 – 0.25 mm with >50% of grains exhibiting a strained, elongated habit. Quartz has undulatory extinction with angles averaging $\sim 11^\circ$. Plagioclase has experienced mild sericitization and many plagioclase grains are strongly optically zoned indicating core-to-rim compositional variation. Some plagioclase feldspars have a poikiloblastic texture with inclusions that are predominantly quartz, biotite, and traces of zircon. Hornblende varies in modal percentage among study samples (Fig. 12).

Three-hundred and one point counts were conducted on sample JCQ-1 with 1 mm spacing to quantify overall mineralogy. Relative abundances are as follows: quartz (42.5%), plagioclase (24.9%), biotite (15.6%), epidote (12.2%), potassium feldspar (2.9%), hornblende (1.9%), opaques (tr.), zoisite (tr.), zircon (tr.), sphene (tr.), and calcite (tr.). Epidote is a common constituent of regionally metamorphosed rocks of intermediate to mafic composition and is favored over clinozoisite in Fe-rich rocks, but is typically not stable in middle to upper amphibolite-facies conditions. Mineralogy and abundance of



Figure 11. Representative hand sample of Junction City quarry phases: A) JCQ-1 is a moderate to fine-grained quartz-plagioclase-biotite-hornblende gneiss; and B) JCQ-3 is a hornblende-rich gneiss.

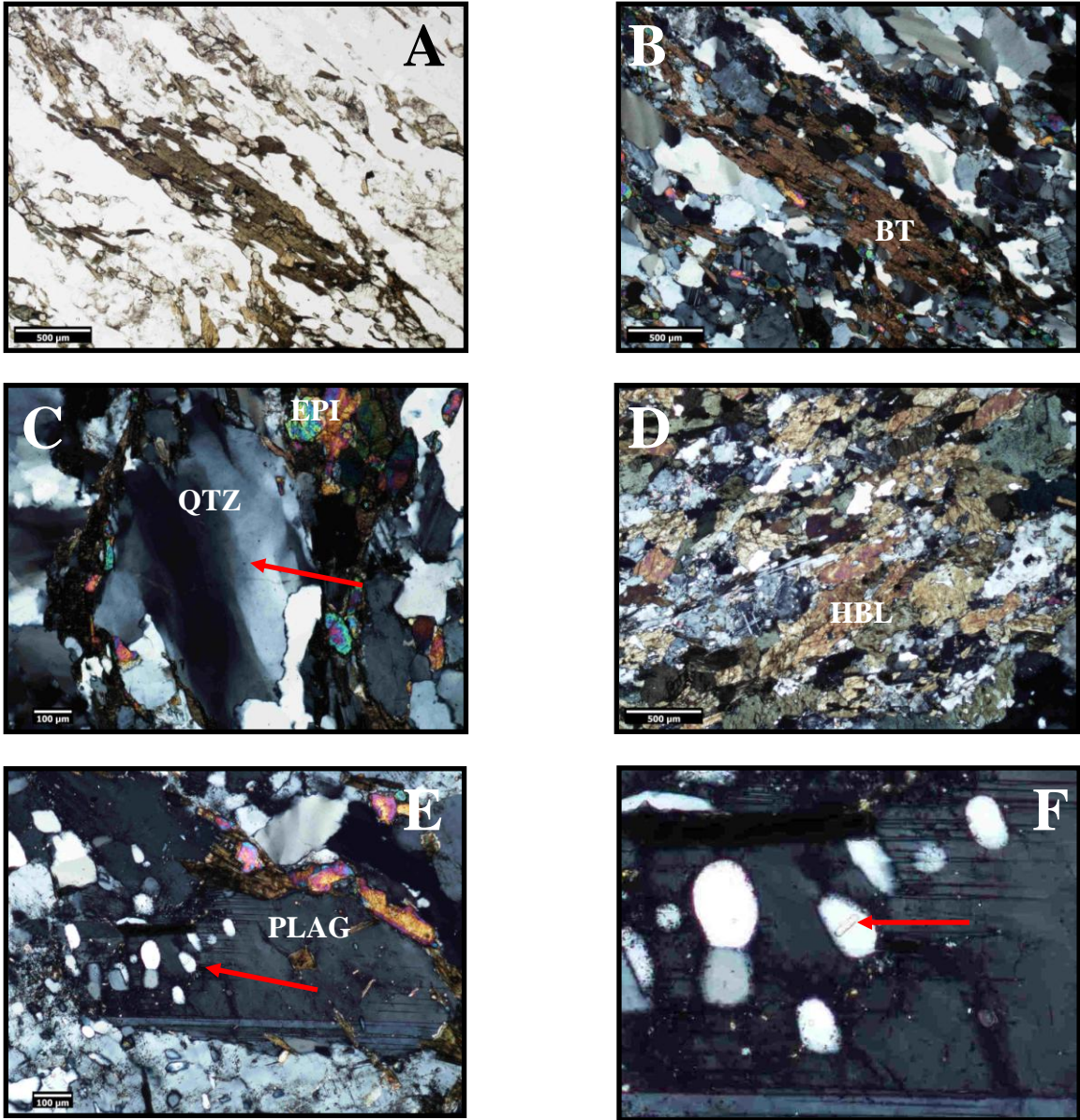


Figure 12. Thin section photomicrographs of Junction City quarry gneiss in plane polarized illumination (A), and crossed polarized illumination (B-F): A) JCQ-1 is a quartz-biotite gneiss with strained quartz and biotite defining the foliation with a quartz + plagioclase + biotite + epidote gross assemblage; B) same view as 'A' in crossed-polarized light; C) JCQ-1 with undulose extinction quartz grains (arrow); D) JCQ-3 is a hornblende-rich gneiss; E) JCQ-1 poikiloblastic texture in plagioclase with inclusions of quartz, biotite, and zircon (highlighted with red arrow and seen in picture F); and F) inclusions in plagioclase with centered quartz inclusion possessing zircon inclusion (arrow).

epidote would seem to indicate epidote-amphibolite to lower amphibolite-facies metamorphic conditions with temperature conditions likely between 500 – 600 °C.

6.3 MACON QUARRY

Samples from the Macon Quarry in Macon, Georgia, are typically granitic gneiss with a pink orthoclase-rich pegmatitic phase. In hand sample, the gneissic foliation is defined by thin melanocratic layers of biotite, and leucocratic, white to pink layers defined by quartz, alkali-feldspar, and plagioclase (Fig. 13). Gneissic texture is generally not pervasive in thin section with only weak preferential alignment of biotite and localized alkali-feldspar. Sample MQ-3 is medium-grained with average grain size approximately 0.5 -1.0 mm. Plagioclase displays sericitization. Quartz has undulatory extinction with angles averaging 5°. Overall crystal habit is subhedral and equigranular. The metamorphic assemblage is quartz + plagioclase + alkali-feldspar + biotite + hornblende (Fig. 14). A pegmatitic phase with coarse (2 – 4 mm) alkali-feldspar along with quartz, plagioclase, and biotite is observed. Point counting was conducted on MQ-3 overall mineralogy. Three-hundred counts were made with 1 mm spacing for sample MQ-3. Relative abundances are as follows: quartz (41.0%), plagioclase (21.6%), alkali-feldspar (17%), biotite (15.3%), hornblende (2.0%), sericite (1.6%), epidote (1.0%), calcite (tr.), zircon (tr.), and apatite (tr.). Mineralogy indicates likely metamorphic conditions up to amphibolite-facies conditions. Macon quarry samples have a similar appearance in hand sample to those of the Barin quarry although rocks in the Macon quarry do not have the same high degree of folding.

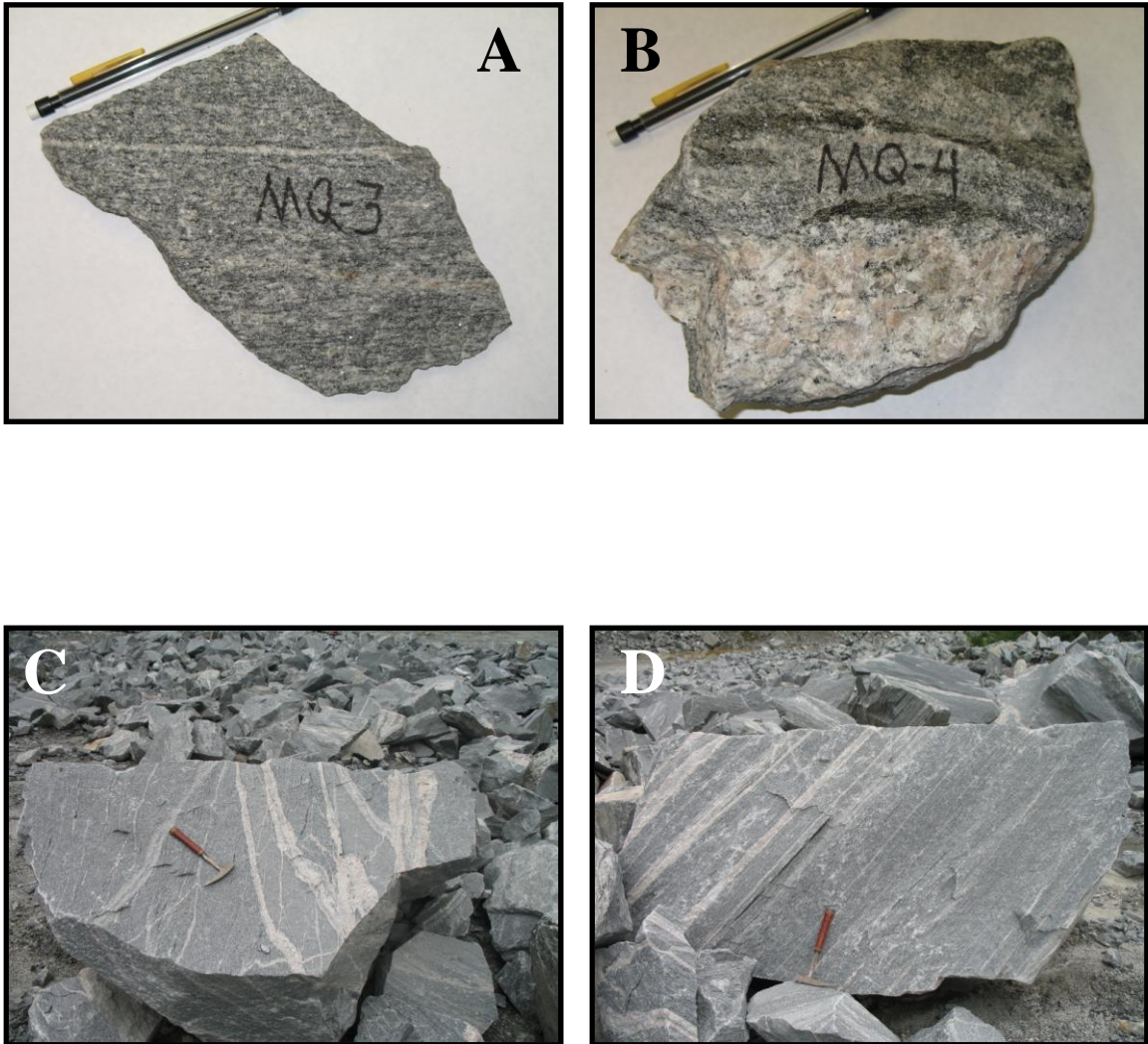


Figure 13. Representative hand sample view of Macon quarry phases: A) MQ-3 with gneissic foliation; B) MQ-4 with contact between granitic gneiss and coarse-grained, alkali-feldspar rich pegmatite; C) pegmatite veins cross-cutting gneissic foliation; and D) gneissic texture parallel to pegmatite at far left end of block.

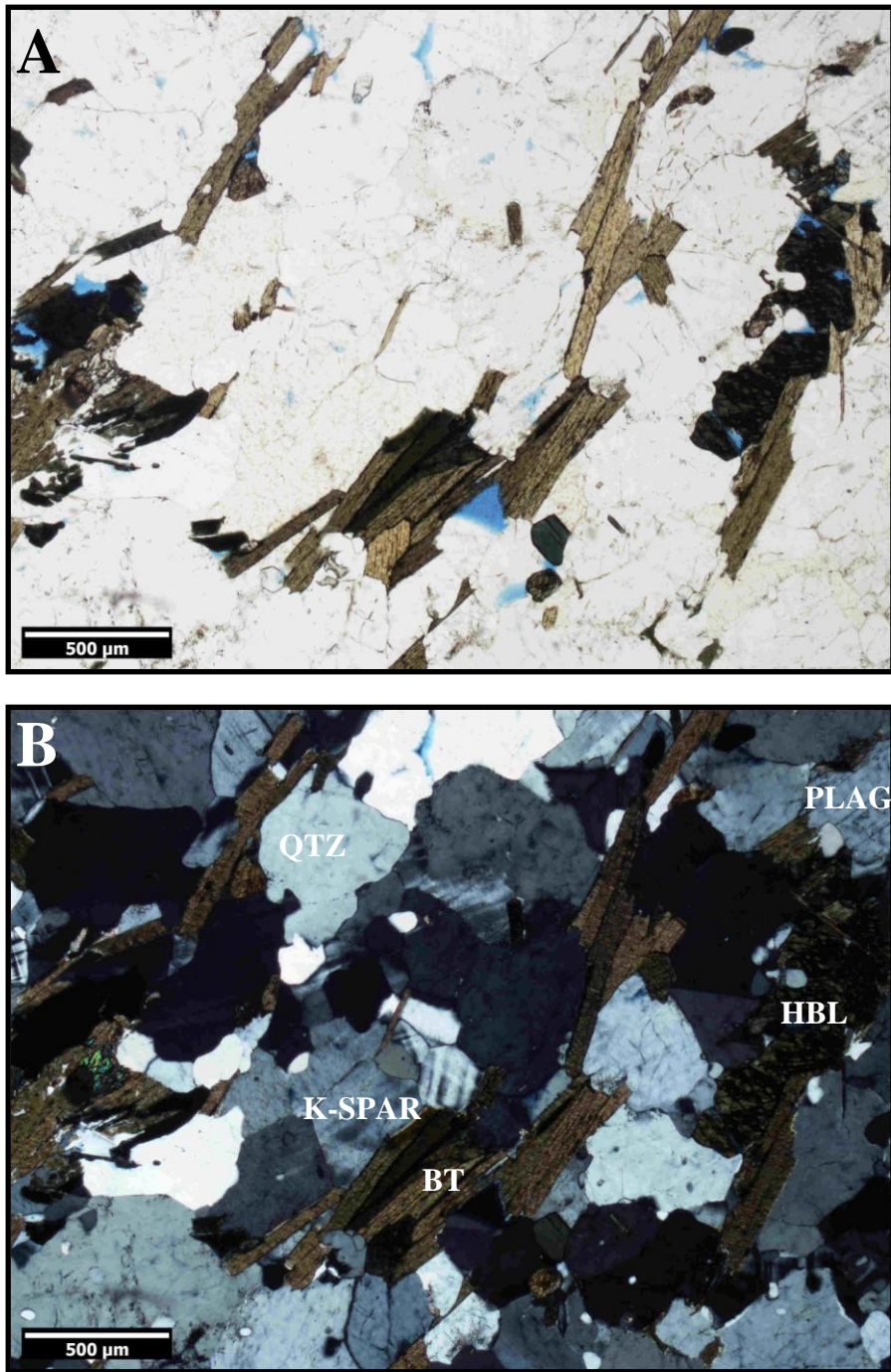


Figure 14. Thin section photomicrographs of Macon quarry gneiss with pictures observed at the same scale: A) MQ-3 granitic gneiss with weakly-defined foliation attributed to biotite with quartz, alkali-feldspar, and plagioclase under plane polarized illumination; and (B) same view under cross polarized illumination.

6.4 NOTASULGA QUARRY

Samples from the Notasulga Quarry in Notasulga, Alabama, are a metamorphosed granite. Hand samples have a weak gneissic foliation defined predominantly by biotite; however, foliation is not pervasive in thin section (Fig. 15). Large, pink, orthoclase porphyroblasts are apparent and some have an augen-type appearance. Overall, the rock is medium to coarse grained (1.0 – 1.5 mm) with porphyroblasts averaging between 2 – 4 mm. The metamorphic assemblage is quartz + alkali-feldspar + plagioclase + biotite + muscovite (Fig. 16). Quartz occurs as large crystals filling interstitial spaces between alkali-feldspar porphyroblasts. Quartz has weak undulatory extinction with angles of $<5^\circ$ indicating a low degree of lattice strain. Alkali-feldspar has characteristic tartan-plaid twinning. Approximately half of observed plagioclase grains have mild to moderate zoning indicating possible rim-to-core compositional variation. Fewer plagioclase grains show sericitization and myrmekite as intergrowths with quartz. Muscovite and biotite are common and appear randomly oriented. Point counting was conducted on sample NQ-1 to quantify overall mineralogy. Three-hundred and six counts were made with 1 mm spacing. Relative abundances are as follows: alkali-feldspar (37.9%), quartz (32.6%), plagioclase (18.9%), biotite (6.8%), muscovite (3.5%), apatite (tr.), and zircon (tr.).

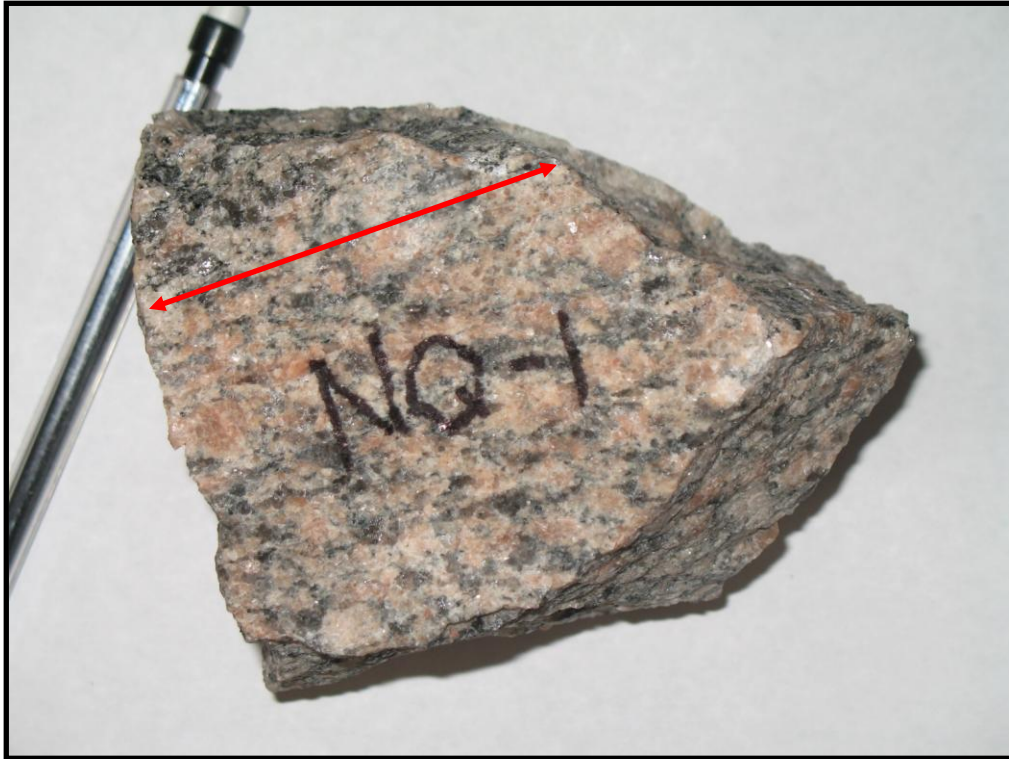


Figure 15. Sample NQ-1 from the Notasulga quarry with weakly defined gneissosity (shown with arrow) defined by biotite and abundant quartz and alkali-feldspar (orthoclase).

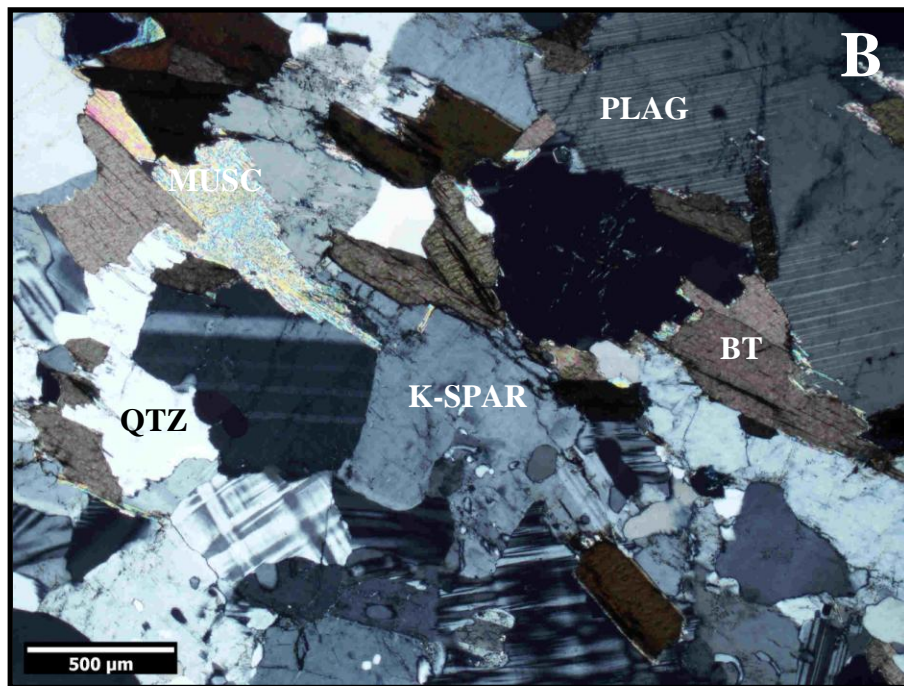
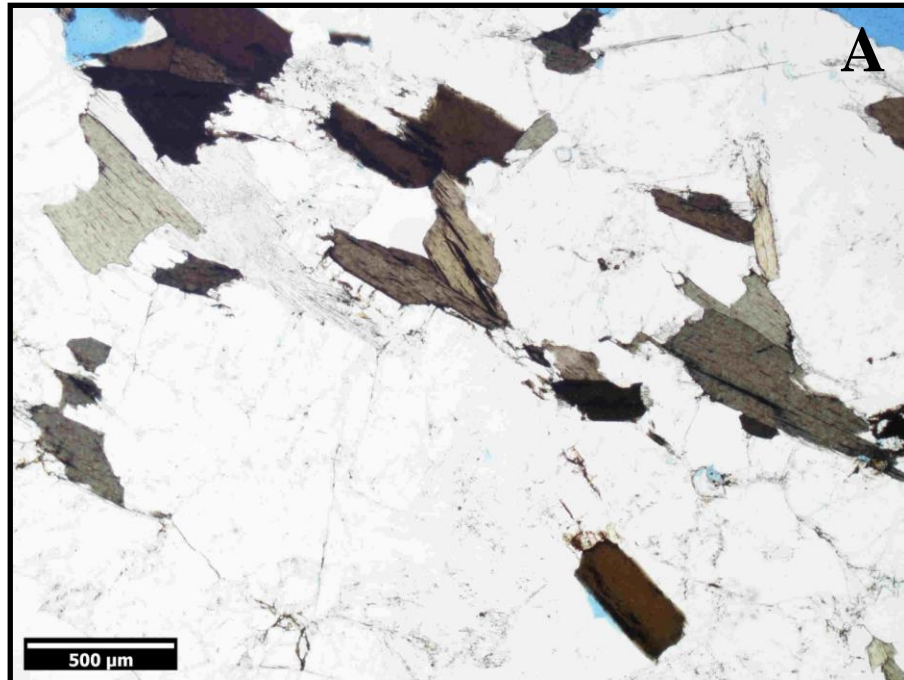


Figure 16. Thin section photomicrographs of Notasulga quarry metagranite sample NQ-1 with pictures observed at the same scale: A) biotite (dark brown) and muscovite (pale yellow) under plane polarized illumination; and B) metamorphic assemblage of alkali-feldspar, quartz, plagioclase, biotite and muscovite under crossed polarized illumination.

CHAPTER 7: PETROLOGY

7.1 INTRODUCTION

Rocks of the Barin locale are migmatitic and thus appear to have undergone fractional melting. This indicates that rocks achieved sufficiently-high temperatures for partial melting of a wet, calc-alkaline granitoid. Fractional melting is a function of protolith or rock composition, pressure, and fluids. As fluid pressure increases, the temperature of initial melting decreases. When fluid pressures are above approximately 3.5 kb and temperatures are minimally 650 – 700 °C then rocks containing quartz + two feldspars (plagioclase and alkali-feldspar) are suitable candidates for partial melting (Blatt et al., 2006). Partial melting of rocks at the Barin locale has resulted in a recrystallized melanocratic and leucocratic layered occurrence. According to Blatt et al. (2006), when resident water pressures reach 5 kb, the minimum temperature for partial melting to occur in a quartz + albite + orthoclase system is approximately 660 °C. Microprobe analyses of hornblende, biotite, plagioclase, and alkali feldspar analyze elemental composition, identify potential chemical zonation, and detect possible evidence of cation-exchange among phases such as hornblende and biotite.

Thermobarometers appropriate to hornblende – plagioclase – alkali-feldspar assemblages are commonly applied to rocks from igneous settings. Analyses are used to calculate pressures on the basis of the aluminum-in-hornblende geobarometer of Johnson and Rutherford (1989). Metamorphic temperatures were calculated using the hornblende

– plagioclase thermometer of Blundy and Holland (1990) with the Windows-based computer program Hb-Pl 1.2 and the two-feldspar ternary thermometer for feldspars from Fuhrman and Lindsley (1988). A two-feldspar solvus and compositional-dependant temperatures were calculated utilizing the Windows-based computer program SOLVCALC developed by Wen and Nekvasil (1994). These thermobarometers are applied with the assumption that parameters governing equilibrium among these phases are similar in the high-grade metamorphic (migmatitic) setting of the study samples (particularly the Barin quarry) as in igneous settings.

All EMP analyses were conducted on a single polished thin section typical of the alkali-feldspar-quartz-biotite migmatitic gneiss at the Barin locale. The thin section was cut from the same rock as sample BQ-1 (Fig. 8). Areas of interest were pre-selected on the microprobe section on the basis of mineralogy (hornblende, biotite, plagioclase, alkali-feldspar), grain-shape (euhedral versus anhedral), grain contacts (mineral adjacency to other grains analyzed), and overall optical grain features (evidence of zonation or perthitic exsolution in feldspar), and selected areas were circled with carbon ink and photomicrographed (Fig. 17). Analyses include rim-and-core spot point analyses and rim-core-rim complete line traverses; analyses labeled ‘rim’ are typically within 50 μm of the grain boundary.

Elemental analysis of hornblende and biotite include silicon, titanium, aluminum, chromium, iron, manganese, magnesium, calcium, sodium, and potassium. Silicon, aluminum, calcium, sodium, and potassium were analyzed in feldspars.

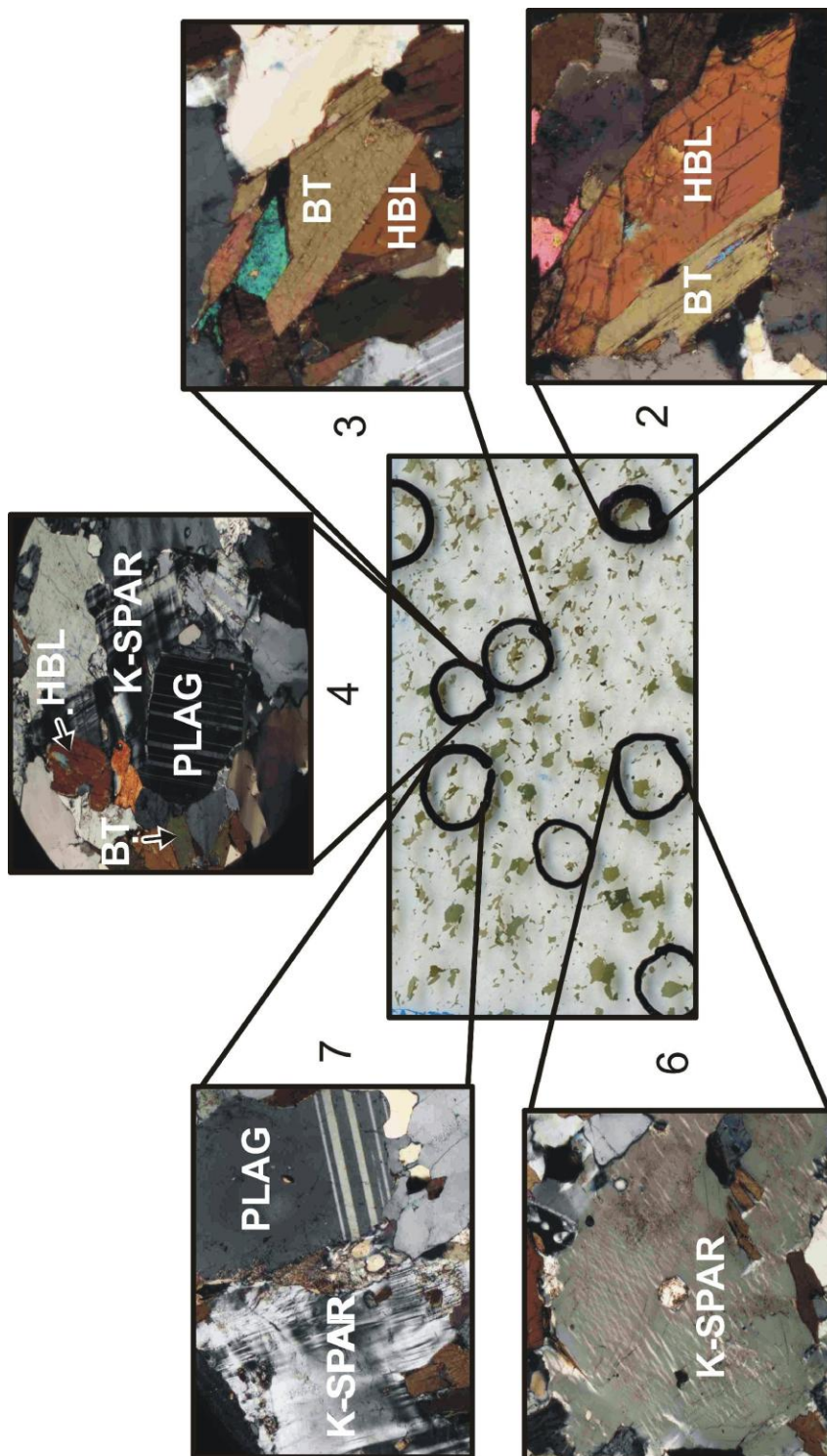
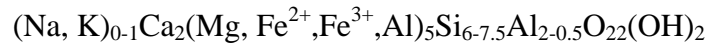


Figure 17. Microprobe thin section with black circled areas indicating initial areas of interest and highlighted circles demonstrating actual grains analyzed. Thin section size is standard 4.5 x 2.5 cm. All pictures taken under cross-polarized light with 4x magnification (BT = biotite, HBL = hornblende, K-SPAR = alkali-feldspar, PLAG = plagioclase)

7.1.1 HORNBLLENDE AND BIOTITE

Hornblende is a lithologically diverse mineral occurring in a wide variety of igneous and metamorphic settings. Such versatility is facilitated by the vast availability of cation substitution sites within the lattice for hornblende



with simple cation exchanges (e.g. $\text{Fe} = \text{Mg}$, $\text{Na} = \text{K}$), coupled exchanges ($\text{NaSi} = \text{CaAl}$), and cationic exchanges ($\text{F} = \text{OH}$, etc.) (Deer et al., 1992). Although hornblende can occur in many rock types, it is characteristic of intermediate and calc-alkaline igneous phases such as diorite, granodiorite, andesite, dacite, and their metamorphosed equivalents. However, hornblende may also occur in granitic assemblages and is one of the most common phases in medium to high-grade regional metamorphic assemblages ranging up to lower-granulite facies conditions (Deer et al., 1992).

Biotite is a phyllosilicate that represents an incomplete range of compositional variation among a Fe-rich end member (Annite) and a Mg-rich end member (Phlogopite). Biotite, like hornblende, possesses the potential for cation substitution in several sites and the formula for biotite is as follows



Biotite is a very common constituent of rocks from a wide range of igneous and metamorphic settings. Biotite associations occur with felsic to intermediate igneous rocks such as granite, granodiorite, and intermediate calc-alkaline rocks. It is a common component of regionally metamorphosed rocks from greenschist-facies conditions through higher-grade migmatized rocks (Neese, 2000).

Point analyses of hornblende and biotite, including single analyses of selected spots and line traverses, are presented in appendix 1. Average elemental percentages of Fe, Mg, and Ca for hornblende were calculated based on 23 point analyses producing 13.44, 5.91, and 7.89%, respectively, yielding an Mg / (Mg+Fe) ratio of ~0.30. The Al content of hornblendes from BQ-1 is also notable and exists in a roughly 1:1 ratio with Mg. Hornblende in BQ-1 is consistently edenitic (Fig. 18). Hornblende derived from intermediate igneous and calc-alkaline compositions typically possesses an Mg ratio of ~0.5 (Deer et al., 1992). Cation substitutions resulting in increased percentages of Al⁴⁺, Al⁶⁺, Ti, Fe³⁺, Na, and K with corresponding decreases in Si, Fe²⁺, Mg, and Ca correlate with increasing metamorphic grade (Deer et al., 1992). Calcium is generally similar in concentration from the core to rim of the amphibole. The Mg/Fe ratio of biotite and edenitic amphibole increase from the core to the rims of crystals, regardless of which phase the biotite or edenite is in contact with. The increasing Mg/Fe ratios of these phases are consistent with zoning of elements during growth through increasing temperature and prograde metamorphism.

7.1.2 PLAGIOCLASE AND ALKALI-FELDSPAR

Alkali feldspars include a solid solution series with varying content of potassium and sodium. The chemical formula for alkali feldspars varies from KAlSi₃O₈ to NaAlSi₃O₈. Based on thin section observations of twins in microcline and orthoclase, each occur at the Barin locale. The plagioclase end-members include sodium-rich albite (NaAlSi₃O₈) and calcium-rich anorthite (CaAl₂Si₂O₈). Substitution of cations between albite and anorthite involves a coupled exchange with the vector NaSi = CaAl. Within metamorphic rocks, plagioclase composition generally is equivalent to metamorphic

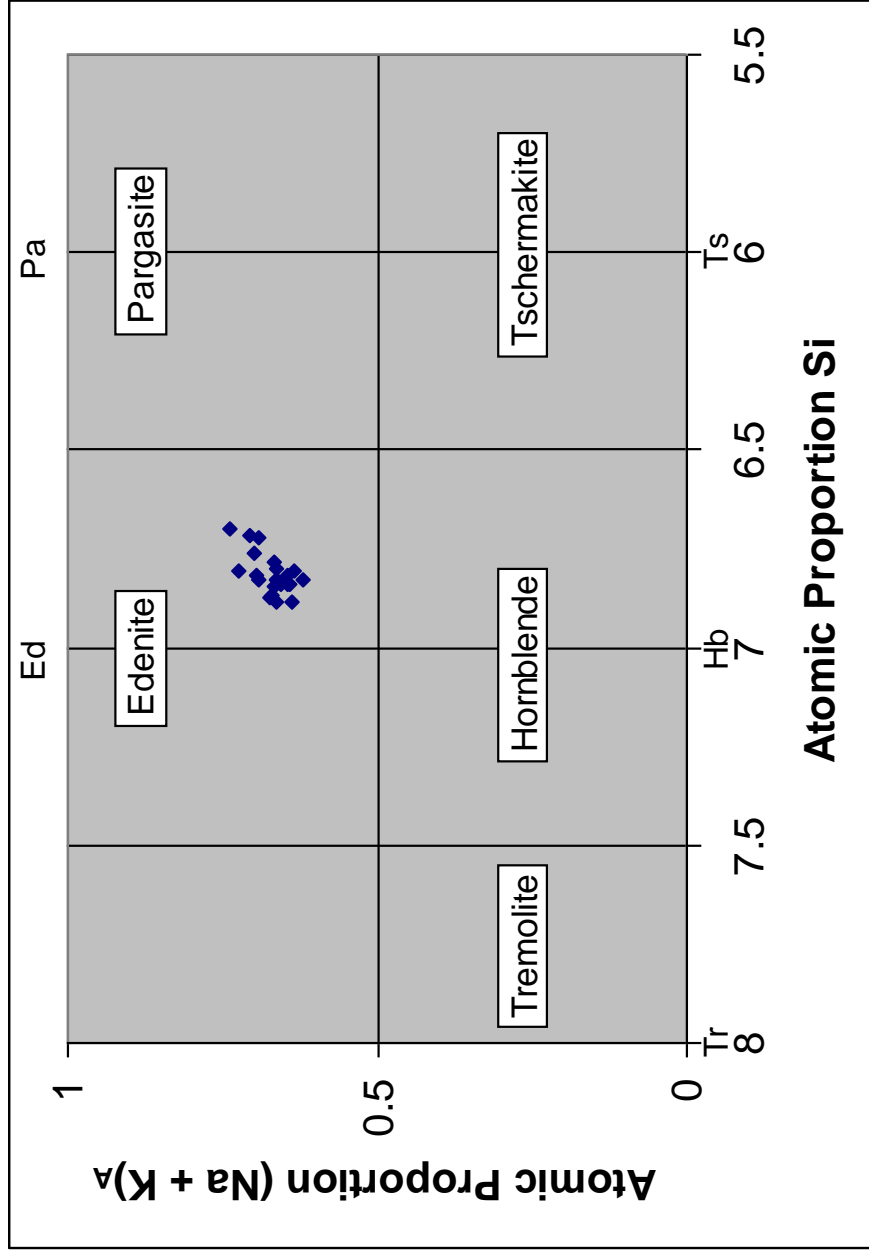
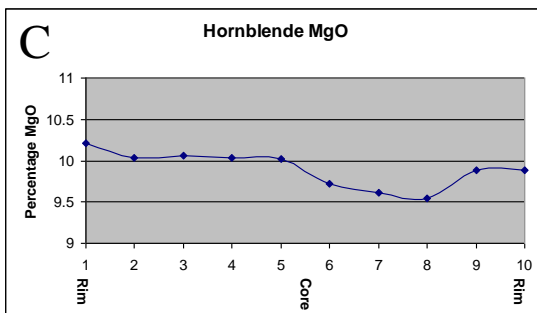
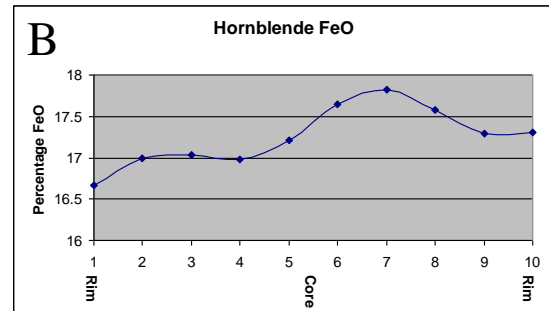
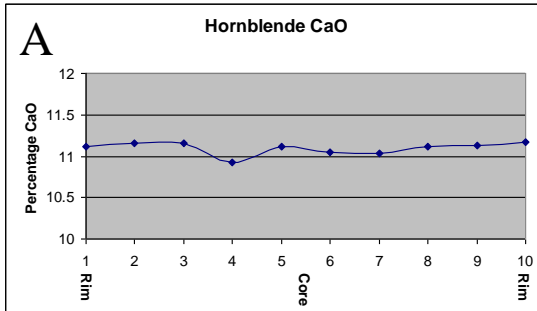


Figure 18. Chart demonstrating chemical variation of calcic amphiboles according to measured atomic proportion of Si and (Na + K) in the A site. End members shown include Ed = edenite, Pa = pargasite, Ts = tschermakite, Hb = hornblende, and Tr = tremolite. Points are based on twenty-two microprobe analyses of amphibole.

LINE TRAVERSES:



CORE AND RIM ANALYSES:

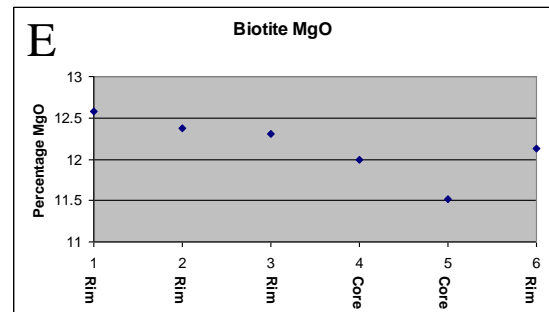
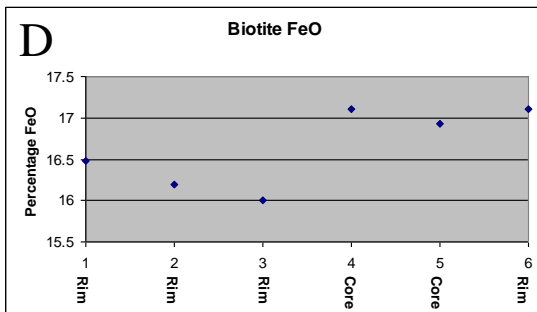


Figure 19. A) Hornblende line traverse analysis CaO; B) hornblende line traverse analysis FeO; C) hornblende line traverse analysis MgO; D) biotite point analyses FeO; and E) biotite point analyses MgO.

grade, and also a function of protolith composition. Plagioclase composition of rocks with a calc-alkaline affinity often possess plagioclase with An content of 30 or higher (Deer et al., 1992).

Analyses of alkali-feldspar and plagioclase are presented in appendix 1. The abundances of K, Na, and Ca in plagioclase are within the compositional range of plagioclase of andesine variety. At thin section scale, plagioclase is likely in equilibrium with relatively consistent composition, prograde zoning preserved, distinct grain contacts, and general lack of alteration. However, alkali-feldspar disequilibrium is indicated by slight compositional differences and exsolution textures (see discussion in section 7.4).

7.2 ALUMINUM-IN-HORNBLLENDE GEOBAROMETER

The total concentration of aluminum in hornblende (Al_{tot}) is a function of rock bulk composition, mineral assemblage, and pressure. Studies have quantified the ability to infer pressure conditions based on the content of aluminum within hornblende of calc-alkaline granitoids (Hammarstrom and Zen, 1986; Hollister et al., 1987; Johnson and Rutherford, 1989). This geobarometer is typically limited to igneous calc-alkaline rocks with the assemblage of quartz + plagioclase + potassium-feldspar + hornblende + biotite + sphene + an Fe-Ti oxide (Vyhnal et al., 1991). The presence of other aluminum-bearing minerals such as garnet can drastically affect total aluminum in hornblende (Vyhnal et al., 1991). Hammarstrom and Zen (1986) empirically derived the following equation to derive pressure from Al content:

$$P (\pm 3 \text{ kb}) = -3.92 + 5.03 Al_{tot}$$

Johnson and Rutherford (1989) experimentally refined this equation further to yield the following relationship:

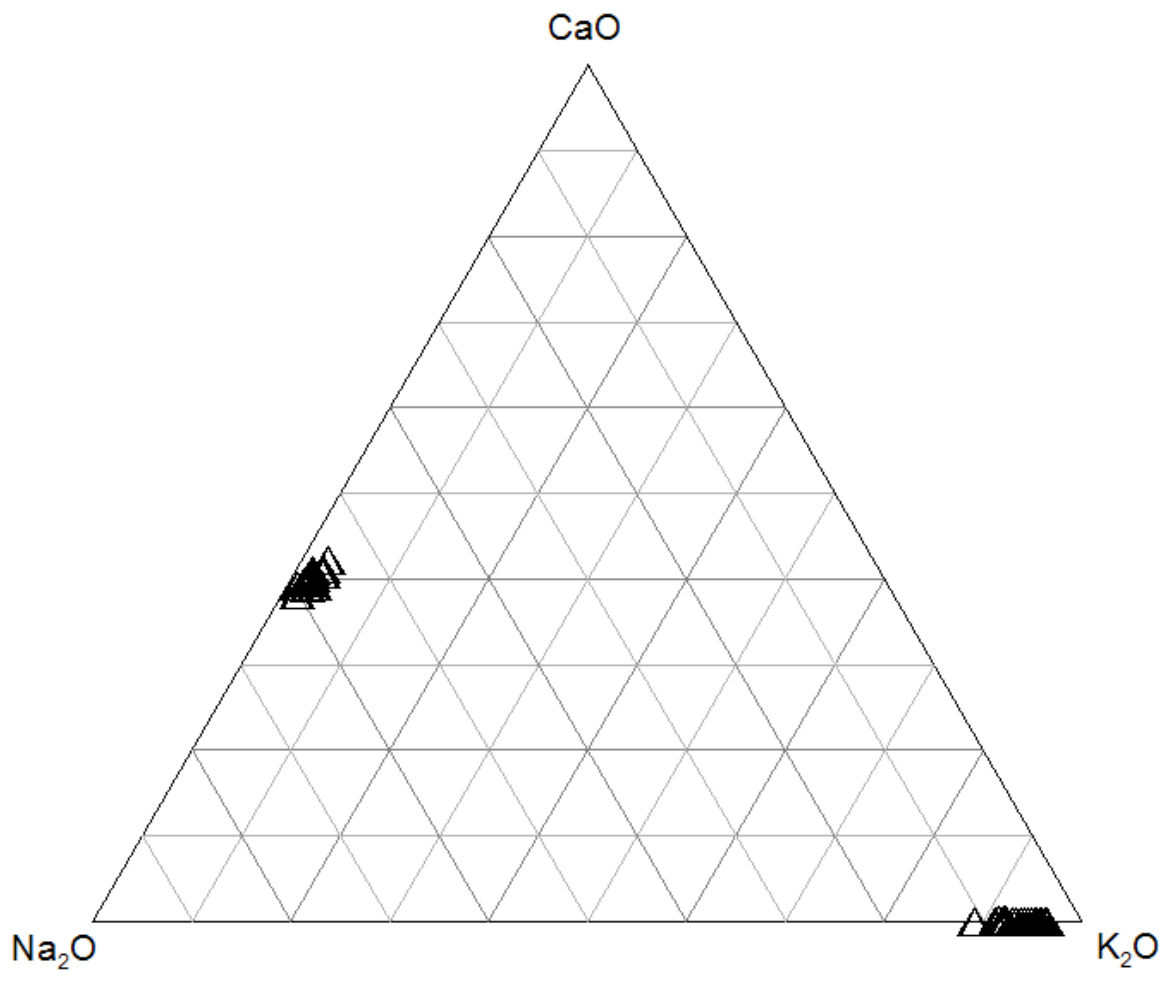


Figure 20. CaO, Na₂O, and K₂O ternary diagrams representing selected plagioclase and alkali-feldspar compositions from EMP. Plagioclase is of andesine variety.

$$P (\pm 0.5 \text{ kb}) = -3.46 + 4.23 \text{ Al}_{\text{tot}}$$

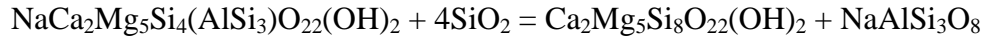
This relationship was derived from simulated igneous conditions in vapor-pressure experiments with temperature conditions ranging from 740 – 780 °C (Johnson and Rutherford, 1989). In the present study, this method is applied to the high-grade metamorphic gneisses derived from calc-alkaline granitoids in the Barin locale. Aluminum content in hornblende (averaged from 22 single point analyses; appendix 1) yields an atomic proportion of $\text{Al}_{\text{tot}} = 2.10$. Applying to the equation of Johnson and Rutherford (1989) yields 5.4 kb with a maximum error of ± 0.5 kb.

Thus, application of the aluminum in hornblende barometer to this equilibrium assemblage yields pressures of $\sim 5.4 \pm 0.5$ kb at peak metamorphic conditions. Assuming roughly 0.25 kb of pressure per kilometer of burial (with intermediate to granitic crust) minimum depth of burial due to tectonic loading (i.e. thrusting) is inferred to be ~ 22 kilometers for rocks at this locality. Propagation of the standard deviation in microprobe data through the geobarometric calculations indicate average pressure = 5.4 kb, maximum pressure = 6.0 kb, minimum pressure = 5.0 kb, and a median = 5.4 kb.

7.3 HORNBLLENDE – PLAGIOCLASE GEOTHERMOMETER

Hornblende and plagioclase analyses can be coupled for utilization as a geothermometer (Blundy and Holland, 1990). Amphiboles are present in a wide range of igneous and metamorphic assemblages, particularly calc-alkaline granitoids and metamorphic amphibolites (Blundy and Holland, 1990). The inherent ability of hornblende to accommodate different cation arrangements in multiple sites allow it considerable range of occurrence in many different settings with stability from 1 – 23 kb and 400 – 1150 °C (Blundy and Holland, 1990).

Blundy and Holland (1990) present a temperature-dependent calibration of the aluminum content in hornblende with the albite content of coexisting plagioclase. This hornblende-plagioclase geothermometer is derived from the following reaction:



representing edenite + quartz = tremolite + albite, respectively (Holland and Blundy, 1994). The thermometric equation for temperature derivation as determined by Blundy and Holland (1990) is as follows:

$$T = (0.677 P - 48.98 + Y) / (-0.0429 - 0.008314 \ln K)$$

where P = pressure in kb, Y = term representing plagioclase non-ideality, and $K = [(Si - 4)/(8 - Si)] * X_{ab}$ (% albite). The applications of this thermometer include a wide range of hornblende-plagioclase coupled occurrences including plutonic and volcanic igneous rocks as well as greenschist to lower granulite facies metamorphics (Blundy and Holland, 1990). This thermometer is applicable to rocks from the Barin locale on the basis of percent oxide abundances as determined by microprobe analysis.

The hornblende-plagioclase thermometer uses a Windows based program, HbPl 1.2, developed by Holland and Blundy (1994) incorporating the above equation. Required input includes oxide weight percent of SiO₂, TiO₂, Al₂O₃, Cr₂O₃, Fe₂O₃, FeO, MnO, MgO, CaO, Na₂O, K₂O, and X_{ab}. This arrangement provides for the distinction of ferrous (Fe²⁺, expressed as FeO) and ferric (Fe³⁺, expressed as Fe₂O₃) iron. However, microprobe analyses do not distinguish between Fe²⁺ and Fe³⁺. Due to a structural vacancy and the hydrous nature of amphiboles, estimation of ferric iron is troublesome (Spear, 1995). The ferrous to ferric iron ratio was calculated for Barin hornblende based on the method outlined in Holland and Blundy (1994). This method allows the derivation of an

acceptable range for ferric iron content by stoichiometrically limiting ferric and ferrous iron to prescribed amphibole sites. For hornblende in this study, the ferrous to ferric iron ratio was determined at 0.75 and 0.25, respectively.

Hornblende-plagioclase thermometer calculations for sample BQ-1 yield temperatures ranging from 656 to 708 °C. These temperatures assume pressures of a 5 kb environment, as estimated of P_{\max} (~5.4 kb) indicated by the aluminum in hornblende barometer. Analyses compare rim (hornblende) to rim (plagioclase) results, and rim-rim analysis produces temperatures averaging 674 °C assuming 5 kb. The accuracy of the geothermometer is reported to be ± 23 °C where Si ~ 6.7 at 650 °C (Blundy and Holland, 1990).

Although there is some zoning of Fe and Mg in biotite and amphibole there is little zoning or variation of Na and Ca in plagioclase or amphibole. Thus, the temperatures calculated for any plagioclase and amphibole composition determined in the thin section are similar. To evaluate the variation in composition and effect on temperature calculation Monte Carlo style statistical simulations were employed. The temperatures calculated provide valuable insight into conditions of peak metamorphism. Approximately twenty analyses for hornblende and plagioclase (rim, core, and intermediate locations in grains) were used to generate ~100 random combinations with a resulting mean of 686 ± 15 °C and a standard error of the mean equal to 1.5 °C (Fig. 21). Pressure for each of the ~100 points was also calculated according to the previously described aluminum-in-hornblende equation of Johnson and Rutherford (1989). The resulting synthetic pressure-temperature pairs are shown in figure 21 and demonstrate the estimated metamorphic conditions experienced at depth for the Barin locale.

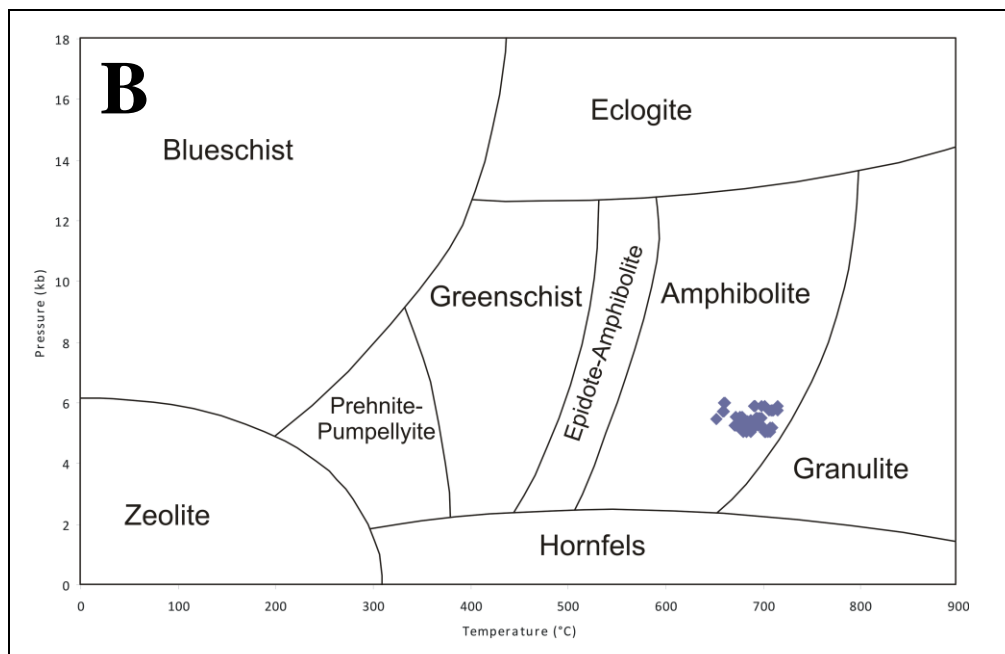
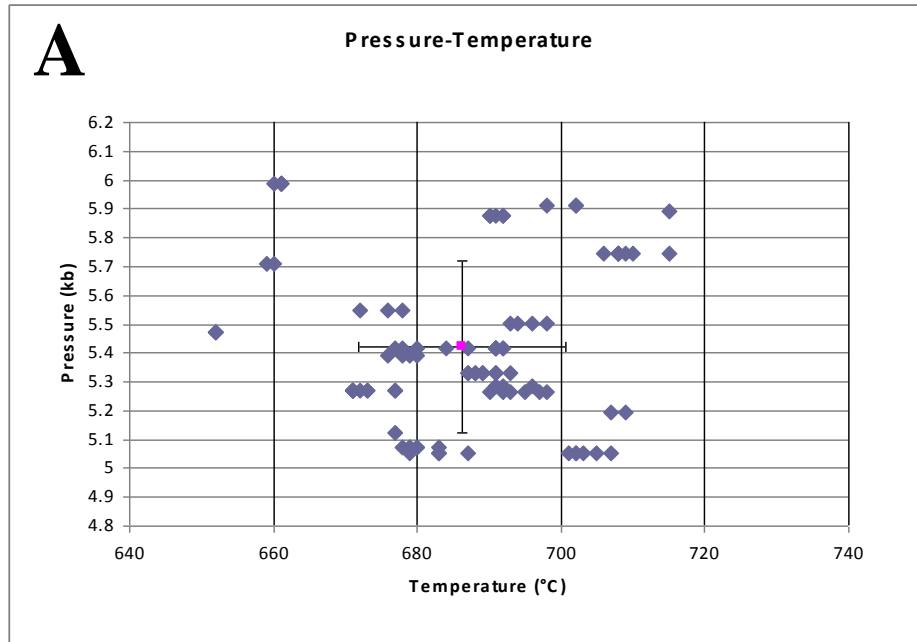


Figure 21. A) Pressure-temperature graph of ~100 analyses of the hornblende-plagioclase geothermometer from the Barin locale (BQ-1). Temperatures range from 652 – 715 °C and pressures range from 5.0 – 6.0 Kb with a standard deviation of 14.7 implied by error bars. B) Pressure-temperature diagram of ~100 analyses from figure A with metamorphic facies distribution. All analyses fall within amphibolite metamorphic facies (modified from Blatt et al., 2006).

7.4 TWO-FELDSPAR GEOTHERMOMETER

The presence and coexistence of two-feldspars (plagioclase and an alkali-feldspar) can be utilized as a geothermometer. At sufficiently high temperatures cation exchange can readily occur between feldspars. Within a ternary feldspar system (anorthite, albite, orthoclase) complete solid-solution exists between anorthite and albite and albite and orthoclase at high-temperatures associated with igneous plutonic and volcanic crystallization or sufficiently high temperatures associated with a metamorphic event (Fuhrman and Lindsley, 1988). The composition of the feldspars at equilibrium is primarily a function of temperature with a secondary dependence on pressure. In practice, it is reported that this thermometer is susceptible to re-equilibration following peak metamorphism, through exsolution or cation-exchange with fluids (Fuhrman and Lindsley, 1988). The relatively high standard deviation (~15%) is consistent with disequilibrium among the feldspars. Inspection of analyses reported in appendix 1 and figure 22 indicate that variation of alkali-feldspar compositions likely was caused by exsolution of albite from K-feldspar (see also discussions in Fuhrman and Lindsley (1988)).

Temperature estimates for feldspars were calculated based on microprobe analyses of plagioclase and alkali-feldspar (orthoclase) of sample BQ-1. The Windows-based computer program SOLVCALC (Wen and Nekvasil, 1994) was used to develop a ternary feldspar solvus and plot compositions with corresponding tie lines (Fig. 22). An initial ternary feldspar solvus was calculated based on the method of Fuhrman and Lindsley (1988) with conditions of 686 °C and 5.4 kb as previously determined and the fractions and the mole percentages of albite, orthoclase, and anorthite (Appendix 1).

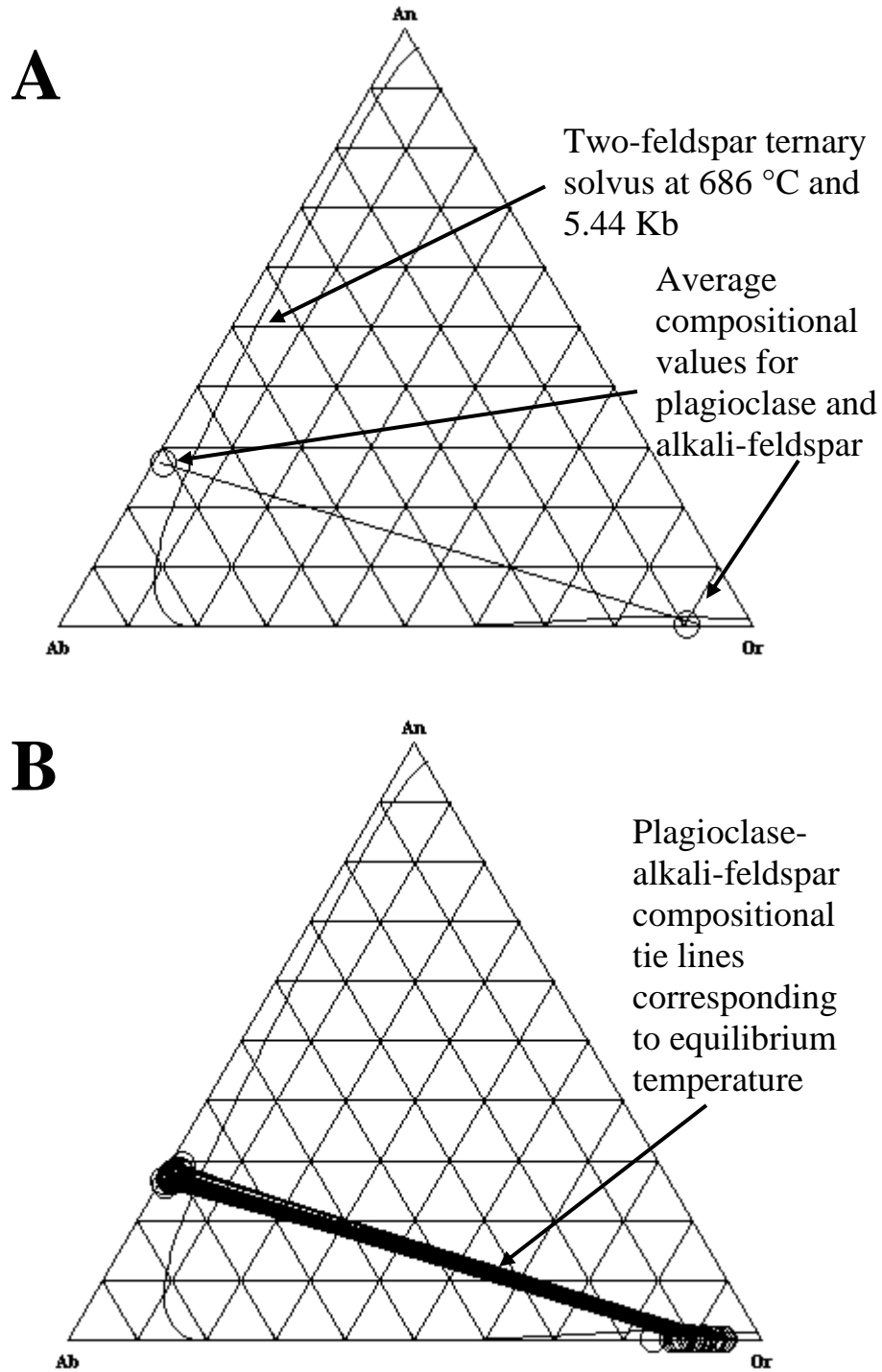


Figure 22. Anorthite, albite, and orthoclase feldspar ternary diagram with feldspar solvus as determined by SOLVCALC with the maximum given metamorphic conditions of 686 °C and 5.4 Kb. A) Solvus with tie lines between average plagioclase and alkali-feldspar compositions for BQ-1; B) tie lines of 91 randomly calculated plagioclase and alkali-feldspar compositions.

The mole fractions measured for feldspars are not compatible with the calculated solvus, but instead yield a temperature for this two-feldspar system of 437 °C at 5.4 kb. This temperature does not correspond to peak metamorphic temperature associated with the Alleghanian event but instead represents a temperature at which feldspars reached equilibrium and cation exchange ceased. This is interpreted to indicate that this rock did not immediately quench, but Na-Ca-K exchange continued among feldspars and perhaps other phases. A Monte Carlo approach was used to better assess the range of feldspar composition and its effect on calculated temperatures, resulting in a mean of 422 ± 65 °C.

CHAPTER 8: GEOCHRONOLOGY

Geochronology is important to developing an increased understanding of the sequence and timing of geologic events such as post-peak metamorphic cooling and subsequent unroofing of collisionally-derived orogenic belts. The geochronologic investigation of this study utilizes $^{40}\text{Ar}/^{39}\text{Ar}$ analyses to evaluate $\sim 500\text{ }^{\circ}\text{C} - 300\text{ }^{\circ}\text{C}$ cooling history and (U-Th)/He analyses to evaluate $\sim 200\text{ }^{\circ}\text{C} - 70\text{ }^{\circ}\text{C}$ cooling history. $^{40}\text{Ar}/^{39}\text{Ar}$ analyses are presented for hornblende, muscovite, and biotite from the Barin locale, and (U-Th)/He analyses on zircon and apatite are presented from the Notasulga, Barin, Junction City, and Macon locales (Fig. 8).

8.1 (U-Th)/He ANALYSES

(U-Th)/He analysis of apatite ideally represents age determined by a closure temperature ca. $70 - 80\text{ }^{\circ}\text{C}$, while zircon represents age determined by a closure temperature ca. $180 - 200\text{ }^{\circ}\text{C}$. (U-Th)/He analysis of apatite was conducted on samples from the Barin, Macon, and Notasulga locales while zircon analysis was conducted on the three aforementioned locales with addition of the Junction City locale (Table 1). Samples from the Junction City locale did yield small apatite crystals, but the apatites were not suitable for analysis due to the presence of inclusions. Four apatite analyses from the Barin locale separated from sample BQ-1 (Fig. 8) reveal ages of 118.9, 131.7, 116.6, and 114.2 Ma with an average of $120.3 \pm 7.2\text{ Ma}$ (standard deviation = 7.8, 94% confidence level) . Four analyses were conducted on apatite from the Macon locale.

APATITE		
Sample	Age (Ma)	± (Ma) 6%
BQ-1-1	118.9	7.1
BQ-1-2	131.7	7.9
BQ-1-3	116.6	7.0
BQ-1-4	114.2	6.9
BQ-1 Average	120.3	7.2
MQ-3-1	117.2	7.0
MQ-3-2*	827.1	49.6
MQ-3-3*	386.1	23.2
MQ-3-4	119.9	7.2
MQ-3 Average	118.5	7.1
NQ-1-1*	453.4	27.2
NQ-1-2	190.3	11.4
NQ-1-3	160.3	9.6
NQ-1-4*	339.9	20.4
NQ-1 Average	175.3	10.5

ZIRCON		
Sample	Age (Ma)	± (Ma) 6%
BQ-1-1*	364.9	29.2
BQ-1-2	221.6	17.7
BQ-1-3	206.8	16.5
BQ-1 Average	214.2	17.1
BQ-6-1	163.8	5.1
BQ-6-2	169.6	5.6
BQ-6-3	154.6	12.4
BQ-6 Average	162.7	7.7
MQ-3-1	187.7	15.0
MQ-3-2	172.5	13.8
MQ-3-3	193.2	15.5
MQ-3 Average	184.5	14.8
NQ-1-1	189.1	15.1
NQ-1-2	215.4	17.2
NQ-1-3	170.3	13.6
NQ-1 Average	191.6	15.3
JCQ-1-1	208.2	16.7
JCQ-1-2	252.7	20.2
JCQ-1-3	233.1	18.6
JCQ-1 Average	231.3	18.5

Table 1. (U-Th)/He ages for apatite (left) and zircon (right); BQ = Barin locale, MQ = Macon locale, NQ = Natasulga locale, JCQ = Junction City locale. Asterisk (*) represents sample with anomalous age not considered for statistical average. See appendix for analytical results.

Apatite separates from sample MQ-3 (Fig. 13) yield ages of 117.2, 119.9, 386.1, and 827.1 Ma. Apatites ages older than ~190 Ma are not geologically reasonable and are likely attributed to the presence of uranium and thorium-rich inclusions producing excess alpha decays. The two geologically reasonable results yield an average of 118.5 ± 7.1 Ma (standard deviation = 1.9). Four analyses were conducted on apatite from the Notasulga locale. Apatite separates from sample NQ-1 (Fig. 15) yield ages of 160.3, 190.3, 339.9, and 453.4 Ma. The latter two analyses are not considered for calculation of an average age. The two logical results yield an average of 175.3 ± 10.5 Ma (standard deviation = 21.2). Apatite, with closure generally coinciding with the ~70 °C isotherm, were elevated above this isotherm at the Barin, Macon, and Notasulga locales at 120 ± 7.2 , 118.5 ± 7.2 , and 175.2 ± 10.5 Ma, respectively.

Three zircon analyses were conducted for each of the phases represented at the Barin locale including migmatitic gneissic phase (BQ-1) and the pegmatite phase (BQ-6). Three analyses for zircon from the Barin locale (BQ-1) yield ages of 206.8, 221.6, and 364.9 Ma. Ages above ~250 Ma are considered geologically unreasonable and are attributed to the presence of uranium and thorium-rich inclusions producing excess alpha decays. The two geologically sensible results average $214.2 \text{ Ma} \pm 17.1 \text{ Ma}$ (standard deviation = 10.4). The pegmatitic phase, BQ-6 yields three zircon ages of 154.6, 163.8, and 169.6 with an average of $162.7 \text{ Ma} \pm 7.7 \text{ Ma}$ (standard deviation = 7.5). Three zircon analyses were conducted on separates from sample MQ-3 from the Macon locale. MQ-3 yields zircon ages of 172.5, 187.7, and 193.2 Ma with an average of $184.5 \text{ Ma} \pm 14.8 \text{ Ma}$ (standard deviation = 10.7). Three zircon analyses were conducted on separates from sample NQ-1 from the Notasulga locale with resulting ages of 170.3, 189.1, and 215.4

Ma with an average of 191.6 ± 15.3 Ma (standard deviation = 22.6). Three zircon analyses were also conducted on separates from sample JCQ-1 (Fig. 11) from the Junction City locale, yielding zircon closure temperature ages of 208.2, 233.1, and 252.7 Ma with an average of 231.3 ± 18.5 Ma (standard deviation = 22.3). In comparison to apatite, (U-Th)/He analysis of zircon is generally interpreted to reflect closure coinciding with the ~ 200 °C isotherm as crust is exhumed. Along the ~ 190 km transect of this project the 200 °C isotherm was achieved between 231.3 and 162.7 Ma. From west to east, closure reflects 191.6, 214.2 (162.7 for pegmatite phase, BQ-6), 231.3, and 184.5 Ma possibly indicating more rapid exhumation in central part of the transect between the Barin and Junction City locales. The fairly large error (average error ~ 14.6 Ma) provides for relative agreement of the zircon ages.

Inductively coupled plasma mass spectrometry (ICP-MS) was conducted for each grain producing an age in order to quantify, in parts per million, the proportions of uranium and thorium within the system. Utilizing this information, a Th/U ratio is easily calculated. For apatite the Th/U ratios are 0.3, 0.2, and 2.8, respectively, for the Barin, Macon, and Notasulga locales. The Notasulga apatites have roughly three times the amount of thorium versus uranium than that of the other two locales. High uranium content will produce greater alpha particle emission. The Notasulga apatite represent ages that are ~ 55 Ma older than the Barin locale. All U, Th, and He data are provided in appendix 3.

Zircons typically will incorporate higher proportions of both uranium and thorium as compared to apatite. Calculated Th/U reveal ratios of 0.4, 0.0 (see below), 0.5, 0.4, and 0.4, respectively, for the Barin quarry samples and BQ-6, Macon, Notasulga, and

Junction City locales. Ratios are generally consistent with thorium content fluctuating from 40 to 50% of that of uranium, with the exception of sample BQ-6 from the Barin locale. The Th/U ratio of 0.0 represents a strong disparity in the high concentration of uranium and low content of thorium. Sample BQ-6 averages 1342.4 ppm uranium and 16.0 ppm thorium. This large uranium content leads to a significantly greater alpha particle measurement of 960.0 ncc/ μ g. Pegmatites typically possess a granitic-like composition, and granitic compositions are typically associated with higher natural uranium content as compared to the adjacent migmatitic gneiss. Pegmatites also possess the ability to concentrate specific chemical constituents through chemical fractionation such as Li, Rb, Cs, Be, Ga, B, P, F, Mn, Nb, Ta, Zr, Hf, Sn, and U, enriching these constituents by a factor of 10^3 to 10^4 over average granitic compositions (London, 1992). Such concentrations are observed in the present study, where the uranium content of BQ-1 (the gneissic host-rock) is almost eight times less than BQ-6 revealing an average of 172.5 ppm. See table 1 for (U-Th)/He data.

8.2 $^{40}\text{Ar}/^{39}\text{Ar}$ ANALYSES

$^{40}\text{Ar}/^{39}\text{Ar}$ analysis quantifies retention of radiogenically produced ^{40}Ar from the natural decay of ^{40}K . In plutonic rocks, retention of ^{40}Ar occurs below the threshold temperature or closure temperature for each mineral analyzed with experimentally-determined, broadly accepted closure temperatures for hornblende (~ 500 °C), muscovite (~ 350 °C), and biotite (~ 300 °C) (e.g. Hodges, 1991). $^{40}\text{Ar}/^{39}\text{Ar}$ analyses were conducted on hornblende, muscovite, and biotite from the Barin locale utilizing both single crystal total fusion (SCTF) and incremental heating (IH) methods.

8.2.1 HORNBLLENDE

Thirty hornblende crystals from sample BQ-1 and 10 from sample BQ-7 were analyzed for the Barin locale. These consisted of 20 single crystal total fusion (SCTF) and 20 incremental heating (IH). SCTF of hornblende yields closure temperature mean age of 298.5 ± 3.1 Ma with a MSWD = 13. This high MSWD value is likely attributed to some non-atmospheric extraneous argon in a few crystals producing older ages (304, 310 Ma) while other crystals may be rich in defects (288 Ma) causing a lower closure temperature (Fig. 23). IH was conducted on 10 hornblende crystals with 20 heating steps for sample BQ-1 yielding a plateau age of 286.38 ± 0.43 Ma incorporating 66.1% of ^{39}Ar .

IH analysis was also conducted on 10 hornblende crystals with 21 steps for sample BQ-7 yielding a plateau age of 292.18 ± 0.48 Ma incorporating 96.8% of ^{39}Ar . Figure 23 B is more discordant, with ages increasing to ~ 292 Ma, where as 97% of release defines figure 23 C. The SCTF and IH ages are not consistent which is likely attributed to the presence of excess, non-atmospheric argon and possible defects among the crystals. The preferred age for the edenitic hornblende is 292.18 ± 0.48 Ma (Fig. 23 C) as this incremental heating result produces a plateau incorporating 97% of the ^{39}Ar corresponding to the timing for retention of argon. Based on an effective grain size of ~ 200 μm as determined by petrography and sieve analysis, and using the diffusion parameters of Harrison (1981) and the model of Dodson (1973), these crystals reached isotopic closure at ~ 527 $^{\circ}\text{C}$.

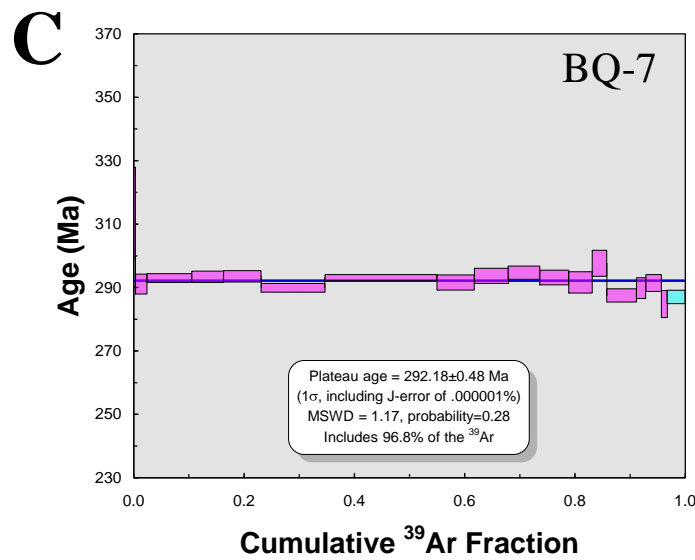
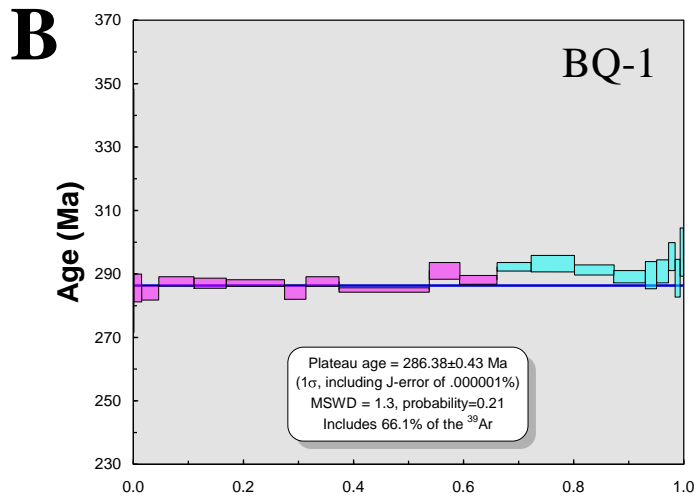
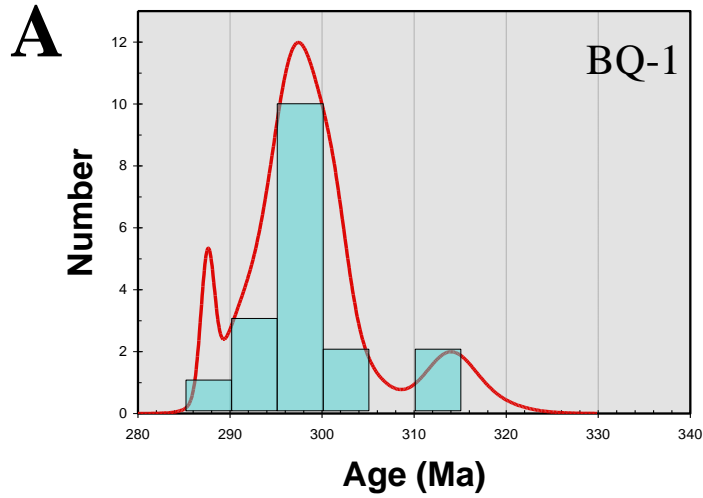


Figure 23. Hornblende incremental heating and single crystal total fusion ⁴⁰Ar/³⁹Ar analyses (plateau steps are magenta and rejected steps cyan, IH box heights are 1σ: A) SCTF (BQ-1) with mean of 298.5 ± 3.1 Ma; B) IH (BQ-1) with plateau age of 286.4 ± 0.4 Ma including ~66% of the ³⁹Ar; C) IH (BQ-7) with plateau age of 292.2 ± 0.5 Ma including ~97% of ³⁹Ar. The age of 292.2 Ma is the preferred age for hornblende of this locale due to the high percentage of argon included in the calculated plateau.

8.2.2 BIOTITE

Thirty biotite crystals were analyzed from sample BQ-1 from the Barin locale. This sample represents the overall migmatitic gneissic phase. SCTF ages of biotite yield a mean of 283.5 ± 2.0 Ma at the 95% confidence level (Fig. 24). These ages have a MSWD = 2.7 and a probability = 0.005. The low probability could be attributed to excess argon in the system. Incremental heating was conducted on 20 biotite crystals from the same sample. Two separate incremental heating analyses were conducted with 10 crystals per hole. The first incremental heating analysis utilized 13 heating steps and produced a plateau age of 283.0 ± 0.78 Ma (Fig. 24 B). This plateau includes 95.2% of measured ^{39}Ar and carries an MSWD = 1.5 and a probability of 0.15. The second incremental heating analysis utilized 9 heating steps and produced a plateau age of 284.8 ± 1.0 Ma incorporating 100% of the ^{39}Ar (Fig. 24 C). This incremental heating analysis produced a MSWD = 1.6 and a probability = 0.12. These ages are the same within uncertainty, and yield a combined estimate of 284 ± 1.0 Ma. The consistency of SCTF ages and plateau ages indicate that the age of 283.6 Ma is the timing for retention of argon in biotite at the Barin locale. Based on an effective grain size diameter of ~ 200 μm as determined by petrography and sieve analysis, and using the diffusion parameters for biotite of Harrison et al., (1985) and the model of Dodson (1973) these crystals reached isotopic closure at ~ 312 °C.

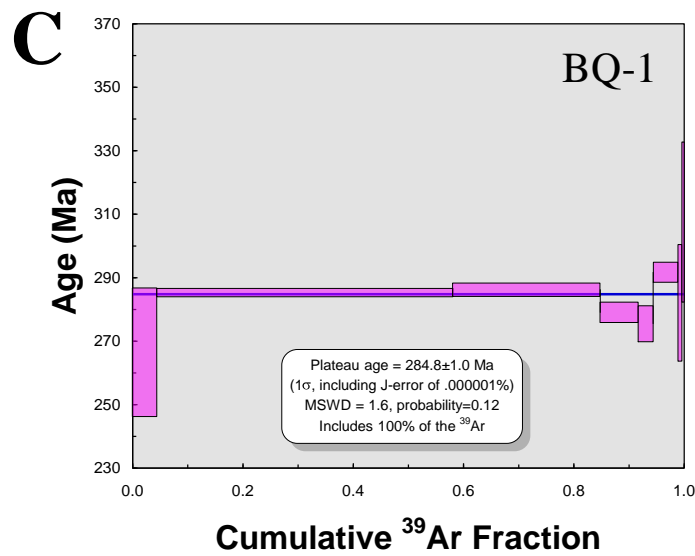
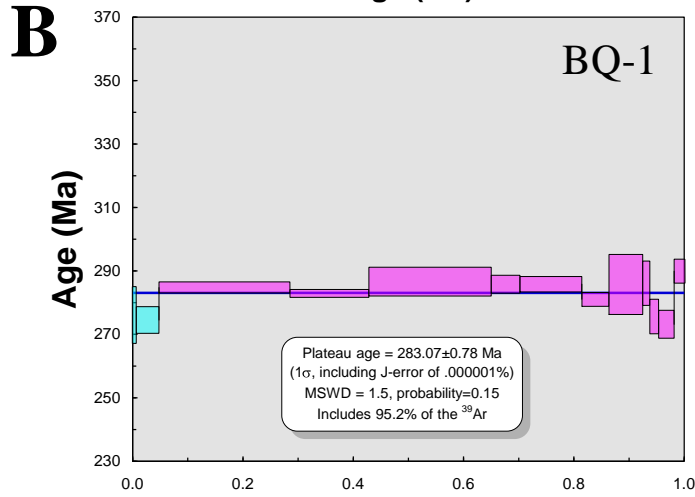
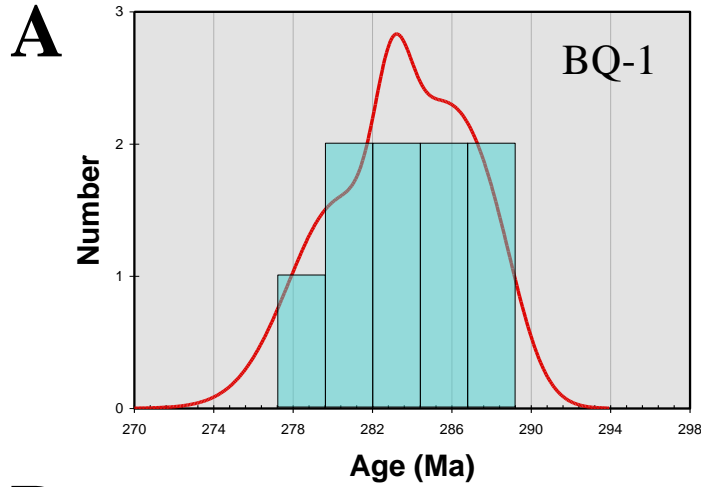


Figure 24. Biotite incremental heating and single crystal total fusion ⁴⁰Ar/³⁹Ar analyses for sample BQ-1 (plateau steps are magenta and rejected steps cyan, IH box heights are 1σ: A) SCTF with mean of 283.5 ± 2.0 Ma; B) IH with plateau age of 283.1 ± 0.8 Ma including ~95% of the ³⁹Ar; C) IH with plateau age of 284.8 ± 1.0 Ma including ~100% of ³⁹Ar. The age of 284.8 Ma is the preferred age for biotite of this locale due to the high percentage of argon included in the calculated plateau.

8.2.3 MUSCOVITE

About twenty muscovite crystals from sample BQ-6 were analyzed from the Barin locale. The muscovites were separated from the pegmatitic phase (Fig. 8). These SCTF ages of individual muscovites define a mean of 276.1 ± 3.1 Ma with a MSWD = 5.2 (Fig. 25). Potential for the accumulation of excess, non-atmospheric argon is indicated by a few crystals indicating older ages. Muscovite ages vary by ~ 30 Ma indicating possible recrystallization, excess argon, and crystals rich with defects. Ideally, closure temperature for muscovite is approximately 350 °C falling in between closure for hornblende and biotite. However, these ages produce a mean age that is approximately 8.7 m.y. younger than biotite ages. Based on an effective grain size of ~ 200 μm as determined by petrography and sieve analysis, and using the diffusion parameters of Hames and Bowring (1994) and the model of Dodson (1973), these crystals reached isotopic closure at 383 °C. Potential problems exist due the muscovite originating from a separate phase than the gneissic phase from which the hornblende and biotite were collected.

Muscovite was also analyzed from a sample of the Moffitt's Mill Schist. SCTF ages of ~ 10 crystals define a mean of 284.7 ± 2.6 Ma with an MSWD = 9.2 (Fig. 25 C). This age records the timing for retention of argon in muscovite at the Moffitt's Mill locality, congruent with regional cooling estimates and compatible with muscovite from Steltenpohl and Kunk (1993); it is not considered for modeling purposes, however, due to geographic distance from the Barin locale.

Muscovite from the Barin locale is anomalously younger than biotite. A possible explanation involves the nature of the pegmatite itself. Pegmatites are characterized and

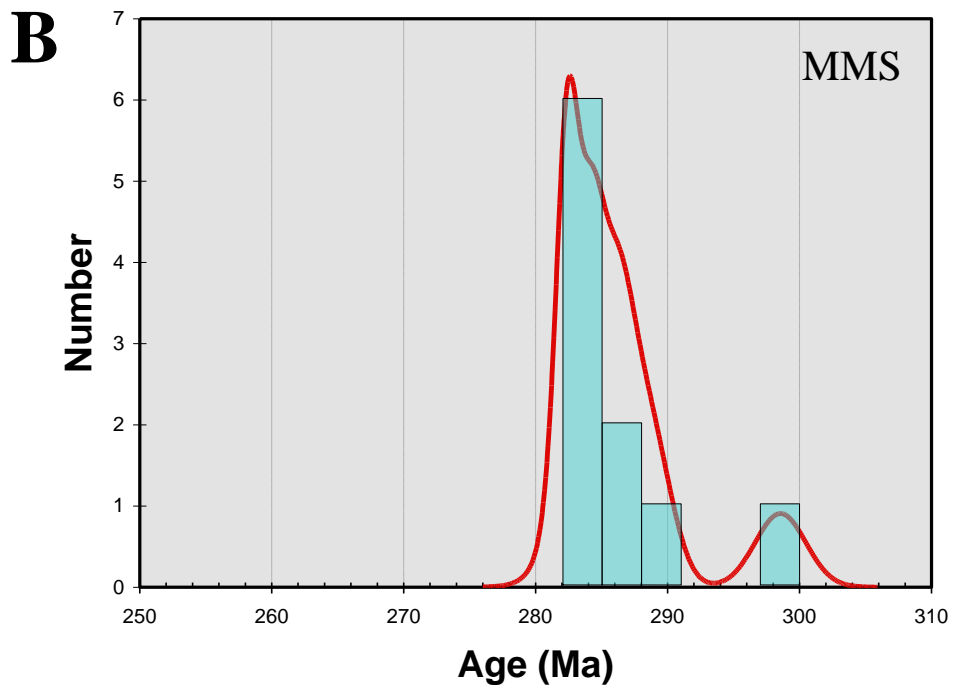
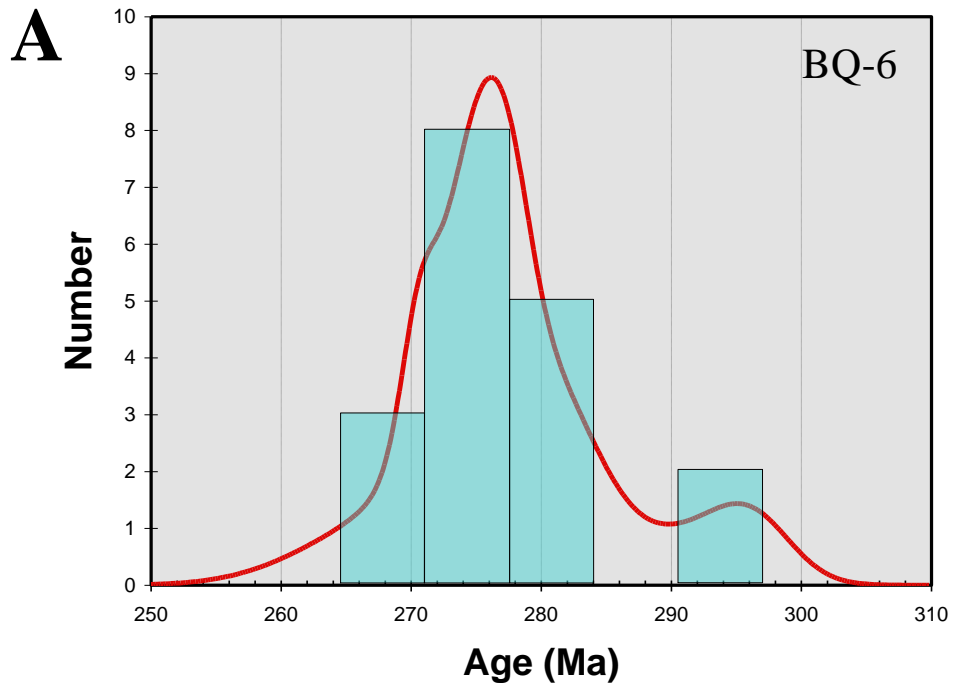


Figure 25. Muscovite single crystal total fusion $^{40}\text{Ar}/^{39}\text{Ar}$ analyses: A) Barin locale from pegmatite sample BQ-6 with mean age of 276.1 ± 3.1 Ma; B) Moffitt's Mill Schist with mean age of 284.7 ± 2.6 Ma.

identified on the basis of alkaline to peraluminous granitic composition and coarse grain size (typically > 1 cm) (Blatt et al., 2006). Pegmatite formation is typically attributed to a fluid-like, melt-induced remobilization of granitic components necessary to typically form abundant quartz and alkali-feldspar in a hydrous system. This granitic chemical mixture recrystallizes with a characteristically larger grain size. The remobilization and concentration of certain chemical constituents is evident in sample BQ-6 by the presence of muscovite which is not observed in the adjacent gneissic phase. This could be interpreted to indicate mobilization and subsequent concentration of sufficient potassium and, more importantly, aluminum in the pegmatoidal phase to enable muscovite growth. Pegmatites are characteristically late-stage features, but should demonstrate synchronous timing with regional post-metamorphic cooling. Pegmatite occurs as blebs within the host-rock and generally concentrated along migmatitic foliation and not as large cross-cutting features.

(U-Th)/He zircon analyses also yield anomalous ages between the pegmatite and host-rock gneiss. Zircons from the BQ-1 gneiss are 214.2 ± 17.1 Ma while zircons from the BQ-6 pegmatite phase are 162.7 ± 7.7 Ma, a roughly 51.5 m.y. discrepancy. It is likely that muscovite in the pegmatite phase crystallized after biotite or grew for a longer period of time in the pegmatite phase resulting in the younger age. Residual fluids of the pegmatite could enable muscovite crystallization after biotite. This is the preferred explanation for this discrepancy. It is also possible that biotite ages are incorrect and appear older, but this interpretation is unlikely due to the lack of excess argon from incremental heating analyses.

CHAPTER 9: DISCUSSION AND CONCLUSIONS

9.1 INTRODUCTION

This study constrains a relatively complete temperature-time evolution for Piedmont rocks of Alabama and Georgia with a combination of high temperature thermochronology ($^{40}\text{Ar}/^{39}\text{Ar}$ age of hornblende, muscovite, and biotite) and low-temperature thermochronometry (U-Th/He ages of apatite and zircon). The present study also provides peak P-T estimates for gneisses in the Uchee terrane through application of mineral thermobarometry. These data are combined and used as constraints for numerical modeling to derive a comprehensive model of pressure-temperature-time evolution for Alleghanian to Mesozoic events for the southernmost Appalachians. This analysis and model have implications for understanding the regional Alleghanian tectonic event and the evolution of the rifted margin of North America at the Coastal Plain unconformity.

9.2 GEOCHRONOLOGY AND PETROLOGY

The $^{40}\text{Ar}/^{39}\text{Ar}$ age of 292.2 ± 0.5 Ma for hornblende from the Barin locale in North Columbus, Georgia, is interpreted to record the timing of ^{40}Ar retention during cooling in that phase (Fig. 26). Closure is interpreted to have occurred at 527°C (on the basis of standard diffusion calculations with parameters discussed previously). The $^{40}\text{Ar}/^{39}\text{Ar}$ age of 284.8 ± 1.0 Ma for biotite from the Barin locale records the timing of ^{40}Ar retention, which is interpreted to have occurred at 312°C . $^{40}\text{Ar}/^{39}\text{Ar}$ analysis of pegmatitic muscovite of 276.1 ± 3.1 Ma is interpreted to record argon retention

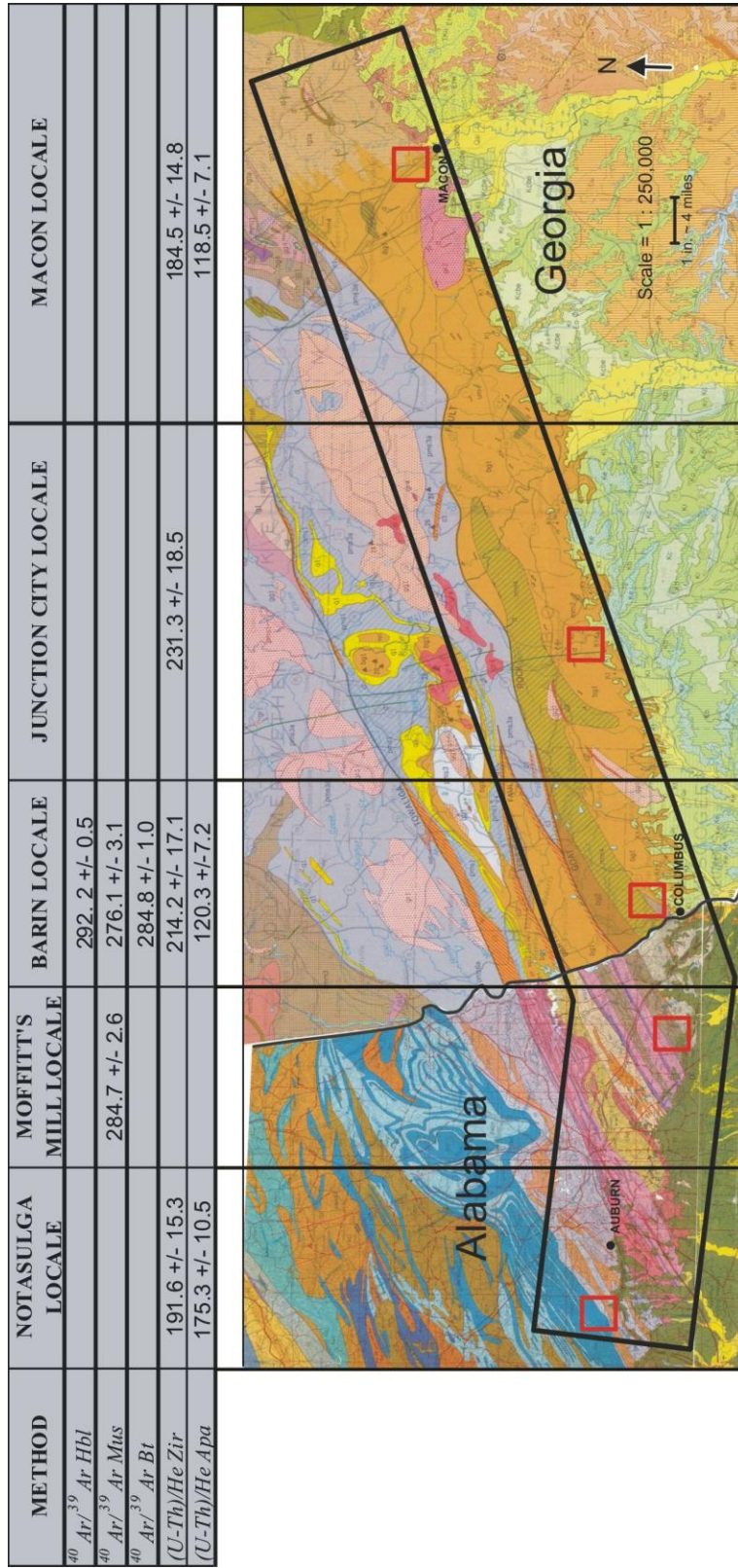


Figure 26. Map with sample localities (red boxes) and chart with ages of minerals dated from each locale. All ages are in Ma.

on the basis of closure at 383°C. However, this age is not included in later thermal modeling discussions (see discussion in section 8.2.3). These ages reflect cooling in response to unroofing of samples following Alleghanian crustal thickening. With the hornblende ages of ~292 Ma and biotite ages of ~284 Ma, a cooling rate from ~500 to 300 °C is calculated to be ~25 °C/m.y. However, initial cooling may be even more rapid for a short time from peak metamorphic conditions to ~500 °C as supported by U-Pb zircon ages of ~300 Ma recording Alleghanian overprint (Steltenpohl et al., 2008). The recorded age measurements are compatible with previous age assessments of hornblende and biotite in the South Carolina Piedmont (see discussion, section 9.2) and the Uchee terrane of Alabama.

The cooling rate between biotite closure and (U-Th)/He closure in zircon (~200 °C) is much slower at the Barin locale. The average biotite age of ~284 Ma and average (U-Th)/He zircon age of ~214 Ma can be used to calculate an average cooling rate of ~1.7 °C/m.y. The cooling rate between (U-Th)/He closure of zircon and apatite is even slower, constrained by the respective ages of ~214 Ma and ~120 Ma for apatite, to ~1.1 °C/m.y. for this late history. At the timing of closure of apatite rocks reached a temperature of ~70 °C at near-surface (<2 km) conditions.

(U-Th)/He thermochronometry of zircon and apatite from Notasula, Alabama, to Macon, Georgia, indicate regional uplift and cooling through the 200 – 180 °C isotherm from ~231 – 184 Ma corresponding to Early Jurassic to Late Triassic. Apatite closure temperature ages indicate continuing uplift and cooling through ~70°C from 120.3 – 118.5 Ma in Georgia and 175.3 Ma in Alabama corresponding to Early Cretaceous to Middle Jurassic. Barin locale average ages of zircon and apatite are 214.2 and 120.3 Ma,

respectively, while Macon locale ages for zircon and apatite are 184.5 and 118.5 Ma, respectively. Junction City locale zircon ages are the oldest of the present study at 231.3 Ma. Zircon and apatite ages for the Notasulga locale are 191.6 and 175.3 Ma, respectively, yielding a 16.3 m.y. difference indicating a cooling rate of ~ 7 °C/m.y. The Notasulga locale possesses the oldest apatite age in the present study along with the shortest time interval between zircon and apatite closure. This is interpreted as corresponding to notably faster Jurassic uplift rate than central Georgia. Inferred Mesozoic cooling rates for the Barin and Macon locales are ~ 1.1 °C/m.y. and ~ 1.6 °C/m.y., respectively.

(U-Th)/He ages from the central Appalachian Piedmont of North Carolina and south-central Virginia tend to be younger than determined in the present study. Spotila et al. (2004) determined (U-Th)/He ages relevant to the origin of the Blue Ridge escarpment and used the analyses to understand near-surface erosional behavior related to escarpment migration. Spotila et al. (2004) determined apatite ages within the Blue Ridge and Inner Piedmont to fall within a range from 204 – 122, and 106 – 68 Ma, respectively. Apatite helium ages as determined in this study are more compatible with Blue Ridge ages for locales near the Blue Ridge/Piedmont boundary in the central Appalachians. Spotila et al. (2004) observed an eastward younging trend among apatite fission track ages which they attributed to the westward migration of the Blue Ridge escarpment.

In the present study, apatite ages tend to young to the east, in comparison with central Appalachian apatite ages (see Spotila et al., 2004). However, the eastward progression of younger apatite ages in the present study is attributed to approaching a rifted margin rather than escarpment migration. Evidence is not observed for major

escarpment migration in the southernmost Appalachians comparable to the drastic escarpment of North Carolina and Virginia, but a southeast to northwest directed Piedmont to Blue Ridge transect perpendicular to strike would perhaps provide more of a definitive answer. Central Appalachian Piedmont apatite fission track ages are as young as Late Cretaceous (68 Ma), while southern Appalachian ages from the present study are Early Cretaceous at the youngest. Younger, Late Cretaceous ages in apatite are perhaps buried beneath the Coastal Plain of Georgia. Pangea breakup occurred ca. 200 Ma along the eastern margin of Laurentia which is indicated by ~200 Ma dikes of the central Atlantic magmatic province in central Georgia. The transect of the present study from Notasulga (westernmost locale) to Macon (easternmost locale) accounts for approximately 190 km. The eastward younging trend of apatite ages in the present study are attributed to elevated geotherms (providing for younger closure) due to increased heat flow related to the rifted margin of Pangea.

9.3 THERMAL MODELING

Computer modeling was conducted to depict potential pressure-temperature-time (P-T-t) paths for the Barin locale to develop an increased understanding of the post-Alleghanian exhumational paths that current surface exposures experienced. The modeling program 1DT by Haugerud (1986) was used for modeling purposes. The 1DT program allows for user-defined parameters to generate geothermal gradients and graphical P-T-t paths according to user-specified conditions.

A model was constructed for the time period from 330 – 110 Ma to incorporate the maximum thickening attributed to Alleghanian thrusting as well as incorporating results from the previously discussed experimentally determined geochronometers.

Calculated closure temperatures for hornblende, muscovite, and biotite for this study correspond to 527, 383, and 312 °C, respectively. Slight variations in closure temperature of 10 – 30 °C will not have an appreciable effect on calculations, and the broadly accepted closure temperatures of 500, 350, and 300 °C are used for modeling purposes. Muscovite results of the Barin locale are not included in the model. However, the timing predicted by the model derived for the Barin locale passes through 350°C conditions consistent with Moffitt's Mill Schist muscovite ages of ca. 285 Ma as reported by Steltenpohl and Kunk (1993) and 284.7 Ma as determined in the present study. Temperature versus time, depth (pressure) versus temperature, and depth versus time were derived through the modeling (Figs. 27, 28, 29). The model assumes the onset of a geologically instantaneous ($t \sim 100,000$ years) Alleghanian thrust event beginning at approximately 330 Ma and incorporates a seven-stage history including the tectonic loading thrust event, regional continental heating, attainment of peak metamorphic conditions, and post-peak metamorphic cooling and erosional uplift. Modeled thrust sheet thickness is 20 km.

The model results (Fig. 27, 28, 29) agree with the previously determined parameters establishing amphibolite-facies of ~ 686 °C and ~ 5.4 kb and are interpreted to represent the peak metamorphic conditions in the model path. The model provides for approximately 9 m.y. of post-thrusting regional heating to attain peak metamorphic temperatures. The model also correlates well to the aluminum-in-hornblende estimate for maximum pressure. Pressure estimates from this geobarometer yield 5.4 kb corresponding to roughly 19 km as a minimum depth of peak conditions (assuming 3.5 km/kb). This model implies original depth of samples in the footwall block of ~ 9.5 km,

THERMAL MODEL SETUP			
STAGE	TIME	VELOCITY	THRUST
1	$1.00 \cdot 10^6$	0.00	Yes
2	$1.00 \cdot 10^7$	0.00	No
3	$3.00 \cdot 10^7$	-0.85	No
4	$4.50 \cdot 10^7$	-0.40	No
5	$6.00 \cdot 10^7$	-0.05	No
6	$1.30 \cdot 10^8$	-0.02	No
7	$2.20 \cdot 10^8$	-0.03	No
MODEL PARAMETERS			
Thermal Conductivity: 2.00 W/mK			
Density: $2.78 \cdot 10^3$ kg/m ³			
Heat Capacity: $1.00 \cdot 10^3$			
Heat Generation:			
	Top: $2.00 \cdot 10^{-6}$ W/m ³		
	Bottom: $2.00 \cdot 10^{-6}$ W/m ³		
	Z: 25 km		
Surface Temperature: 0.0 °C			
Initial Basal Flux: $3.00 \cdot 10^{-2}$ W/m ²			
	Constant: yes		
Thrust Sheet Thickness: 20 km			
Total Model Time: $2.2 \cdot 10^8$ years			
Number of Layers: 1			
Number of Stages in Uplift History: 7			
Time-Step: $4.0 \cdot 10^5$ years			
Maximum Depth: 50 km			
Maximum Temperature: 750°C			

Table 2. Modeling parameters, including time and uplift velocity utilized; negative value for velocity indicates velocity toward surface.

BARIN LOCALE TIME - TEMPERATURE HISTORY

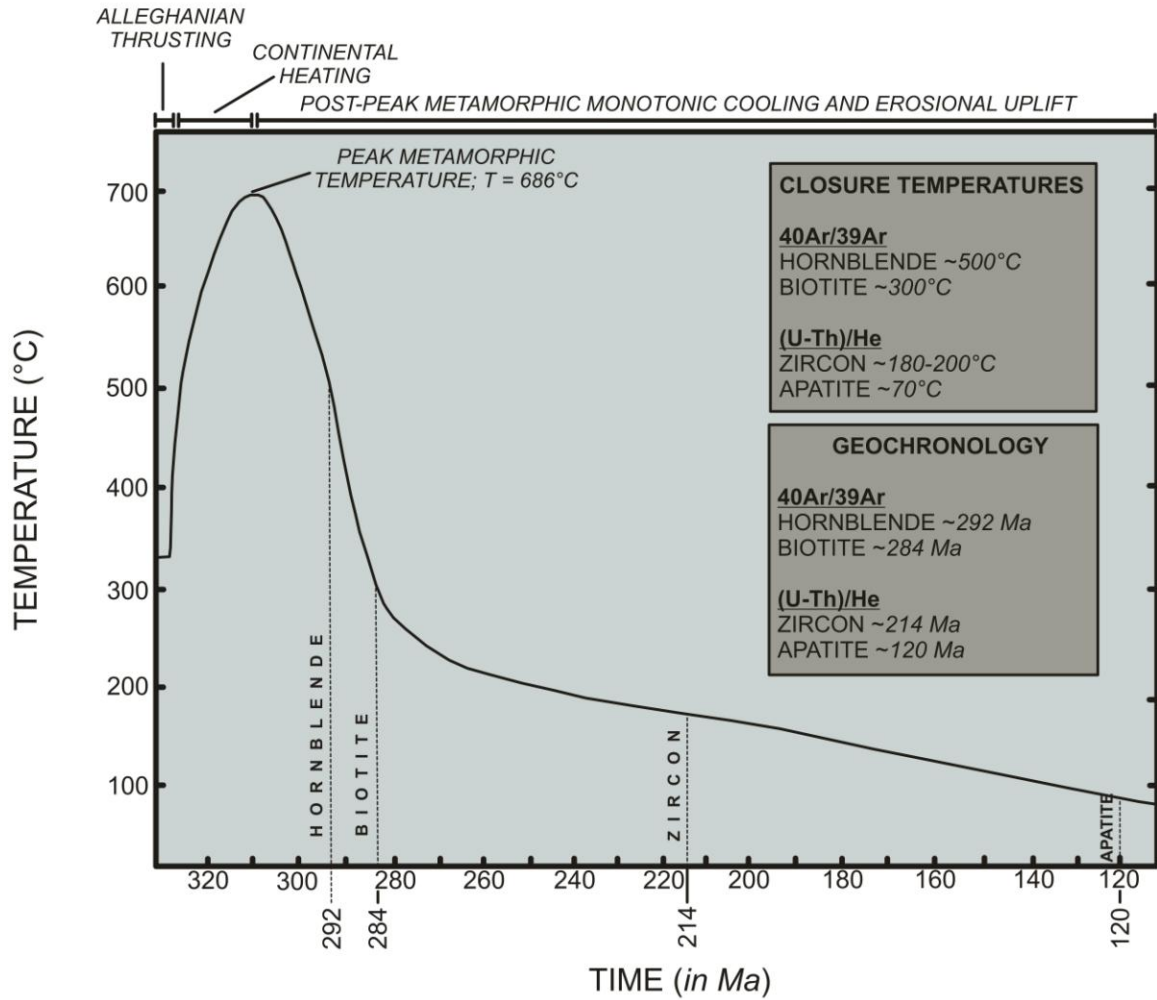


Figure 27. Time-temperature thermal history of the Barin locale. Age constraints are provided by ⁴⁰Ar/³⁹Ar and (U-Th)/He geochronometers. See text and table 2 for model setup and parameters.

BARIN LOCALE DEPTH (PRESSURE) - TEMPERATURE HISTORY

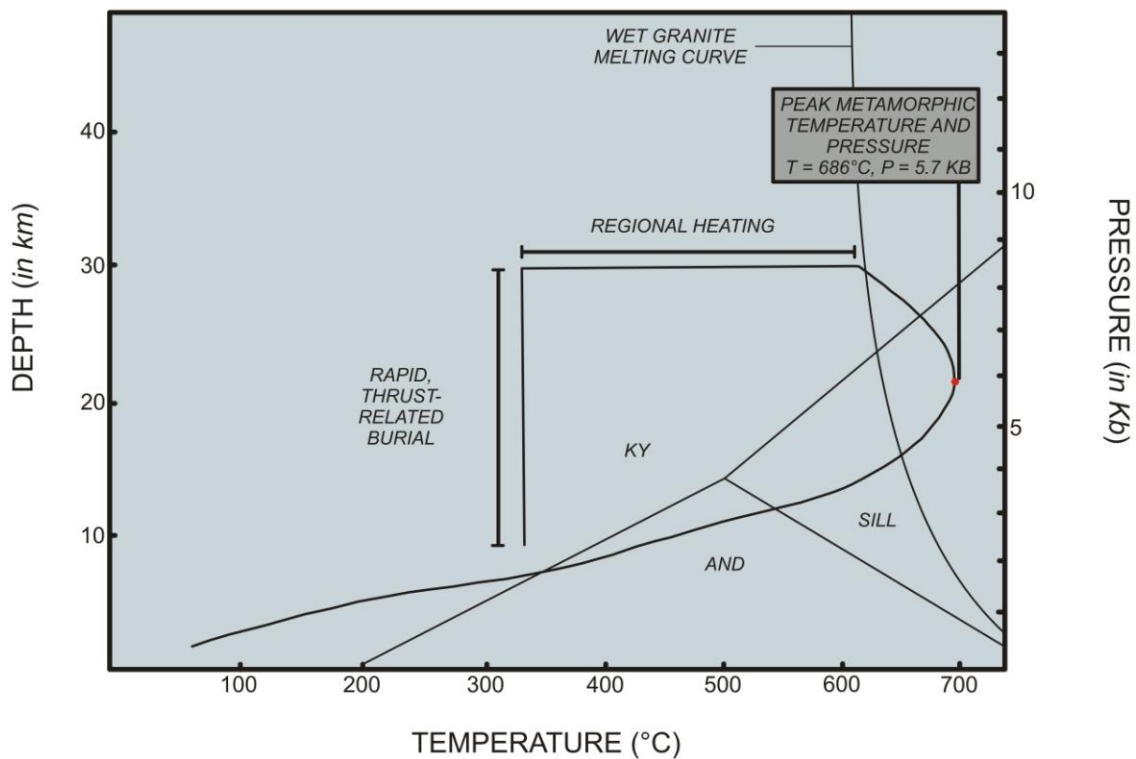


Figure 28. Depth (pressure) – temperature history of the Barin locale. Maximum depth achieved attributed to thrust sheet burial is approximately 29.5 km and peak metamorphic conditions achieved are approximately 686 °C and 5.7 Kb (indicated by red dot). Assumed depth pressure relationship is 3.5 km/Kb. Aluminum silicate triple point indicated at 4 Kb and 500 °C and wet-granite melting curve (Blatt et al., 2006).

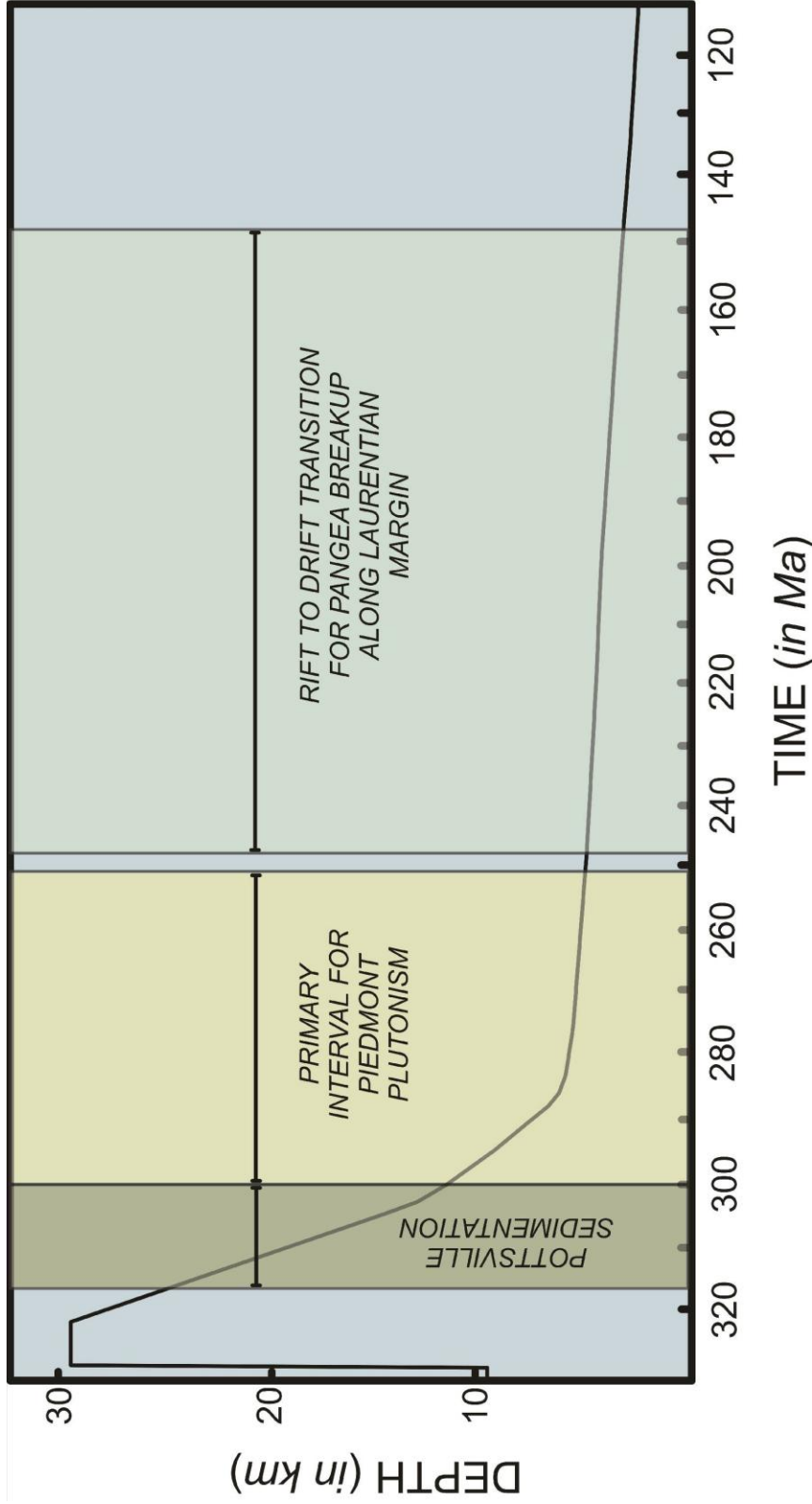


Figure 29. Depth – time history as for the Alleghanian orogeny as demonstrated in the model developed for the Barin locale (see discussion in section 9.2). Major post-Alleghanian events depicted include Pennsylvanian Pottsville Formation sediment accumulation (~315 – 300 Ma), Piedmont plutonism (~300 – 250 Ma), and the rift-to-drift transition due to development of a passive margin along the eastern Laurentian margin (~200 Ma for rifting).

which experienced a post-thrusting maximum depth up to 29.5 km (Fig. 29) corresponding to approximately 8.4 kb. However, maximum temperature, and thus corresponding peak metamorphic pressures were achieved at approximately 20 km (~5.7 kb) according to the model, in relative agreement to that determined by the aluminum-in-hornblende geobarometer (~5.4 kb). After peak metamorphism, cooling and erosional uplift govern the model. Hornblende closure on the cooling path occurs at 292 Ma and biotite closure at 284 Ma, followed by zircon closure at 214 Ma and apatite at 120 Ma. To achieve a path corresponding to the previous geochronometers initial erosion is set to 0.85mm/yr, which corresponds to approximately 850 m of material removal per million years. This erosional rate gradually decreases over the seven steps to a minimum of 0.02 mm/yr (Table 2).

The results of the model for the present study can also be compared to other thermochronology studies across the Piedmont of Alabama, Georgia, and South Carolina. Dallmeyer et al. (1986) report a cooling estimate from ~500 – 300 °C for the eastern South Carolina Piedmont from 295 – 285 Ma in relative agreement with the present study of cooling for the same temperature interval from 292 – 284 Ma. The model of the present study is also in agreement with Dallmeyer et al. (1986) estimates for peak metamorphic conditions at approximately 310 Ma (Fig. 29) and Secor et al. (1986), which provides a window from 315 – 295 for peak metamorphism. During the 500 – 300 °C temperature interval, the model of the present study predicts a rapid cooling rate of 25 °C/m.y. corresponding to rapid uplift of 0.85 mm/yr, comparable with an estimated value of 20 °C/m.y. reported for the South Carolina Piedmont (uplift of 0.6 mm/yr: Dallmeyer et al., 1986). The present study is also in agreement with previous Alabama-Georgia

geochronologic studies. Steltenpohl and Kunk (1993) point to a clustering of hornblende ages ca. 292 Ma over the southern Piedmont of Alabama and Georgia and estimate peak amphibolite-facies conditions for the Uchee terrane from 320- 292 Ma in agreement with the model presented in this study of peak conditions at 310 Ma. In view of the similar thermal histories determined in the present study and also in Dallmeyer (1978), Dallmeyer et al. (1986), Secor et al. (1986), Steltenpohl and Kunk (1993), and Steltenpohl et al. (2008), the Carboniferous to Permian P-T-t pathway determined for the Barin locale is likely representative of the entire southern Piedmont.

This study provides valuable information on several key questions regarding the Alleghanian orogeny and post-Alleghanian tectonic evolution. Questions that could be posed include the following. What was the sedimentation response to orogenic unroofing? What was the influence and timing of the Alleghanian orogeny on post-Alleghanian plutonism? What relationships are observed between the study area and development of the passive margin along the Laurentian margin? Does evidence exist for passage of the Bermuda hotspot?

Following peak metamorphism at ca. 310 Ma, a ~15 m.y. period of orogenic unroofing at a modeled rate of 0.85 mm/yr governed the southern Piedmont. This period of maximum post-Alleghanian erosion led to removal of >15 km of material. Appalachian depositional basins, such as the Black Warrior and Cahaba basins, are a likely destination for post-Alleghanian erosional sediments. Rapid orogenic sedimentation is one consequence to be expected from this removal of material. The Pennsylvanian Pottsville Formation is a 3,000 m+ thick sedimentary unit within the foreland basin of central Alabama (Hewitt, 1984, Peavy, 2008). The age for the Pottsville

Formation is Pennsylvanian. Timing for rapid sedimentation of the Pottsville corresponds to the most rapid period of erosional exhumation of the southern Appalachians (Fig. 28). Erosional unroofing of the southern Piedmont is potentially a source for Pottsville sedimentation.

A second consequence of rapid decompression of high-grade rocks of roughly granitic composition involves the generation of melts. Carboniferous plutons are very common across the Piedmont of central Georgia (e.g., Stone Mountain granite, Danburg granite, and Siloam granite) with granite reaching Elberton batholithic proportions. The primary interval for Alleghanian plutonism is constrained from ~320 to 250 Ma (Speer et al., 1994). According to the model developed for this study, this interval overlaps the period following rapid orogenic unroofing. This depressurization is likely a source of generation of the melts at depth (see discussion in Speer et al., 1994) (Fig. 28).

The supercontinent Pangea formed due to the convergence of Laurentia and Gondwana. Pangea rifting occurred ~200 Ma with evidence from the central Atlantic magmatic province (CAMP) (Hames et al., 2000; Morris et al., 2006). Dikes associated with CAMP occur in central Georgia in the Piedmont. Triassic to Jurassic rift basins are also known beneath the Coastal Plain of southeast Georgia (known as the south Georgia rift) as shown by seismic reflection data (McBride, 1990). These factors provide evidence for the rifting of Pangea and formation of a passive margin along Eastern North American. The low-temperature apatite ages (as young as Late Cretaceous) exhibit a younging trend from west to east across the study area, and indicate substantiated heat flow in the eastern Piedmont due to crustal thinning.

Previous studies estimate passage of the Bermuda hotspot beneath the southern Appalachians between 100 – 50 Ma (Baksi, 1997; Cox and Van Arsdale, 2002). Magmatic evidence of hotspot migration is not observed in the southern Appalachians due to intense crustal thickening attributed to thrust sheet emplacement of three Appalachian orogenies. The lowest-temperature geochronometer in this study is apatite and it yields the youngest age of the entire study (Macon locale, 118.5 Ma). If hotspot migration had a significant influence on the southern Appalachians within the area of the present study, then low-temperature, and thermally more sensitive, geochronometers such as (U-Th)/He apatite would be reset to likely reflect Late Cretaceous to early Paleogene elevated heat flow. Thus, no evidence was observed within the present study for Bermuda hotspot passage as rocks were already exhumed to the near-surface when the hotspot passed beneath the area.

9.4 CONCLUSIONS

The following conclusions are reached from this study.

1. Localized cooling from 500 – 300 °C of the Barin locale occurred relatively quickly from approximately 292 – 284 Ma with an inferred cooling rate of 25 °C/m.y.
2. The model developed for this study correlates very well to previous reports for the Piedmont of South Carolina, Georgia, and Alabama and likely represents generalized conditions and exhumation history for the southern Piedmont of east-central Alabama and west-central Georgia.
3. A (U-Th)/He database has been expanded within the southern Appalachians which regionally indicate zircon ($T_c \sim 180 - 200$ °C) and apatite ($T_c \sim 70$ °C) closure

across the southernmost Piedmont of Alabama at Georgia at 231.3 – 184.5 Ma and 175.3 – 118.5, respectively.

4. Peak metamorphic temperature and pressure at the Barin locale reached amphibolite-facies conditions estimated at 686 °C and 5.4 kb, respectively.
5. Thermal modeling of the Barin locale reveals post-Alleghanian thrust history and erosionally governed cooling with induced rates of uplift ranging from 0.85mm/yr to 0.02 mm/yr to accommodate experimentally determined geochronometers.
6. Post-Alleghanian Piedmont plutonism is likely attributed to rapid decompression of the southern Piedmont with removal of 15+ km of material over <20 m.y.
7. The sedimentological response of rapid unroofing (up to 0.85 mm/yr) is likely manifest in formations such as the Pennsylvanian Pottsville Formation whose deposition correlates to timing of rapid, post-Alleghanian exhumation.
8. Mesozoic rifting through passive margin development appears to be recorded by an eastward-younging trend indicated by (U-Th)/He apatite ages.
9. No evidence of passage of the Bermuda hotspot is observed within the data derived from this study area.

REFERENCES

- Adams, M.G., Stewart, K.G., Trupe, C.H., and Willard, R.A., 1995, Tectonic significance of high-pressure metamorphic rocks and dextral strike-slip faulting along the Taconic suture, *in* Hibbard, J.P., van Staal, C.R., and Cawood, P.A., eds., *Current Perspectives in the Appalachian-Caledonian Orogen*: Geological Association of Canada, Special Paper 41, p. 21-42.
- Anderson, T.M., 1981, Application of fission track studies to the dynamo-thermal history of a metamorphic terrane, South Georgia Piedmont: M.S. thesis, Tallahassee, Florida, Florida State University, 102 p.
- Baksi, A.K., 1997, The timing of Late Cretaceous Alkalic Igneous Activity in the Northern Gulf of Mexico Basin, Southeastern USA: *Journal of Geology*, v. 105, p. 629 – 643.
- Bentley, R.D., and Neathery, T.L., 1970, Geology of the Brevard fault zone and related rocks of the Inner Piedmont of Alabama: Alabama Geological Society, 8th Annual Field Trip Guidebook, p. 1-79.
- Bentley, R.D., Neathery, T.L., and Scott, J.C., 1985, Geology and mineral resources of Lee County, Alabama: Geological Survey of Alabama Bulletin 107, 110 p.
- Blatt, H., Tracy, R.J., and Owens, B.E., 2006, *Petrology Igneous, Sedimentary, and Metamorphic*: New York, W.H. Freeman and Company, 530 p.
- Blundy, J.D., Holland, T.J., 1990, Calcic amphibole equilibria and a new amphibole-plagioclase thermometer: *Contributions to Mineralogy and Petrology*, v. 104, p. 208-224.
- Butler, 1972, Age of Paleozoic regional metamorphism in the Carolinas, Georgia, and Tennessee southern Appalachians: *American Journal of Science*, v. 272, p. 319-333.
- Chalokwu, C.I., 1989, Epidote-amphibolite to amphibolite facies transition in the southern Appalachian Piedmont: P-T conditions across the garnet and calc-silicate isograds: *Geology*, v. 17, p. 491-494.
- Chalokwu, C.I., and Kuehner, S.M., 1992, Quantitative evaluation of the role of fluids in the formation of symplectic amphibolites from the Southern Appalachian

Piedmont; implications for the retrograde P-T path: Geological Society of America Abstracts with Programs, v. 24, no. 2, p. 7.

- Chowns, T.M., and Williams, C.T., 1983, Pre-Cretaceous rocks beneath the Georgia Coastal Plain-regional implications, *in* Gohn, G.S., ed., Studies related to the Charleston, South Carolina, Earthquake of 1886 – tectonics and seismicity: U.S. Geological Survey Professional Paper 1313-L, 42 p.
- Cook, F., Albaugh, D., Brown, L., Kaufman, S., Oliver, J., and Hatcher, R., 1979, Thin skinned tectonics in the crystalline southern Appalachians – COCORP Seismic-reflection profiling of the Blue Ridge and Piedmont: *Geology*, v. 7, p. 563-567.
- Corrie, S.L., and Kohn, M.J., 2007, Resolving the timing of orogenesis in the Western Blue Ridge, southern Appalachians, via in situ ID-TIMS monazite geochronology: *Geology*, v. 35, no. 7, p. 627-630.
- Cox, R.T., and Van Arsdale, R.B., 2002, The Mississippian Embayment, North America: a first order continental structure generated by the Cretaceous superplume mantle event: *Journal of Geodynamics*, v. 34, p. 163-176.
- Dallmeyer, R. D., 1978, $^{40}\text{Ar}/^{39}\text{Ar}$ Incremental-release ages of hornblende and biotite across the Georgia Inner Piedmont: Their bearing on Late Paleozoic-Early Mesozoic tectonothermal history: *American Journal of Science*, v. 278, p. 124-149.
- Dallmeyer, R.D., and Van Breeman, O., 1981, Rb-Sr whole-rock and $^{40}\text{Ar}/^{39}\text{Ar}$ mineral ages of the Togus and Hallowell quartz monzonite and Three Miles Pond granodiorite plutons, south-central Maine; Their bearing on post-Acadian cooling history: *Contributions to Mineralogy and Petrology*, v. 78, p. 61-73.
- Dallmeyer, R.D., Wright, J.E., Secor, D.T., and Snoke, A.W., 1986, Character of the Alleghanian orogeny in the southern Appalachians: Part II. Geochronological constraints on the tectonothermal evolution of the eastern Piedmont in South Carolina: *Geological Society of America Bulletin*, v. 97, p. 1329-1344.
- Dallmeyer, R.D., 1989, Contrasting Accreted Terranes in the Southern Appalachian Orogen, Basement Beneath the Atlantic and Gulf Coastal Plains, and West African Orogens: *Precambrian Research*, v. 42, p. 387-409.
- Dallmeyer, R.D., Roden, M.F., and Swansom, S.E., 2005, Geologic Overview of the Elberton, GA Area *in* Roden, M.F., Schroeder, P.A., and Swanson, S.E., eds., *Geologic Investigations of Elberton Granite and Surrounding Rocks: Georgia Geological Society Guidebooks*, v. 25, no. 1, p. 1-16.

- Deer, W.A., Howie, R.A., and Zussman, J., 1992, *An Introduction to the Rock-Forming Minerals*: New York, Longman Scientific & Technical, 696 p.
- Dodson, M., 1973, Closure temperature in cooling geochronological and petrological system: *Contributions to Mineralogy and Petrology*, v. 40, no. 3, p. 259-274.
- Drake, A., Sinha, A., Laird, J., and Guy, R., 1989, The Taconic orogen, *in* Hatcher, R., Thomas, W., and Viele, G., eds., *The Appalachian-Ouachita Orogen in the United States*: Boulder, Colorado, Geological Society of America, *The Geology of North America*, v. F-2, p. 101-177.
- Dunkl, I., Danisik, M., Picotti, V., and Frisch, W., von Eynatten, H., and Castellarin, A., 2006, (U-Th)/He thermochronology – methodology and a case study: dating of faulting in the Southern Alps: *Tektonik, struktur- und Kristallingeologie*, v. 11, p. 45-47.
- Ehlers, T., and Farley, K., 2003, Apatite (U-Th)/He thermochronometry: methods and applications to problems in tectonic and surface processes: *Earth and Planetary Science Letters*, no. 206, p. 1-14.
- England, P.C., and Thompson, A.B., 1984, Pressure-temperature-time paths of regional metamorphism, Part I: Heat transfer during the evolution of regions of thickened continental crust: *Journal of Petrology*, v. 25, p. 894-928.
- Farley, K., 2000, Helium diffusion from apatite: General behavior as illustrated by Durango fluorapatite: *Journal of Geophysical Research*, v. 105, no. B2, p. 2903-2914.
- Farley, K.A., Wolf, R., and Silver, L., 1996, The effects of long alpha-stopping distances on (U-Th)/He ages: *Geochimica et Cosmochimica Acta*, v. 60, no. 21, p. 4223-4229.
- Fuhrman, M.L., and Lindsley, D.H., 1988, Ternary-feldspar modeling and thermometry: *American Mineralogist*, v. 73, p. 201-215.
- Glover, L., Speer, J., Russell, G., Farrar, S., 1983 Ages of regional metamorphism and ductile deformation in the central and southern Appalachians: *Lithos*, v. 16, p. 223-245.
- Goldberg, S.A., and Burnell, J.R., 1987, Rubidium-strontium geochronology of the Farmville granite, Alabama Inner Piedmont, *in* Drummond, M.S., and Green, N.L., eds., *Granites of Alabama*: Tuscaloosa, Alabama, Alabama Geological Survey, p. 251-257.

- Gradstein, F.M., Ogg, J.G., Smith, A.G., Bleeker, W., and Lourens, L.J., 2004, A new Geologic Time Scale, with special reference to Precambrian and Neogene: *Episodes*, v. 27, no. 2, p. 83-100.
- Hames, W.E., Renne, P.R., and Ruppel, C., 2000, New evidence for geologically instantaneous emplacement of earliest Jurassic Central Atlantic magmatic province basalts on the North American margin: *Geology*, v. 28, no. 9, p. 859-862.
- Hamilton, E.I., 1965, *Applied Geochronology*, London, Academic Press Inc. 267 p.
- Hammarstrom, J.M., and Zen, E., 1986, Aluminum in hornblende: An empirical igneous geobarometer: *American Mineralogist*, v. 71, p. 1297-1313.
- Hanley, T. B., Chalokwu, C. I., and Steltenpohl, M. G., 1997, Constraints on the location of the Carolina/Avalon terrane boundary in the southernmost exposed Appalachians, western Georgia and eastern Alabama *in* Glover, L., and Gates, A. E., eds., *Central and Southern Appalachian Sutures: results of the EDGE Project and Related Studies: Boulder, Colorado, Geological Society of America Special Paper 314*, p. 15-24.
- Hanley, T.B., 1986, Petrography and structural geology of Uchee Belt Rocks in Columbus Georgia, and Phenix City, Alabama: *Geological Society of America Centennial Field Guide-Southeastern Section*, p. 297-300.
- Hanley, T.B., Kar, A., Burnley, P.C., Scanlan, M., Wilson, C., Bratton, G., James, R., 2005, Phenix City Gneiss amphibolite and associated rocks of the Uchee belt, western Georgia and eastern Alabama *in* Steltenpohl, M., ed., *New Perspectives on Southernmost Appalachian Terranes, Alabama and Georgia: Alabama Geological Society, 42nd Annual Field Trip Guidebook*, p. 1-18.
- Harris, L., and Bayer, K., 1979, Sequential development of the Appalachian orogen above a master decollement – a hypothesis: *Geology*, v. 7, p. 568-572.
- Harrison, T.M., Celerier, J., Aikman, A.B., Hermann, J., and Heizler, M.T., 2009, Diffusion of ⁴⁰Ar in muscovite: *Geochimica et Cosmochimica Acta*, v. 73, p. 1039-1051.
- Harrison, T.M., Duncan, I., and McDougall, I., 1985, Diffusion of ⁴⁰Ar in biotite: Temperature, pressure and compositional effects: *Geochimica et Cosmochimica Acta*, v. 49, p. 2461-2468.
- Hatcher, R., 1978, Tectonics of the western Piedmont and Blue Ridge, Southern Appalachians; review and speculation: *American Journal of Science*, v. 278, no. 3, p. 276-304.

- Hatcher, R., 1987, Tectonics of the Southern and Central Appalachian Internides: Annual Reviews Earth and Planetary Science, v. 15, p. 337-362.
- Hatcher, R., 1989, Appalachians introduction, *in* Hatcher, R., Thomas, W., and Viele, G., eds., The Appalachian-Ouachita Orogen in the United States: Boulder, Colorado, Geological Society of America, The Geology of North America, v. F-2, p. 1-5.
- Hatcher, R., Thomas, W., Geiser, P., Snoke, A., Mosher, S., and Wiltschko, D., 1989, Alleghanian orogen *in* Hatcher, R., Thomas, W., and Viele, G., eds., The Appalachian-Ouachita Orogen in the United States: Boulder, Colorado, Geological Society of America, The Geology of North America, v. F-2, p. 233-318.
- Hatcher, R.D., 1989, Tectonic synthesis of the U.S. Appalachians, *in* Hatcher, R.D., Thomas, W.A., and Viele, G.W., eds., The Appalachian-Ouachita Orogen in the United States: Boulder, Colorado, Geological Society of America, The Geology of North America, v. F-2, p. 511-535.
- Hatcher, R., 2005, North America: Southern and Central Appalachians *in* Selley, R.C., Cocks, L.R., and Plimer, I.R., eds., Encyclopedia of Geology volume 4: Oxford, Elsevier, p. 72-81.
- Hatcher, R., 2007, The Appalachians; an accretionary and collisional orogen: Geological Society of America Abstracts with Programs, v. 39, no. 1, p. 36.
- Haugerud, R.A., 1986, 1DT; an interactive, screen-oriented microcomputer program for simulation of 1-dimensional geothermal histories: U.S. Geological Survey Open-File Report OF 86-0511, 19 p.
- Hewitt, J.L., 1984, Geologic overview, coal, and coalbed methane resources of the Warrior Basin-Alabama and Mississippi, *in* Rightmire, C.T., Eddy, G.E., and Kirr, J.N., eds., Coalbed methane resources of the United States: American Association of Petroleum Geologists Studies in Geology Series, no. 17, p. 73-104.
- Hibbard, J.P., Stoddard, E.F., Secor, D.T., Dennis, A.J., 2002, The Carolina Zone: overview of Neoproterozoic to Early Paleozoic peri-Gondwanan terranes along the eastern flank of the southern Appalachians: Earth-Science Reviews, v. 57, p. 299-339.
- Hibbard, J.P., van Staal, C.R., and Miller, B.V., 2007, Links among Carolina, Avalonia, and Ganderia in the Appalachian peri-Gondwanan realm: Geological Society of America Special Paper, v. 433, p. 291-311.

- Hobbs, B., Cabiles, L., Beville, S., Kar, A., Burnley, P., and Hanley, T.B., 2004, Constraints on the P-T path for uplift of the Uchee Belt based on microthermometry of fluid inclusions in metamorphic rock: Geological Society of America Abstracts with Programs, v. 36, no. 5, p 79.
- Hodges, K.V., 1991, Pressure-temperature-time paths: Annual Reviews in Earth and Planetary Science, v. 19, p. 207-236.
- Holland, T.J., and Blundy, J.D., 1994, Non-ideal interactions in calcic amphiboles and their bearing on amphibole-plagioclase thermometry: Contributions to Mineralogy and Petrology, v. 116, p. 433-447.
- Hollister, L.S., Grissom, G.C., Peters, E.K., Stowell, H.H., and Sisson, V.B., 1987, Confirmation of the empirical correlation of Al in hornblende with pressure of solidification of calc-alkaline plutons: American Mineralogist, v. 72, 231-239.
- Johnson, M.C., and Rutherford, M.J., 1989, Experimental calibration of the aluminum-in-hornblende geobarometer with application to Long Valley caldera (California) volcanic rocks: Geology, v. 17, 837-841.
- King, D.T., and Skotnicki, M.C., 1992, Upper Cretaceous Stratigraphy and relative sea-level changes, Gulf Coastal Plain of eastern and central Alabama: AAPG Memoir, v. 53, p. 317-331.
- Lavallee, S., 2003, Timing of the accretion of the Carolina Zone to Laurentia: Petrologic and Geochronologic analysis: M.S. thesis, Auburn, Alabama, Auburn University, 90 p.
- Lippolt, H., Leitz, M., Wernicke, R., and Hagedorn, B., 1994, (Uranium + thorium)/helium dating of apatite: experience with samples from different geochemical environments: Chemical Geology (Isotope Geoscience Section), no. 112, p. 179-191.
- London, D., 1992, The Application of Experimental Petrology to the Genesis and Crystallization of Granitic Pegmatites: The Canadian Mineralogist, v. 30, p. 499-540.
- McBride, J.H., 1990, Constraints on the structure and tectonic development of the early Mesozoic South Georgia Rift, Southeastern United States; seismic reflection data processing and interpretation: Tectonics, v. 10, no. 5, p. 1065-1083.
- McDougall, I., and Harrison, M.T., 1999, Geochronology and Thermochronology by the $^{40}\text{Ar}/^{39}\text{Ar}$ Method, Second Edition, New York, Oxford University Press. 269 p.

- Merrihue, C., and Turner, G., 1966, Potassium-Argon Dating by Activation with Fast Neutrons: *Journal of Geophysical Research*, v. 71, no. 11, p. 2852-2857.
- Milla, K.A., and Ragland, P.C., 1992, Early Mesozoic Talbotton diabase dikes in west-central Georgia; compositionally homogeneous high-Fe quartz tholeiites: *Geological Society of America Special Paper*, v. 268, p. 347-359.
- Morris, D.P., Hames, W.E., and Salters, V., 2006, The Clubhouse Crossroads flood basalts in the context of the CAMP and SDRS: *Geological Society of America Abstracts with Programs*, v. 38, no. 3, p. 8.
- Neese, W.D., 2000, *Introduction to Mineralogy*: New York, Oxford University Press, 442 p.
- Nier, A.O., 1950, A redetermination of the relative abundances of the isotopes of carbon, nitrogen, oxygen, argon, and potassium: *Physical Review*, v. 77, p. 789-793.
- Osberg, P., Tull, J., Robinson, P., Hon, R., and Butler, J., 1989, The Acadian orogen, *in* Hatcher, R., Thomas, W., and Viele, G., eds., *The Appalachian-Ouachita Orogen in the United States*: Boulder, Colorado, Geological Society of America, *The Geology of North America*, v. F-2, p. 179-232.
- Osborne, W.E., Szabo, M.W., Neathery, T.L., Copeland, C.W., 1988, *Geologic Map of Alabama, Northeast sheet*: Geological Society of Alabama, scale 1:250,000, 1 sheet.
- Peavy, T., 2008, *Provenance of Lower Pennsylvanian Pottsville Formation, Cahaba Basin, Alabama*: M.S. Thesis, Auburn University, 123 p.
- Pickering, S.M., ed., 1976, *Geologic Map of Georgia*: Georgia Department of Natural Resources, scale 1:500,000, 1 sheet.
- Rankin, D., 1976, Appalachian Salients and Recesses: Late Precambrian Continental Breakup and the Opening of the Iapetus Ocean: *Journal of Geophysical Research*, v. 81, no. 32
- Rast, N., 1989, The evolution of the Appalachian chain: *in* Bally, A., and Palmer, A, eds., *The Geology of North America – An overview*: Boulder, Colorado, Geological Society of America, *The Geology of North America*, v. A, p. 323-348.
- Reiners, P., Farley, K., Hickey, H., 2002, He diffusion and (U-Th)/He thermochronometry of zircon: initial results from Fish Canyon Tuff and Gold Butte: *Tectonophysics*, no. 349, p. 297-208.

- Rodger, F.T., 1997, A geologic history of the north-central Appalachians; Part 1, Orogenesis from the Mesoproterozoic through the Taconic Orogeny: *American Journal of Science*, v. 297, no. 6, p. 551-619.
- Secor, D.T., Snoke, A.W., and Dallmeyer, R.D., 1986, Character of the Alleghanian orogeny in the southern Appalachians: Part III. Regional tectonic relations: *Geological Society of America Bulletin*, v. 97, p. 1345-1353.
- Soderlund, P., Juez-Larre, J., Page, L., and Dunai, T., 2005, Extending the time range of apatite (U-Th)/He thermochronometry in slowly cooled terranes, Palaeozoic to Cenozoic exhumation history of southeast Sweden: *Earth and Planetary Science Letters*, no. 239, p. 266-275.
- Spear, F.S., 1995, *Metamorphic Phase Equilibria and Pressure-Temperature-Time Paths*, Washington D.C., Mineralogical Society of America, 797 p.
- Speer, J.A., McSween Jr., H.Y., Gates, A.E., 1994, Generation, Segregation, Ascent, and Emplacement of Alleghanian Plutons in the Southern Appalachians: *The Journal of Geology*, v. 102, p. 249-267.
- Steiger, R.H., and Jäger, E., 1977, Subcommittee on geochronology: convention on the use of decay constants in geo- and cosmochronology: *Earth and Planetary Science Letters*, v. 36, p. 359-362.
- Steltenpohl, M.G. and Kunk, M., 1993, $^{40}\text{Ar}/^{39}\text{Ar}$ thermochronology and Alleghanian development of the southernmost Appalachian Piedmont, Alabama and southwest Georgia: *Geological Society of America Bulletin*, v. 105, p. 819-833.
- Steltenpohl, M.G., 2003, More and more timing information indicate a more significant role for the Alleghanian event in the Alabama Piedmont: *Geological Society of America Abstracts with Programs*, v. 35, no. 1, p. 9.
- Steltenpohl, M.G., 2005, A primer on terranes of the southernmost Appalachians of Alabama and Georgia *in* Steltenpohl, M., ed., *New Perspectives on Southernmost Appalachian Terranes, Alabama and Georgia*: Alabama Geological Society, 42nd Annual Field Trip Guidebook, p. 1-18.
- Steltenpohl, M.G., Cook, R.B., Grimes, J.E., Keefer, W.D., Heatherington, A., and Mueller, P., 2005, Geology of the Brevard Zone in the Hinge of the Tallassee Synform, Alabama Fall Line: Implications for Southern Appalachian Tectonostratigraphy *in* Steltenpohl, M.G., ed., *New Perspectives on Southernmost Appalachian Terranes, Alabama and Georgia*: Alabama Geological Society, 42nd Annual Field Trip Guidebook, p. 125-148.

- Steltenpohl, M.G., Mueller, P.M., Heatherington, A.L., Hanley, T.B., and Wooden, J.L., 2008, Gondwanan/peri-Gondwanan origin for the Uchee terrane, Alabama and Georgia: Carolina zone or Suwanee terrane (?) and its suture with Grenvillian basement of the Pine Mountain window: *Geosphere*, v. 4, no. 1, p. 131 – 144.
- Stewart, K., and Miller, B., 2001, The tectonic implications of 460 Ma eclogite along the Taconic Suture in the eastern Blue Ridge of North Carolina: *Geological Society of America Abstracts with Programs*, v. 33, no. 2, p. 65.
- Szabo, M.W., Copeland, C.W., 1988, Geologic Map of Alabama, Southeast sheet: Geological Survey of Alabama, scale 1:250,000, 1 sheet.
- Thomas, W., 1989, Stratigraphy and Evolution of the Foreland, *in* Hatcher, R., Thomas, W., Geiser, P., Snoke, A., Mosher, S., and Wiltschko, D., 1989, Alleghanian orogen *in* Hatcher, R., Thomas, W., and Viele, G., eds., *The Appalachian-Ouachita Orogen in the United States*: Boulder, Colorado, Geological Society of America, *The Geology of North America*, v. F-2, p. 237-245.
- Thompson, A.B., and Ridley, J.R., 1987, Pressure-temperature-time (P-T-t) histories of orogenic belts: *Phil. Trans. R. Soc. London*, v. 321, p. 27-45.
- Tull, J.F., 1980, Overview of the sequence of timing of deformational events in the Southern Appalachians; evidence from the crystalline rocks, North Carolina to Alabama, *in* Wones, D.R., ed., *The Caledonides in the USA: Memoir – Virginia Polytechnic Institute, Department of Geological Sciences*, no. 2, p. 167-177.
- Vyhnal, C.R., McSween, H.Y., Speer, J.A., 1991, Hornblende chemistry in southern Appalachian granitoids: Implications for aluminum hornblende thermobarometry and magmatic epidote stability: *American Mineralogist*, v. 76, 176-188.
- Warnock, A., Zeitler, P., Wolf, R., and Bergman, S., 1997, An evaluation of low-temperature apatite U-Th/He thermochronometry: *Geochemica et Cosmochimica Acta*, v. 61, no. 24, p. 5371-5377.
- Wen, S., and Nekvasil, H., 1994, SOLVCALC: An interactive graphics program package for calculating the ternary feldspar solvus and for two-feldspar geothermometry: *Computers and Geosciences*, v. 20, no. 6, p. 1025-1040.
- Wiltschko, D., 1989, Description of structures: Southern Appalachians *in* Hatcher, R., Thomas, W., Geiser, P., Snoke, A., Mosher, S., and Wiltschko, D., 1989, Alleghanian orogen *in* Hatcher, R., Thomas, W., and Viele, G., eds., *The Appalachian-Ouachita Orogen in the United States*: Boulder, Colorado, Geological Society of America, *The Geology of North America*, v. F-2, p. 253-275.

- Wiltschko, D., and Geiser, P., 1989, Overview of the Appalachian Foreland *in* Hatcher, R., Thomas, W., Geiser, P., Snoke, A., Mosher, S., and Wiltschko, D., 1989, Alleghanian orogen *in* Hatcher, R., Thomas, W., and Viele, G., eds., The Appalachian-Ouachita Orogen in the United States: Boulder, Colorado, Geological Society of America, The Geology of North America, v. F-2, p. 245-253.
- Wolf, R., Farley, K., and Silver, L., 1996, Helium diffusion and low-temperature thermochronometry of apatite: *Geochemimica et Cosmochimica Acta*, v. 51, p. 2865-2868.
- Zeitler, P., Herczeg, A., McDougall, I., and Honda, M., 1987, U-Th-He dating of apatite: A potential thermochronometer: *Geochemimica et Cosmochimica Acta*, v. 61, no. 24, p. 5371-5377.

APPENDICES

APPENDIX 1: EMP ANALYSES

Probe Data	Homblende									
Mineral:	1	2	3	4	5	6	7	8	9	10
Number:										
Label:										
Coordinates:										
X:	76.8095	76.78	76.7507	76.7212	76.6917	76.6625	76.633	76.6035	76.574	76.8453
Y:	35.2072	35.1798	35.152	35.1242	35.0967	35.069	35.0412	35.0138	34.986	35.2252
Oxide Percent										
SiO2	42.32	42.73	42.77	43.13	41.8	42	41.5	42.28	42.63	42.51
TiO2	0.9816	1.1286	0.9731	1.0015	1.1252	1.0914	1.0634	1.0594	0.9014	0.7832
Al2O3	10.86	10.98	10.71	10.72	11.48	11.75	11.62	11.2	11.11	11.03
Cr2O3	0	0	0.0078	0	0.0133	0.0263	0.0328	0.0476	0	0.0356
FeO(total)	17	17.04	16.98	17.21	17.64	17.82	17.58	17.29	17.3	16.66
FeO	12.82759	12.85777	12.8125	12.98605	13.31051	13.44633	13.26524	13.04641	13.05396	12.57104
Fe2O3	4.172412	4.182229	4.167503	4.223954	4.329491	4.37367	4.314765	4.243588	4.246043	4.088964
MnO	0.3722	0.4701	0.4476	0.4697	0.4788	0.4496	0.4452	0.4311	0.4936	0.4107
MgO	10.04	10.06	10.04	10.02	9.72	9.61	9.54	9.88	9.88	10.21
CaO	11.16	11.15	10.92	11.12	11.05	11.03	11.11	11.13	11.17	11.11
Na2O	1.4066	1.3469	1.3456	1.3154	1.3619	1.4101	1.4247	1.3176	1.2042	1.278
K2O	1.2496	1.2042	1.2384	1.1369	1.3108	1.3254	1.412	1.2561	1.2041	1.1919
Oxide Total:	95.39	96.1	95.42	96.13	95.98	96.52	95.73	95.9	95.88	95.22
Atomic Proportions										
Si	6.82	6.826	6.876	6.884	6.722	6.716	6.699	6.784	6.831	6.841
Ti	0.119	0.1356	0.1177	0.1202	0.1361	0.1312	0.1291	0.1278	0.1086	0.0948
Al	2.0629	2.0675	2.0295	2.017	2.176	2.215	2.2108	2.1183	2.0979	2.0922
Cr	0	0	0.001	0	0.0017	0.0033	0.0042	0.006	0	0.0045
Fe	2.2906	2.2765	2.2829	2.2975	2.3725	2.3826	2.3735	2.3206	2.318	2.2422
Mn	0.0508	0.0636	0.061	0.0635	0.0652	0.0609	0.0609	0.0586	0.067	0.056
Mg	2.4111	2.3952	2.405	2.3843	2.3291	2.2912	2.296	2.3637	2.3606	2.4481
Ca	1.9262	1.9089	1.8808	1.9012	1.9036	1.8896	1.9219	1.9134	1.9173	1.9159
Na	0.4395	0.4172	0.4195	0.4071	0.4246	0.4371	0.4459	0.4099	0.3742	0.3987
K	0.2569	0.2454	0.254	0.2315	0.2689	0.2703	0.2908	0.2571	0.2462	0.2447
O	24	24	24	24	24	24	24	24	24	24
Cation Total:	16.377	16.336	16.328	16.306	16.4	16.397	16.432	16.359	16.321	16.338
Na+K	0.6964	0.6626	0.6735	0.6386	0.6935	0.7074	0.7367	0.667	0.6204	0.6434
Fe+Mg+Mn	4.7525	4.7353	4.7489	4.7453	4.7668	4.7347	4.7304	4.7429	4.7456	4.7463

Probe Data																					
Mineral:	Homblende																				
Number:	11	12	13	14	14	23	15	24	25	16	17	18	19	20							
Label:	12	13	14	14	23	24	25	16	17	18	19	20	4								
Coordinates:																					
X:	76.6122	76.8305	76.3162	67.475	67.3982	67.475	67.5685	67.472	65.1065	65.1525	65.2398										
Y:	34.9392	34.756	35.2907	42.573	42.6465	42.7315	42.77	42.77	42.77	42.71	42.46										
Oxide Percent																					
SiO2	42.57	42.65	41.89	42.67	42.41	42.44	42.39	42.77	42.71	42.71	42.46										
TiO2	0.9168	0.9201	0.5824	0.8091	1.073	1.0928	1.0468	1.0468	0.6416	0.6416	0.4488										
Al2O3	10.62	10.97	11.6	11.31	10.82	11.11	10.87	11.51	11.11	11.11	11.83										
Cr2O3	0.0351	0.0176	0.0467	0.0136	0.0126	0	0	0.0531	0	0	0.0185										
FeO(total)	17.28	17.05	17.59	17.67	17.75	17.79	17.07	17.55	16.89	16.89	17.97										
FeO	13.03887	12.86532	13.27278	13.33315	13.39351	13.42369	12.88041	13.2426	12.74459	13.55952											
Fe ₂ O ₃	4.241134	4.184684	4.317219	4.336854	4.356489	4.366306	4.189593	4.307402	4.145414	4.410485											
MnO	0.512	0.436	0.424	0.4493	0.4038	0.3772	0.4827	0.4672	0.4545	0.4368											
MgO	10.22	10.03	9.6	9.69	9.82	9.77	9.97	9.65	9.65	9.65	9.24										
CaO	11.06	11.04	11.16	11.19	11.11	11.05	11	10.95	11.06	11.06	11.27										
Na2O	1.3032	1.3389	1.4246	1.252	1.4636	1.2759	1.3829	1.2735	1.3249	1.262											
K2O	1.2273	1.2191	1.2241	1.262	1.3066	1.3067	1.268	1.2091	1.2029	1.1813											
Oxide Total:	95.75	95.68	95.54	96.32	96.17	96.22	95.48	96.1	95.04	96.11											
Atomic Proportions																					
Si	6.841	6.843	6.76	6.82	6.806	6.798	6.826	6.837	6.887	6.887	6.805										
Ti	0.1108	0.111	0.0707	0.0972	0.1295	0.1316	0.1267	0.0804	0.0778	0.0778	0.0541										
Al	2.0119	2.0749	2.2072	2.1298	2.0462	2.0981	2.0626	2.1676	2.1117	2.1117	2.2341										
Cr	0.0045	0.0022	0.006	0.0017	0.0016	0	0	0.0067	0	0	0.0023										
Fe	2.3221	2.2882	2.374	2.3621	2.3819	2.3829	2.298	2.3452	2.2772	2.2772	2.4087										
Mn	0.0697	0.0593	0.058	0.0608	0.0549	0.0512	0.0658	0.0633	0.0621	0.0621	0.0593										
Mg	2.4474	2.3987	2.309	2.3073	2.3495	2.3314	2.3931	2.3001	2.3207	2.3207	2.2063										
Ca	1.9046	1.897	1.9292	1.9161	1.9098	1.8969	1.8976	1.8752	1.9112	1.9112	1.9353										
Na	0.406	0.4165	0.4458	0.3879	0.4554	0.3962	0.4317	0.3947	0.4143	0.4143	0.3922										
K	0.2516	0.2495	0.252	0.2573	0.2675	0.267	0.2604	0.2465	0.2475	0.2475	0.2415										
O	24	24	24	24	24	24	24	24	24	24	24										
Cation Total:	16.369	16.34	16.412	16.34	16.402	16.353	16.362	16.316	16.31	16.31	16.339										
Na+K	0.6576	0.666	0.6978	0.6452	0.7229	0.6632	0.6921	0.6412	0.6618	0.6618	0.6337										
Fe+Mg+Mn	4.8392	4.7462	4.741	4.7302	4.7863	4.7655	4.7569	4.7086	4.66	4.66	4.6743										

Probe Data											
Mineral:	Biotite										
Number:	1	2	3	4	5	6	7	8	9	10	
Label:	15	16	17	18	19	20	21	22	27	1	
Coordinates:											
X:	76.3185	76.3042	76.5532	76.665	76.4315	76.4855	76.508	76.306	67.546	67.519	
Y:	35.2797	35.2795	34.995	34.8567	34.9805	34.9063	34.785	35.0783	42.7635	42.777	
Oxide Percent											
SiO2	36.74	36.29	36.96	36.9	36.08	36.61	35.76	36	36.47	36.35	
TiO2	1.6429	1.4703	1.8068	1.8502	2.0856	2.2221	1.862	1.6728	2.1956	2.0939	
Al2O3	16.8	16.62	17.9	17.11	16.8	17.15	16.58	16.23	16.69	16.3	
Cr2O3	0.0146	0.0238	0.0253	0.0141	0.0208	0	0.0528	0.0146	0.0469	0.0189	
FeO	16.29	16.48	16.2	16.01	17.1	16.93	16.65	17.11	17.9	17.75	
MnO	0.2873	0.3242	0.2641	0.2681	0.2752	0.3101	0.2773	0.282	0.3563	0.3485	
MgO	12.23	12.58	12.37	12.3	12	11.52	12.65	12.13	12.05	11.92	
CaO	0.2149	0.0535	0.0517	0.0443	0	0.008	0.1249	0.0173	0.0189	0.0029	
Na2O	0.0968	0.1052	0.0765	0.0138	0.055	0.0021	0.043	0.044	0.1141	0.1001	
K2O	9.23	9.63	9.81	10	9.45	9.82	8.4	9.68	9.71	9.81	
Oxide Total:	93.55	93.58	95.47	94.52	93.88	94.57	92.39	93.18	95.56	94.69	
Atomic Proportions											
Si	3.062	3.039	3.019	3.0485	3.0165	3.035	3.017	3.0405	3.0105	3.03	
Ti	0.10295	0.0926	0.111	0.11495	0.1311	0.13855	0.11815	0.10625	0.1363	0.1313	
Al	1.6505	1.64	1.723	1.666	1.6555	1.6755	1.6485	1.6155	1.624	1.6015	
Al ^{IV}	0.938	0.961	0.981	0.9515	0.9835	0.965	0.983	0.9595	0.9895	0.97	
Al ^{VI}	0.7125	0.679	0.742	0.7145	0.672	0.7105	0.6655	0.656	0.6345	0.6315	
Cr	0.00095	0.0016	0.00165	0.0009	0.0014	0	0.0035	0.00095	0.00305	0.00125	
Fe	1.1351	1.15405	1.10695	1.1064	1.1955	1.1742	1.17495	1.2086	1.23545	1.2372	
Mn	0.0203	0.023	0.01825	0.01875	0.0195	0.0218	0.0198	0.02015	0.0249	0.0246	
Mg	1.5195	1.5695	1.506	1.515	1.4958	1.42315	1.5905	1.527	1.483	1.48125	
Ca	0.0192	0.0048	0.00455	0.0039	0	0.0007	0.0113	0.00155	0.00165	0.00025	
Na	0.01565	0.0171	0.0121	0.0022	0.0089	0.00035	0.00705	0.0072	0.01825	0.0162	
K	0.98175	1.02905	1.0221	1.0538	1.0076	1.0384	0.9036	1.04255	1.0226	1.04365	
O	12	12	12	12	12	12	12	12	12	12	
Cation Total:	8.508	8.571	8.5245	8.531	8.532	8.508	8.494	8.57	8.56	8.567	
Na+K	0.9974	1.04615	1.0342	1.056	1.0165	1.03875	0.91065	1.04975	1.04085	1.05985	
Fe+Mg+Mn+Al	3.3874	3.42555	3.3732	3.35465	3.3828	3.32965	3.45075	3.41175	3.37785	3.37455	
%Annite	0.427597	0.42373	0.42364	0.422065	0.444209	0.452076	0.424868	0.441804	0.454469	0.455112	
%Phlogopite	0.572403	0.57627	0.57636	0.577935	0.555791	0.547924	0.575132	0.558196	0.545531	0.544888	

Probe Data		Biotite		12	13	14	15	16	17	18	19	20
Mineral:	11	12	13	14	15	16	17	18	19	20	21	22
Number:	2	3	4	5	6	7	8	9	10	11	12	13
Label:												
Coordinates:	X:	67.6187	67.6687	67.5028	67.2112	65.0112	65.0865	65.0455	64.9672	64.9462		
	Y:	42.8502	42.9235	42.997	43.0757	47.669	47.4852	47.3995	47.5138	47.5655		
Oxide Percent												
SiO2	36.75	36.26	36.57	36.25	36.56	36.44	36.28	36.48	36.26	36.59		
TiO2	2.319	2.6951	3.17	2.7114	3.11	2.2688	2.2585	1.9378	2.0187	2.0491		
Al2O3	16.37	16	16.51	16.1	16.48	16.91	16.82	16.97	16.74	17.01		
Cr2O3	0.0402	0.0199	0.0219	0	0.0097	0.0443	0.0677	0.0317	0.0351	0.0088		
FeO	17.74	17.39	17.38	17.95	17.29	17.25	17.3	16.85	17.05	17.22		
MnO	0.3293	0.2812	0.2912	0.3177	0.2558	0.2745	0.3019	0.2886	0.3063	0.3297		
MgO	11.76	11.73	11.46	11.88	11.42	11.59	11.63	11.89	11.98	12.14		
CaO	0	0.0011	0	0	0.0281	0	0.053	0.1472	0	0.0156		
Na2O	0.0406	0.04	0.0765	0	0.0469	0.0652	0	0.0322	0.0596	0.0203		
K2O	9.5	9.65	9.68	9.76	9.75	9.81	9.52	9.69	9.76	9.38		
Oxide Total:	94.85	94.07	95.15	94.97	94.95	94.66	94.22	94.31	94.21	94.77		
Atomic Proportions												
Si	3.047	3.0355	3.022	3.0155	3.0265	3.026	3.0245	3.033	3.025	3.025		
Ti	0.1446	0.16965	0.19675	0.1696	0.19385	0.1417	0.1416	0.12115	0.12665	0.1274		
Al	1.6	1.5785	1.6075	1.578	1.6085	1.6555	1.652	1.663	1.646	1.6575		
Al ^{IV}	0.953	0.9645	0.978	0.9845	0.9735	0.974	0.9755	0.967	0.975	0.975		
Al ^{VI}	0.647	0.614	0.6295	0.5935	0.635	0.6815	0.6765	0.696	0.671	0.6825		
Cr	0.00265	0.0013	0.00145	0	0.00065	0.0029	0.00445	0.0021	0.0023	0.00055		
Fe	1.2305	1.21715	1.20105	1.24845	1.19725	1.1981	1.206	1.1713	1.18915	1.191		
Mn	0.02315	0.01995	0.0204	0.0224	0.01795	0.0193	0.0213	0.0203	0.02165	0.0231		
Mg	1.453	1.46385	1.41105	1.47345	1.409	1.4348	1.4454	1.47295	1.4892	1.49615		
Ca	0	0.0001	0	0	0.0025	0	0.00475	0.0131	0	0.0014		
Na	0.00655	0.0065	0.01225	0	0.00755	0.0105	0	0.0052	0.00965	0.00325		
K	1.0051	1.03075	1.0204	1.0359	1.02965	1.039	1.0119	1.0278	1.03865	0.9894		
O	12	12	12	12	12	12	12	12	12	12		
Cation Total:	8.5125	8.5235	8.493	8.5435	8.4935	8.528	8.512	8.53	8.5485	8.515		
Na+K	1.01165	1.03725	1.03265	1.0359	1.0372	1.0495	1.0119	1.033	1.0483	0.99265		
Fe+Mg+Mn+Al	3.35365	3.31495	3.262	3.3378	3.2592	3.3337	3.3492	3.36055	3.371	3.39275		
%Annite	0.458543	0.453991	0.459802	0.458669	0.459376	0.45505	0.454854	0.442961	0.443986	0.443221		
%Phlogopite	0.541457	0.546009	0.540198	0.541331	0.540624	0.54495	0.545146	0.557039	0.556014	0.556779		

Probe Data												
Mineral:	Alkali Feldspar											
Number:	1	2	3	4	5	6	7	8	9	10		
Label:	1	2	3	4	5	6	7	1	2	3		
Coordinates:	X:											
	Y:	64.9842	65.026	65.1092	65.151	64.7835	64.7835	53.9273	53.7947	53.6623		
Oxide Percent		46.3117	46.1945	46.0775	45.9602	46.0367	46.0367	40.212	40.1713	40.072		
SiO2												
Al2O3		62.84	62.9	63.27	63.17	62.79	62.72	62.87	62.84	62.78		
CaO		18.85	18.92	18.96	18.87	18.7	18.81	18.67	18.76	18.88		
Na2O		0	0.0012	0	0.0189	0	0	0	0	0		
K2O		0.589	1.2192	1.2539	1.3025	0.9567	0.7744	0.6418	1.3426	1.0262		
Oxide Total:		15.35	14.36	14.48	14.22	14.76	15.31	15.19	14.08	14.63		
Atomic Proportions		97.63	97.4	97.97	97.58	97.69	97.58	97.37	97.01	97.31		
Si												
Al		2.96825	2.967	2.9685	2.97175	2.97	2.975	2.97525	2.9725	2.967		
Ca		1.04925	1.052	1.04825	1.04625	1.04875	1.04425	1.041	1.04575	1.052		
Na		0	0.00005	0	0.00095	0	0	0	0	0		
K		0.05395	0.1115	0.11405	0.1188	0.08735	0.07115	0.0589	0.12315	0.09405		
O		0.92475	0.864	0.86675	0.85325	0.8865	0.8955	0.917	0.84975	0.882		
Cation Total:		8	8	8	8	8	8	8	8	8		
Si+Al		4.9965	4.99475	4.99775	4.99125	4.9925	4.986	4.99225	4.991	4.995		
Ca+Na+K		4.0175	4.019	4.01675	4.018	4.01875	4.01925	4.01625	4.01825	4.019		
%Anorthite		0.9787	0.97555	0.9808	0.973	0.97385	0.96665	0.9759	0.9729	0.97605		
%Albite		0	5.13E-05	0	0.000976	0	0	0	0	0		
%Orthoclase		0.055124	0.114295	0.116283	0.122097	0.089696	0.073605	0.060355	0.12658	0.096358		
		0.944876	0.885654	0.883717	0.876927	0.910304	0.926395	0.931048	0.87342	0.903642		

Probe Data																				
Mineral: Alkali Feldspar																				
Number:	11	12	13	14	15	16	17	18	19	20	21									
Label:	4	5	6	7	8	9	10	1	2	3	4									
Coordinates:																				
X:	53.5297	53.397	53.2645	53.132	52.9995	52.867	52.7345	59.4647	59.3322	59.5347	59.5707									
Y:	40.047	39.995	39.9917	39.8762	39.932	39.9267	40.0342	35.0525	33.534	33.9872	34.372									
Oxide Percent																				
SiO2	63.21	63.22	63.17	63.35	63.03	63.4	63.1	62.91	63.09	63.29	62.56									
Al2O3	18.73	18.87	18.86	18.91	18.76	18.73	18.79	18.66	18.75	18.56	18.78									
CaO	0.0154	0.0218	0.0319	0.0059	0.0089	0.0242	0	0	0	0	0.003									
Na2O	0.8849	1.1704	1.2276	1.1886	1.064	1.2924	0.5674	0.7188	0.8487	0.6617	1.6728									
K2O	14.82	14.31	14.69	14.53	14.43	14.38	15.57	15.12	14.67	15.19	13.91									
Oxide Total:	97.67	97.6	97.98	97.99	97.28	97.83	98.03	97.41	97.37	97.7	96.92									
Atomic Proportions																				
Si	2.977	2.97325	2.968	2.97125	2.9755	2.977	2.971	2.9755	2.9775	2.98325	2.9645									
Al	1.03975	1.04625	1.04425	1.0455	1.04375	1.03675	1.043	1.04	1.043	1.031	1.049									
Ca	0.000775	0.0011	0.0016	0.0003	0.00045	0.001225	0	0	0	0	0.00015									
Na	0.0808	0.106725	0.111825	0.1081	0.0974	0.117675	0.0518	0.065925	0.07765	0.060475	0.1537									
K	0.8905	0.85875	0.88025	0.8695	0.86875	0.8615	0.93525	0.9125	0.8835	0.913	0.84075									
O	8	8	8	8	8	8	8	8	8	8	8									
Cation Total:	4.98875	4.98625	5.006	4.99475	4.98575	4.99425	5.001	4.99375	4.9815	4.988	5.008									
Si+Al																				
	4.01675	4.0195	4.01225	4.01675	4.01925	4.01375	4.014	4.0155	4.0205	4.01425	4.0135									
Ca+Na+K																				
	0.972075	0.966575	0.993675	0.9779	0.9666	0.9804	0.98705	0.978425	0.96115	0.973475	0.9946									
%Anorthite																				
	0.000797	0.001138	0.00161	0.000307	0.000466	0.001249	0	0	0	0	0.000151									
%Albite																				
	0.083121	0.110416	0.112537	0.110543	0.100766	0.120028	0.05248	0.067379	0.080789	0.062123	0.154534									
%Orthoclase																				
	0.916082	0.888446	0.885853	0.88915	0.898769	0.878723	0.94752	0.932621	0.919211	0.937877	0.845315									

Probe Data											
Mineral:	Plagioclase										
Number:	1	2	3	4	5	6	7	8	9	10	
Label:	2	3	4	5	6	7	8	9	10	12	
Coordinates:											
X:	65.1272	65.014	64.9007	64.7873	64.674	64.5608	64.4472	64.334	64.2208	64.7873	
Y:	46.842	46.7887	46.734	46.679	46.6262	46.5752	46.5195	46.4667	46.4165	46.6825	
Oxide Percent											
SiO2	60.42	60.56	60.42	60.52	60.46	60.45	60.13	60.37	60.8	59.93	
Al2O3	24.68	24.57	24.68	24.59	24.71	24.7	24.5	24.54	24.5	24.85	
CaO	5.35	5.5	5.35	5.51	5.38	5.39	5.49	5.41	5.14	5.44	
Na2O	7.95	7.71	7.95	7.81	7.94	7.91	7.97	7.79	8.12	7.78	
K2O	0.2047	0.2374	0.2047	0.2763	0.281	0.2382	0.2922	0.2269	0.2135	0.2951	
Oxide Total:	98.61	98.59	98.61	98.71	98.78	98.69	98.39	98.34	98.78	98.29	
Atomic Proportions											
Si	2.71475	2.72075	2.71	2.7175	2.7135	2.7145	2.712	2.719	2.726	2.7035	
Al	1.307	1.30075	1.3125	1.30125	1.307	1.307	1.3025	1.30275	1.2945	1.321	
Ca	0.257575	0.26475	0.26185	0.26515	0.258675	0.2594	0.265325	0.26115	0.2471	0.262975	
Na	0.692975	0.671775	0.685375	0.679975	0.691175	0.6885	0.697075	0.6807	0.705725	0.680425	
K	0.011725	0.0136	0.0135	0.015825	0.016075	0.01365	0.016825	0.01305	0.0122	0.016975	
O	8	8	8	8	8	8	8	8	8	8	
Cation Total:	4.984	4.97175	4.98325	4.97975	4.9865	4.983	4.99375	4.9765	4.98575	4.98475	
Si+Al	4.02175	4.0215	4.0225	4.01875	4.0205	4.0215	4.0145	4.02175	4.0205	4.0245	
Ca+Na+K	0.962275	0.950125	0.960725	0.96095	0.965925	0.96155	0.979225	0.9549	0.965025	0.960375	
%Anorthite	0.267673	0.278648	0.272555	0.275925	0.2678	0.269773	0.270954	0.273484	0.256056	0.273825	
%Albite	0.720142	0.707039	0.713394	0.707607	0.715558	0.716031	0.711864	0.71285	0.731302	0.708499	
%Orthoclase	0.012185	0.014314	0.014052	0.016468	0.016642	0.014196	0.017182	0.013666	0.012642	0.017675	

Probe Data		Plagioclase													
Mineral:		11	12	13	14	15	16	17	18						
Number:		1	3	4	5	6	7	8	9						
Label:															
Coordinates:															
X:	54.2537	54.6303	54.8182	55.0065	55.1948	55.383	55.5712	55.7595							
Y:	40.4972	40.5953	40.6442	40.6932	40.7425	40.7915	40.8405	40.8895							
Oxide Percent															
SiO2	60	60.15	60.23	59.71	60.37	60.13	59.75	60.5							
Al2O3	24.38	24.54	24.82	24.74	24.62	24.31	24.77	24.64							
CaO	5.41	5.41	5.57	5.75	5.43	5.23	5.05	5.34							
Na2O	7.99	7.99	7.73	7.53	7.42	7.87	7.47	8.13							
K2O	0.2198	0.3864	0.4044	0.3679	0.3456	0.2904	0.3666	0.1398							
Oxide Total:	98	98.49	98.75	98.09	98.2	97.84	97.41	98.75							
Atomic Proportions															
Si	2.71525	2.71125	2.70625	2.701	2.72075	2.723	2.71325	2.71525							
Al	1.30025	1.30375	1.31425	1.319	1.30775	1.29775	1.3255	1.3035							
Ca	0.2621	0.261375	0.268	0.278575	0.262425	0.25395	0.2458	0.256775							
Na	0.70145	0.69865	0.673	0.660875	0.64855	0.69065	0.6578	0.707025							
K	0.012675	0.022225	0.023175	0.021225	0.019875	0.016775	0.021225	0.008							
O	8	8	8	8	8	8	8	8							
Cation Total:	4.99175	4.99725	4.98475	4.9805	4.9595	4.982	4.9635	4.9905							
Si+Al	4.0155	4.015	4.0205	4.02	4.0285	4.02075	4.03875	4.01875							
Ca+Na+K	0.976225	0.98225	0.964175	0.960675	0.93085	0.961375	0.924825	0.9718							
%Anorthite	0.268483	0.266098	0.277958	0.289978	0.28192	0.264153	0.26578	0.264226							
%Albite	0.718533	0.711275	0.698006	0.687928	0.696729	0.718398	0.71127	0.727542							
%Orthoclase	0.012984	0.022627	0.024036	0.022094	0.021351	0.017449	0.02295	0.008232							

APPENDIX 2: THERMOBAROMETRY

Hornblende-Plagioclase Geothermometer and Aluminum-in-Hornblende Geobarometer				
HBL #	PLAG #	TEMP	ALUMINUM CONTENT	PRESSURE
20	17	661	2.2341	5.990243
22	2	673	2.0638	5.269874
5	14	715	2.176	5.74448
2	14	696	2.0675	5.285525
13	2	692	2.2072	5.876456
12	10	683	2.0119	5.050337
10	5	679	2.0922	5.390006
16	10	692	2.0981	5.414963
22	11	671	2.0638	5.269874
8	10	696	2.1183	5.500409
22	14	677	2.0638	5.269874
6	18	698	2.215	5.90945
18	2	660	2.1676	5.708948
4	12	680	2.017	5.07191
11	8	701	2.0119	5.050337
22	16	671	2.0638	5.269874
5	5	708	2.176	5.74448
2	7	691	2.0675	5.285525
22	11	671	2.0638	5.269874
11	10	702	2.0119	5.050337
20	10	661	2.2341	5.990243
6	2	702	2.215	5.90945
5	16	708	2.176	5.74448
5	18	706	2.176	5.74448
17	15	695	2.0626	5.264798
16	3	691	2.0981	5.414963
21	15	691	2.0781	5.330363
15	2	709	2.0462	5.195426
5	7	709	2.176	5.74448
22	16	671	2.0638	5.269874
3	10	677	2.0295	5.124785
11	4	703	2.0119	5.050337
4	5	679	2.017	5.07191
5	6	708	2.176	5.74448
4	12	680	2.017	5.07191
21	15	691	2.0781	5.330363
16	2	692	2.0981	5.414963
12	4	683	2.0119	5.050337
8	13	698	2.1183	5.500409
14	12	676	2.1298	5.549054
10	9	676	2.0922	5.390006
18	6	659	2.1676	5.708948
19	8	652	2.1117	5.472491
21	5	687	2.0781	5.330363
13	12	691	2.2072	5.876456
13	4	692	2.2072	5.876456
13	3	690	2.2072	5.876456

Hornblende-Plagioclase Geothermometer and Aluminum-in-Hornblende Geobarometer				
HBL #	PLAG #	TEMP	ALUMINUM CONTENT	PRESSURE
21	4	689	2.0781	5.330363
16	3	691	2.0981	5.414963
20	17	661	2.2341	5.990243
9	2	680	2.0979	5.414117
14	13	678	2.1298	5.549054
17	4	693	2.0626	5.264798
4	5	679	2.017	5.07191
2	8	691	2.0675	5.285525
8	5	694	2.1183	5.500409
16	12	691	2.0981	5.414963
4	15	683	2.017	5.07191
9	11	677	2.0979	5.414117
2	2	692	2.0675	5.285525
21	6	687	2.0781	5.330363
20	12	661	2.2341	5.990243
17	12	692	2.0626	5.264798
22	16	671	2.0638	5.269874
22	2	673	2.0638	5.269874
1	3	697	2.0629	5.266067
15	6	707	2.0462	5.195426
17	1	690	2.0626	5.264798
16	17	691	2.0981	5.414963
12	18	679	2.0119	5.050337
4	11	678	2.017	5.07191
11	14	707	2.0119	5.050337
1	4	698	2.0629	5.266067
8	1	693	2.1183	5.500409
22	3	672	2.0638	5.269874
19	3	652	2.1117	5.472491
21	7	688	2.0781	5.330363
6	4	702	2.215	5.90945
9	5	678	2.0979	5.414117
21	12	688	2.0781	5.330363
10	16	678	2.0922	5.390006
20	3	660	2.2341	5.990243
11	13	705	2.0119	5.050337
21	14	693	2.0781	5.330363
14	9	672	2.1298	5.549054
21	2	689	2.0781	5.330363
10	8	680	2.0922	5.390006
7	14	715	2.2108	5.891684
19	3	652	2.1117	5.472491
12	14	687	2.0119	5.050337
5	2	710	2.176	5.74448
9	14	684	2.0979	5.414117
11	7	702	2.0119	5.050337
16	9	687	2.0981	5.414963
22	14	677	2.0638	5.269874
13	8	690	2.2072	5.876456

Summation of hornblende-plagioclase geothermometer and aluminum-in-hornblende geobarometer statistical analyses

Hornblende-Plagioclase Thermometer		Aluminum in Hornblende Barometer	
Average=	686.2292	Average=	5.423189
Number of Analyses:	96	Number of Analyses:	96
Average Temperature:	686.2291667	Average pressure:	5.423189469
Maximum Value:	715	Maximum Value:	5.990243
Minimum Value:	652	Minimum Value:	5.050337
Mode:	691	Mode:	5.269874
Median:	689	Median:	5.3601845
Standard Deviation:	14.7	Standard Deviation:	0.3

APPENDIX 3: GEOCHRONOLOGY

Date Run: 2/16/09
 Irradiation Package: AU11
 Date of Irradiation: 4/29/2008
 Reactor: McMaster, with Cd shielding
 Monitor Age Assigned*: 28.02 Ma
 Air 40Ar/36Ar: 293.5 ± 1.5
 Sensitivity (moles/V): 8.606E-15
 J-Value: 0.014609

AU11.7i.bio: BQ-1, biotite from the Barin Quarry; fl = 2.290 A

	40Ar (* atm)	39Ar (K)	38(atmCl)	37(Ca)	36*(atm)	%Rad	R	Age (Ma)
1	3.820E-14 + 2.9E-17	2.866E-15 + 6.9E-18	1.21E-17 + 2.7E-19	2.6E-17 + 8.7E-18	1.65E-17 + 1.82E-19	87.2%	11.6260	283.0 ± 0.9
2	2.991E-14 + 2.5E-17	1.499E-15 + 5.8E-18	1.24E-17 + 2.5E-19	2.6E-18 + 6.1E-18	4.26E-17 + 6.05E-19	57.9%	11.5580	281.5 ± 3.6
3	1.575E-14 + 2.5E-17	1.266E-15 + 4.8E-18	3.97E-18 + 9.0E-20	3.0E-17 + 7.4E-18	3.22E-18 + 1.20E-19	94.0%	11.6896	284.4 ± 1.4
4	7.177E-15 + 8.8E-18	5.357E-16 + 2.1E-18	1.47E-18 + 3.8E-20	1.7E-17 + 4.3E-18	2.85E-18 + 8.83E-20	88.3%	11.8261	287.5 ± 1.8
5	1.148E-14 + 1.4E-17	8.637E-16 + 3.3E-18	2.46E-18 + 5.1E-20	8.1E-18 + 5.0E-18	4.23E-18 + 1.04E-19	89.1%	11.8399	287.8 ± 1.6
6	1.485E-14 + 3.0E-17	1.198E-15 + 4.9E-18	3.42E-18 + 5.8E-20	5.0E-18 + 6.0E-18	2.60E-18 + 6.86E-20	94.8%	11.7518	285.8 ± 1.4
7	1.414E-14 + 3.2E-17	9.966E-16 + 4.9E-18	4.46E-18 + 1.1E-19	4.7E-18 + 6.4E-18	9.04E-18 + 1.20E-19	81.1%	11.5104	280.4 ± 2.1
8	9.367E-15 + 1.4E-17	7.360E-16 + 3.3E-18	2.38E-18 + 5.4E-20	5.7E-19 + 3.8E-18	3.19E-18 + 1.73E-19	89.9%	11.4451	278.9 ± 2.2
9	1.057E-14 + 2.1E-17	7.853E-16 + 4.1E-18	3.24E-18 + 1.1E-19	1.3E-17 + 4.7E-18	4.98E-18 + 1.99E-19	86.1%	11.5889	282.2 ± 2.6

AU11.7i.hbl: BQ-1, hornblende from the Barin Quarry; fl = 2.290 A

	40Ar (* atm)	39Ar (K)	38(atmCl)	37(Ca)	36*(atm)	%Rad	R	Age (Ma)
1	5.272E-15 + 9.0E-18	4.209E-16 + 2.6E-18	1.90E-18 + 6.1E-20	1.24E-15 + 1.4E-17	2.46E-19 + 5.57E-20	98.6%	12.3537	299.3 ± 3.0
2	4.436E-15 + 7.8E-18	3.527E-16 + 2.9E-18	1.24E-18 + 4.9E-20	1.10E-15 + 2.1E-17	3.63E-19 + 5.60E-20	97.6%	12.2742	297.6 ± 3.3
3	7.266E-15 + 1.2E-17	5.770E-16 + 2.9E-18	2.17E-18 + 5.7E-20	1.46E-15 + 1.4E-17	5.62E-19 + 6.60E-20	97.7%	12.3052	298.3 ± 2.1
4	5.633E-15 + 1.3E-17	4.471E-16 + 2.8E-18	1.77E-18 + 4.9E-20	1.34E-15 + 4.6E-17	3.79E-19 + 5.55E-20	98.0%	12.3468	299.2 ± 2.6
5	5.169E-15 + 1.3E-17	4.246E-16 + 2.6E-18	1.77E-18 + 7.1E-20	1.34E-15 + 5.1E-17	2.16E-19 + 3.59E-20	98.8%	12.0220	291.9 ± 2.6
6	4.061E-15 + 8.0E-18	3.333E-16 + 3.3E-18	1.55E-18 + 5.8E-20	9.20E-16 + 1.6E-17	-9.59E-20 + -7.14E-20	100.7%	12.2700	297.5 ± 3.9
7	3.066E-15 + 5.0E-18	2.409E-16 + 1.8E-18	1.00E-18 + 3.5E-20	6.65E-16 + 2.1E-17	1.27E-19 + 2.49E-20	98.8%	12.5706	304.2 ± 2.9
8	1.943E-15 + 7.0E-18	1.421E-16 + 8.6E-19	3.67E-19 + 2.7E-20	3.97E-16 + 1.1E-17	2.95E-19 + 5.29E-20	95.5%	13.0554	314.9 ± 4.3
9	2.388E-15 + 9.1E-18	1.961E-16 + 1.4E-18	4.02E-19 + 2.0E-20	6.12E-16 + 2.5E-17	1.20E-20 + 3.97E-21	99.9%	12.1586	295.0 ± 3.2
10	5.197E-15 + 6.1E-18	4.150E-16 + 2.8E-18	2.73E-18 + 1.5E-19	1.14E-15 + 4.4E-17	3.60E-19 + 3.37E-20	98.0%	12.2646	297.3 ± 2.4
11	5.231E-15 + 6.7E-18	4.124E-16 + 3.2E-18	2.32E-18 + 1.0E-19	1.12E-15 + 1.8E-17	4.94E-19 + 4.24E-20	97.2%	12.3299	298.8 ± 2.7
12	4.486E-15 + 8.0E-18	3.522E-16 + 2.1E-18	2.32E-18 + 6.2E-20	8.97E-16 + 1.3E-17	5.02E-19 + 4.52E-20	96.7%	12.3149	298.5 ± 2.4
13	7.595E-15 + 9.8E-18	5.763E-16 + 4.2E-18	2.88E-18 + 7.3E-20	1.10E-15 + 1.6E-17	3.35E-19 + 3.96E-20	98.7%	13.0069	313.9 ± 2.5
14	1.397E-14 + 1.3E-17	1.155E-15 + 2.1E-18	3.68E-18 + 7.0E-20	9.85E-16 + 3.6E-17	1.05E-18 + 5.21E-20	97.8%	11.8287	287.6 ± 0.7
15	4.376E-15 + 5.3E-18	3.513E-16 + 1.6E-18	2.00E-18 + 1.1E-19	1.02E-15 + 2.0E-17	3.06E-19 + 2.85E-20	97.9%	12.2000	295.9 ± 1.8
16	3.497E-15 + 9.0E-18	2.781E-16 + 1.5E-18	1.00E-18 + 3.4E-20	7.97E-16 + 7.5E-18	3.60E-19 + 3.08E-20	97.0%	12.1892	295.7 ± 2.2
17	5.043E-15 + 1.1E-17	3.888E-16 + 1.2E-18	2.00E-18 + 5.9E-20	1.11E-15 + 2.0E-17	6.90E-19 + 3.50E-20	96.0%	12.4484	301.4 ± 1.5
18	4.303E-15 + 7.4E-18	3.522E-16 + 2.7E-18	1.46E-18 + 3.3E-20	9.24E-16 + 8.7E-18	2.80E-19 + 2.71E-20	98.1%	11.9806	291.0 ± 2.6
19	3.583E-15 + 1.1E-17	2.844E-16 + 2.6E-18	1.04E-18 + 4.7E-20	7.20E-16 + 1.8E-17	4.63E-19 + 3.75E-20	96.2%	12.1177	294.1 ± 3.2

Date Run: 2/16/09
 Irradiation Package: AU11
 Date of Irradiation: 4/29/2008
 Reactor: McMaster, with Cd shielding
 Monitor Age Assigned*: 28.02 Ma
 Air-40Ar/36Ar: 293.5 ± 1.5
 Sensitivity (moles/V): 8.606E-15
 J-Value: 0.014609

AU11.7j.bio.ih: BQ-1, biotite from the Barin Quarry; fil = 2.290 A

	40Ar (^ε .atm)	39Ar (K)	38(atm,Cl)	37(Ca)	36*(atm)	%Rad	R	Age (Ma)
a	8.825E-16 + 2.7E-18	6.404E-17 + 4.3E-19	1.99E-19 + 2.2E-20	7.8E-18 + 6.1E-18	5.38E-19 + 7.57E-20	82.0%	11.2964	275.6 + 8.9
b	5.396E-15 + 1.6E-17	3.819E-16 + 2.6E-18	1.40E-18 + 3.9E-20	1.9E-18 + 5.2E-18	3.75E-18 + 1.74E-19	79.5%	11.2290	274.0 + 4.2
c	2.929E-14 + 1.9E-17	2.218E-15 + 9.8E-18	7.30E-18 + 9.8E-20	1.8E-17 + 6.5E-18	1.14E-17 + 3.03E-19	88.5%	11.6825	284.3 + 1.7
d	1.637E-14 + 2.0E-17	1.342E-15 + 3.6E-18	4.82E-18 + 1.8E-19	-5.4E-18 + 5.5E-18	2.74E-18 + 1.81E-19	95.0%	11.6007	282.4 + 1.3
e	2.570E-14 + 2.1E-16	2.064E-15 + 2.6E-17	6.81E-18 + 1.5E-19	9.5E-18 + 5.6E-18	4.79E-18 + 1.32E-19	94.5%	11.7652	286.1 + 4.5
f	6.127E-15 + 1.6E-17	4.890E-16 + 4.1E-18	2.23E-18 + 9.7E-20	1.2E-17 + 6.4E-18	1.33E-18 + 7.00E-20	93.6%	11.7275	285.3 + 2.9
g	1.322E-14 + 7.3E-17	1.052E-15 + 5.7E-18	3.69E-18 + 9.8E-20	5.6E-18 + 5.0E-18	2.97E-18 + 9.31E-20	93.4%	11.7270	285.3 + 2.5
h	5.774E-15 + 1.1E-17	4.590E-16 + 2.0E-18	7.81E-19 + 3.1E-20	1.3E-17 + 6.1E-18	1.65E-18 + 1.04E-19	91.6%	11.5187	280.6 + 2.2
i	7.154E-15 + 1.3E-16	5.697E-16 + 1.5E-17	1.54E-18 + 9.3E-20	9.6E-19 + 6.0E-18	1.60E-18 + 1.02E-19	93.4%	11.7240	285.2 + 9.6
j	1.475E-15 + 1.7E-17	1.170E-16 + 1.9E-18	2.61E-19 + 3.2E-20	-6.5E-18 + 6.0E-18	3.42E-19 + 5.42E-20	93.2%	11.7449	285.7 + 7.0
k	1.846E-15 + 4.2E-18	1.446E-16 + 2.0E-18	8.74E-19 + 8.9E-20	8.7E-18 + 5.4E-18	7.27E-19 + 6.42E-20	88.4%	11.2791	275.2 + 5.4
l	3.315E-15 + 1.0E-17	2.630E-16 + 1.4E-18	8.72E-19 + 3.8E-20	7.2E-18 + 6.1E-18	1.28E-18 + 1.44E-19	88.6%	11.1682	272.7 + 4.4
m	2.473E-15 + 5.4E-18	1.879E-16 + 1.7E-18	6.11E-19 + 2.8E-20	5.1E-18 + 6.6E-18	7.93E-19 + 6.35E-20	90.5%	11.9114	289.4 + 3.8

AU11.7j.bio.ih: BQ-1, biotite from the Barin Quarry; fil = 2.290 A

	40Ar (^ε .atm)	39Ar (K)	38(atm,Cl)	37(Ca)	36*(atm)	%Rad	R	Age (Ma)
a	7.759E-15 + 9.8E-18	1.857E-16 + 2.1E-18	4.30E-18 + 1.5E-19	4.7E-18 + 7.3E-18	1.94E-17 + 3.69E-19	26.0%	10.8752	266.0 + 20.3
b	2.964E-14 + 3.0E-17	2.249E-15 + 8.5E-18	8.44E-18 + 1.6E-19	5.4E-18 + 5.1E-18	1.12E-17 + 1.51E-19	88.9%	11.7102	284.9 + 1.3
c	1.408E-14 + 7.0E-17	1.120E-15 + 5.2E-18	3.23E-18 + 5.4E-20	2.1E-17 + 5.2E-18	3.12E-18 + 8.33E-20	93.5%	11.7489	285.8 + 2.1
d	3.645E-15 + 1.6E-17	2.892E-16 + 2.2E-18	1.39E-18 + 6.5E-20	4.5E-18 + 5.6E-18	1.15E-18 + 6.78E-20	90.7%	11.4309	278.6 + 3.2
e	1.438E-15 + 6.9E-18	1.116E-16 + 1.3E-18	1.76E-19 + 2.5E-20	-4.2E-18 + 5.1E-18	6.08E-19 + 6.15E-20	87.5%	11.2750	275.1 + 5.7
f	2.376E-15 + 6.2E-18	1.879E-16 + 1.0E-18	6.80E-19 + 4.9E-20	2.1E-17 + 1.0E-17	4.15E-19 + 6.43E-20	94.8%	11.9943	291.3 + 3.1
g	3.493E-16 + 2.7E-18	2.911E-17 + 5.8E-19	3.00E-19 + 5.5E-20	6.2E-18 + 6.2E-18	4.23E-20 + 6.73E-20	96.4%	11.5666	281.7 + 18.4
h	2.313E-16 + 2.9E-18	1.927E-17 + 7.4E-19	2.73E-19 + 7.4E-20	2.6E-18 + 6.2E-18	-4.59E-20 + -6.13E-20	105.9%	12.7075	307.2 + 25.3
i	5.651E-17 + 3.4E-18	5.667E-18 + 3.6E-19	1.75E-19 + 6.5E-20	1.1E-18 + 6.7E-18	-3.83E-20 + -6.47E-20	120.0%	11.9667	290.7 + 84.0

Date Run: 2/16/09
 Irradiation Package: AU11
 Date of Irradiation: 4/29/2008
 Reactor: McMaster; with Cd shielding
 Monitor Age Assigned*: 28.02 Ma
 Air 40Ar/36Ar: 293.5 ± 1.5
 Sensitivity (moles/V): 8.606E-15
 J-Value: 0.014609

AU11.7k.hbl.in: BQ-1, homblende from the Barrin Quarry, fil = 2.290 A

	40Ar (% atm)	39Ar (K)	38Ar (atmCl)	37Ca	36Ar (atm)	% Rad	R	Age (Ma)
a	2.164E-16 + 3.7E-18	1.388E-17 + 1.5E-19	2.08E-19 + 5.0E-20	5.51E-17 + 3.7E-17	1.43E-19 + 6.42E-20	80.5%	12.8295	309.9 + 38.4
b	1.896E-15 + 2.3E-18	1.505E-16 + 1.0E-18	4.84E-19 + 2.7E-20	1.84E-17 + 2.7E-17	4.38E-19 + 7.93E-20	93.2%	11.7401	285.6 + 4.4
c	4.403E-15 + 5.6E-18	3.580E-16 + 2.0E-18	1.28E-18 + 7.3E-20	3.98E-17 + 2.5E-17	7.56E-19 + 7.50E-20	94.9%	11.6741	284.1 + 2.3
d	9.039E-15 + 1.6E-17	7.257E-16 + 2.5E-18	2.53E-18 + 4.7E-20	2.23E-16 + 3.7E-17	1.53E-18 + 8.03E-20	95.0%	11.8300	287.6 + 1.4
e	8.199E-15 + 1.0E-17	6.647E-16 + 2.5E-18	2.28E-18 + 1.1E-19	1.04E-15 + 5.0E-17	1.19E-18 + 7.52E-20	95.7%	11.8059	287.1 + 1.6
f	1.472E-14 + 2.4E-17	1.199E-15 + 3.0E-18	5.06E-18 + 6.7E-20	1.83E-15 + 5.4E-17	1.92E-18 + 6.74E-20	96.2%	11.8069	287.1 + 1.0
g	5.554E-15 + 1.3E-17	4.375E-16 + 2.1E-18	1.48E-18 + 8.1E-20	2.39E-16 + 3.2E-17	1.50E-18 + 8.02E-20	92.0%	11.6809	284.3 + 2.2
h	8.653E-15 + 1.0E-17	6.876E-16 + 2.4E-18	3.37E-18 + 1.4E-19	1.03E-15 + 3.4E-17	1.75E-18 + 8.02E-20	94.0%	11.8303	287.6 + 1.5
i	2.242E-14 + 1.5E-17	1.851E-15 + 3.8E-18	6.71E-18 + 7.4E-20	1.84E-15 + 6.8E-17	2.51E-18 + 6.58E-20	96.7%	11.7122	285.0 + 0.7
j	7.944E-15 + 1.8E-17	6.328E-16 + 5.1E-18	2.54E-18 + 9.1E-20	1.23E-15 + 5.0E-17	1.23E-18 + 4.84E-20	95.4%	11.9819	291.0 + 2.6
k	9.351E-15 + 1.5E-17	7.637E-16 + 2.8E-18	3.15E-18 + 9.1E-20	1.43E-15 + 5.2E-17	1.01E-18 + 4.94E-20	96.8%	11.8553	288.2 + 1.4
l	8.592E-15 + 8.2E-18	6.965E-16 + 2.2E-18	3.46E-18 + 2.9E-19	1.35E-15 + 2.8E-17	7.04E-19 + 5.04E-20	97.6%	12.0369	292.2 + 1.3
m	1.110E-14 + 1.6E-17	9.011E-16 + 7.4E-18	5.25E-18 + 1.8E-19	1.89E-15 + 5.6E-17	7.16E-19 + 5.09E-20	98.1%	12.0802	293.2 + 2.6
n	9.956E-15 + 1.1E-17	8.077E-16 + 3.5E-18	3.69E-18 + 7.8E-20	1.38E-15 + 1.5E-16	9.13E-19 + 5.73E-20	97.3%	11.9932	291.3 + 1.6
o	7.965E-15 + 1.3E-17	6.536E-16 + 4.0E-18	2.08E-18 + 9.8E-20	1.35E-15 + 2.8E-17	6.43E-19 + 4.04E-20	97.6%	11.8971	289.1 + 2.0
p	2.773E-15 + 6.1E-18	2.253E-16 + 2.6E-18	1.14E-18 + 3.5E-20	3.91E-16 + 3.0E-17	2.97E-19 + 5.33E-20	96.8%	11.9194	289.6 + 4.2
q	3.077E-15 + 9.7E-18	2.446E-16 + 2.3E-18	1.23E-18 + 7.0E-20	5.15E-16 + 4.3E-17	5.03E-19 + 5.13E-20	95.2%	11.9703	290.8 + 3.6
r	1.790E-15 + 3.1E-18	1.394E-16 + 1.4E-18	6.71E-19 + 3.8E-20	3.43E-16 + 2.4E-17	3.10E-19 + 4.46E-20	94.9%	12.1811	295.5 + 4.4
s	1.271E-15 + 3.5E-18	9.894E-17 + 1.0E-18	5.17E-19 + 3.2E-20	1.43E-16 + 2.3E-17	3.26E-19 + 6.02E-20	92.4%	11.8741	288.6 + 5.9
t	9.367E-16 + 4.2E-18	6.753E-17 + 6.2E-19	4.36E-19 + 6.0E-20	1.24E-16 + 2.2E-17	3.72E-19 + 5.89E-20	88.3%	12.2421	296.8 + 7.7

AU11.7k.hbl.in: BQ-7, homblende from the Barrin Quarry, fil = 2.290 A

	40Ar (% atm)	39Ar (K)	38Ar (atmCl)	37Ca	36Ar (atm)	% Rad	R	Age (Ma)
a	4.327E-17 + 4.0E-18	2.989E-18 + 2.1E-19	3.58E-19 + 1.3E-19	-1.30E-17 + 6.1E-17	1.28E-20 + 6.35E-20	91.3%	13.3505	321.5 + 158.0
b	4.224E-16 + 3.0E-18	2.836E-17 + 2.8E-19	3.59E-19 + 8.7E-20	-3.88E-18 + 5.9E-17	1.83E-19 + 5.43E-20	87.2%	12.9910	313.5 + 14.4
c	2.616E-15 + 4.4E-18	2.061E-16 + 1.5E-18	1.19E-18 + 7.0E-20	4.56E-16 + 3.9E-17	4.96E-19 + 4.65E-20	94.4%	11.9808	291.0 + 3.1
d	1.019E-14 + 1.3E-17	8.190E-16 + 3.1E-18	3.94E-18 + 7.1E-20	1.92E-15 + 5.7E-17	1.04E-18 + 5.42E-20	97.0%	12.0672	292.9 + 1.4
e	7.379E-15 + 1.1E-17	5.911E-16 + 2.9E-18	1.44E-18 + 4.1E-20	1.46E-15 + 5.3E-17	8.02E-19 + 5.42E-20	96.8%	12.0836	293.3 + 1.8
f	8.446E-15 + 1.1E-17	6.827E-16 + 3.4E-18	3.11E-18 + 6.8E-20	1.62E-15 + 5.4E-17	6.47E-19 + 4.85E-20	97.7%	12.0910	293.5 + 1.8
g	1.410E-14 + 2.4E-17	1.161E-15 + 4.7E-18	6.03E-18 + 1.3E-19	2.71E-15 + 6.3E-17	8.37E-19 + 4.25E-20	98.2%	11.9286	289.8 + 1.4
gg	2.516E-14 + 3.1E-17	2.048E-15 + 5.5E-18	9.61E-18 + 1.3E-19	5.04E-15 + 8.0E-17	1.46E-18 + 5.11E-20	98.3%	12.0717	293.0 + 1.0
h	8.376E-15 + 1.1E-17	6.896E-16 + 5.1E-18	3.55E-18 + 7.1E-20	1.76E-15 + 4.8E-17	3.31E-19 + 2.89E-20	98.8%	12.0030	291.5 + 2.3
i	7.622E-15 + 3.3E-17	6.184E-16 + 3.9E-18	3.12E-18 + 7.4E-20	1.48E-15 + 3.1E-17	4.81E-19 + 3.76E-20	98.1%	12.0970	293.6 + 2.4
j	7.159E-15 + 3.3E-17	5.784E-16 + 2.4E-18	2.71E-18 + 5.9E-20	1.39E-15 + 3.4E-17	4.66E-19 + 4.68E-20	98.1%	12.1404	294.6 + 2.1
k	6.513E-15 + 3.2E-17	5.282E-16 + 2.5E-18	2.05E-18 + 6.7E-20	1.33E-15 + 5.4E-17	4.60E-19 + 4.34E-20	97.9%	12.0724	293.0 + 2.3
l	5.193E-15 + 3.1E-17	4.277E-16 + 3.7E-18	1.50E-18 + 4.7E-20	1.22E-15 + 9.1E-17	2.01E-19 + 2.95E-20	98.9%	12.0026	291.5 + 3.4
m	3.347E-15 + 3.1E-17	2.687E-16 + 2.1E-18	1.20E-18 + 6.2E-20	6.12E-16 + 3.7E-17	1.63E-19 + 3.62E-20	98.6%	12.2753	297.6 + 4.1
n	6.524E-15 + 1.3E-17	5.383E-16 + 3.2E-18	2.06E-18 + 4.8E-20	1.28E-15 + 5.0E-17	5.41E-19 + 4.13E-20	97.5%	11.8233	287.5 + 2.0
o	2.170E-15 + 5.0E-18	1.771E-16 + 1.5E-18	7.95E-19 + 4.1E-20	4.43E-16 + 4.0E-17	1.95E-19 + 2.92E-20	97.3%	11.9266	289.8 + 3.3
p	3.460E-15 + 6.1E-18	2.794E-16 + 1.8E-18	1.45E-18 + 4.8E-20	7.18E-16 + 4.2E-17	3.65E-19 + 4.33E-20	96.9%	11.9975	291.4 + 2.6
q	1.262E-15 + 6.0E-18	1.048E-16 + 6.9E-19	3.18E-19 + 3.5E-20	2.60E-16 + 4.4E-17	1.21E-19 + 3.15E-20	97.2%	11.6983	284.6 + 4.3
r	3.933E-15 + 6.4E-18	3.268E-16 + 1.9E-18	1.41E-18 + 6.6E-20	8.09E-16 + 4.0E-17	2.56E-19 + 2.92E-20	98.1%	11.8007	286.9 + 2.1

Date Run: 3/25/09
 Irradiation Package: AU12
 Date of Irradiation: 1/30/2009
 Reactor: McMaster; with Cd shielding
 Monitor Age Assigned*: 98.79 Ma
 Air 40Ar/36Ar: 293.0 + 1.5
 Sensitivity (moles/V): 8.606E-15
 J-Value: 0.014167

AU12.6i musc: BQ-6, muscovite from the Batin Quarry; fil = 2.290 A (1-10), fil = 2.9 (11-20)									
	40Ar (* atm)	39Ar (K)	38Ar (atm, Cl)	37(Ca)	36* (atm)	%Rad	R	Age (Ma)	
1	1.710E-15 + 5.6E-18	1.378E-16 + 1.1E-18	3.05E-19 + 1.5E-20	1.1E-19 + 2.1E-19	2.61E-19 + 7.81E-20	95.5%	11.8458	279.9 + 4.7	
2	2.021E-15 + 4.6E-18	1.586E-16 + 1.4E-18	1.62E-19 + 1.0E-20	7.3E-19 + 2.5E-19	1.85E-19 + 7.00E-20	97.3%	12.4015	292.0 + 4.1	
3	2.120E-15 + 5.3E-18	1.783E-16 + 1.9E-18	1.62E-19 + 9.9E-21	3.7E-19 + 2.6E-19	1.43E-19 + 7.05E-20	98.0%	11.6528	275.7 + 4.2	
4	1.639E-15 + 6.8E-18	1.337E-16 + 1.6E-18	2.25E-19 + 1.6E-20	4.1E-19 + 2.0E-19	2.77E-19 + 7.01E-20	95.0%	11.6492	275.6 + 5.2	
5	2.501E-15 + 5.6E-18	2.006E-16 + 1.1E-18	4.79E-19 + 1.9E-20	6.5E-19 + 2.3E-19	5.84E-19 + 8.10E-20	93.1%	11.6042	274.6 + 3.4	
6	2.150E-15 + 9.3E-18	1.824E-16 + 3.2E-18	2.07E-19 + 7.7E-21	3.4E-19 + 2.4E-19	3.15E-19 + 8.19E-20	95.7%	11.2783	267.4 + 6.0	
7	1.400E-15 + 6.4E-18	1.115E-16 + 9.2E-19	1.74E-19 + 1.1E-20	4.5E-19 + 2.7E-19	4.92E-19 + 8.32E-20	89.6%	11.2568	266.9 + 5.9	
8	1.833E-15 + 1.3E-17	1.503E-16 + 1.8E-18	1.96E-19 + 1.3E-20	7.3E-19 + 2.0E-19	1.09E-19 + 1.15E-19	98.2%	11.9794	282.8 + 6.7	
9	1.536E-15 + 9.8E-18	1.277E-16 + 1.4E-18	2.77E-19 + 1.5E-20	3.5E-19 + 2.6E-19	1.92E-19 + 5.91E-20	96.3%	11.5785	274.0 + 4.9	
10	1.865E-14 + 4.2E-17	1.260E-15 + 6.8E-18	4.88E-18 + 3.0E-19	1.5E-18 + 2.4E-18	1.37E-17 + 4.29E-19	78.3%	11.5867	274.2 + 3.2	
11	2.522E-14 + 3.3E-17	1.924E-15 + 1.6E-17	2.23E-18 + 1.0E-19	-1.8E-18 + 3.0E-18	3.33E-18 + 4.02E-19	96.1%	12.5997	296.3 + 3.0	
12	6.271E-14 + 7.8E-17	3.973E-15 + 2.0E-17	1.80E-17 + 4.5E-19	1.3E-17 + 2.6E-18	5.27E-17 + 1.01E-18	75.2%	11.8632	280.3 + 2.7	
13	2.846E-14 + 8.0E-17	1.864E-15 + 1.1E-17	8.44E-18 + 3.0E-19	3.5E-17 + 3.4E-18	2.07E-17 + 4.70E-19	78.5%	11.9952	283.1 + 3.0	
14	2.777E-14 + 4.6E-17	2.155E-15 + 1.2E-17	4.73E-18 + 2.2E-19	3.5E-18 + 2.6E-18	9.34E-18 + 4.35E-19	90.1%	11.6070	274.6 + 2.2	
15	3.452E-15 + 8.5E-18	2.702E-16 + 7.7E-19	9.09E-19 + 3.4E-20	7.0E-19 + 3.8E-19	9.89E-19 + 5.20E-20	91.5%	11.6943	276.6 + 1.8	
16	4.710E-15 + 5.6E-18	3.977E-16 + 1.5E-18	7.22E-19 + 2.0E-20	5.1E-19 + 3.3E-19	5.67E-19 + 4.52E-20	96.4%	11.4219	270.6 + 1.4	
17	5.927E-15 + 3.3E-18	4.791E-16 + 3.0E-18	1.12E-18 + 3.4E-20	9.2E-19 + 3.4E-19	1.26E-18 + 5.11E-20	93.7%	11.5970	274.4 + 2.0	
18	4.838E-15 + 1.0E-17	3.828E-16 + 1.6E-18	1.16E-18 + 3.5E-20	8.0E-19 + 3.2E-19	1.14E-18 + 5.04E-20	93.0%	11.7585	278.0 + 1.7	

Date Run: 4/5/09
 Irradiation Package: AU12
 Date of Irradiation: 1/30/2009
 Reactor: McMaster, with Cd shielding
 Monitor Age Ass igned*: 98.79 Ma
 Air 40Ar/36Ar: 293.0 + 1.5
 Sensitivity (moles/V): 8.606E-15
 J-Value: 0.014245

AU12:6h.mus: MMS-1, muscovite from the Moffits Mill schist, fil=2.290 A

	40Ar (*.atm)	39Ar (K)	38Ar(atmCl)	37(Ca)	36*(atm)	%Rad	R	Age (Ma)
1	1.011E-14 + 1.5E-17	8.015E-16 + 3.6E-18	2.30E-18 + 5.9E-20	7.8E-19 + 6.6E-19	1.31E-18 + 4.62E-20	96.2%	12.1252	287.4 + 1.5
2	3.838E-15 + 4.8E-18	3.007E-16 + 1.6E-18	5.74E-19 + 2.2E-20	-1.9E-19 + 3.6E-19	1.33E-19 + 4.13E-20	99.0%	12.6340	298.6 + 1.9
3	1.694E-14 + 2.5E-17	1.396E-15 + 3.7E-18	2.80E-18 + 3.8E-20	-1.7E-19 + 3.8E-19	7.10E-19 + 4.28E-20	98.8%	11.9792	284.2 + 0.9
4	7.491E-15 + 7.1E-18	6.138E-16 + 3.6E-18	9.97E-19 + 2.6E-20	-5.9E-19 + 3.9E-19	5.54E-19 + 4.18E-20	97.8%	11.9377	283.3 + 1.8
5	3.717E-15 + 6.7E-18	3.063E-16 + 2.6E-18	3.17E-19 + 1.8E-20	-5.6E-19 + 3.8E-19	1.34E-19 + 4.37E-20	98.9%	12.0044	284.8 + 2.7
6	1.108E-14 + 1.7E-17	9.191E-16 + 1.6E-18	1.57E-18 + 3.2E-20	6.6E-19 + 4.7E-19	4.86E-19 + 3.94E-20	98.7%	11.8962	282.4 + 0.7
7	4.003E-15 + 5.3E-18	3.287E-16 + 1.6E-18	6.44E-19 + 3.2E-20	6.8E-19 + 3.9E-19	2.05E-19 + 3.88E-20	98.5%	11.9948	284.6 + 1.7
8	1.385E-14 + 1.8E-17	1.126E-15 + 5.5E-18	2.18E-18 + 3.2E-20	-6.1E-19 + 5.0E-19	3.72E-19 + 4.70E-20	99.2%	12.2029	289.1 + 1.5
9	1.113E-14 + 1.5E-17	9.213E-16 + 2.6E-18	1.72E-18 + 3.6E-20	4.6E-19 + 4.2E-19	6.06E-19 + 4.36E-20	98.4%	11.8898	282.3 + 0.9
10	1.701E-14 + 1.6E-17	1.366E-15 + 4.8E-18	3.41E-18 + 6.5E-20	3.0E-19 + 4.4E-19	1.78E-18 + 6.16E-20	96.9%	12.0702	286.2 + 1.1

Alabama/Georgia Piedmont Apatite and Zircon (U-Th)/He data (March 2009)

Sample	Age [Ma]	± [Ma] 6%	U [ppm]	Th [ppm]	Sm [ppm]	Th/U	He [ncc/mg]	mass [mg]	Ft	stdev
<i>A P A T I T E</i>										
BQ-1-1	118.9	7.1	11.8	3.5	1.8	0.3	6.66	14.6	0.81	
BQ-1-2	131.7	7.9	46.4	13.0	2.5	0.3	26.92	7.0	0.76	
BQ-1-3	116.6	7.0	26.5	7.2	3.2	0.3	14.40	12.3	0.80	
BQ-1-4	114.2	6.9	9.3	2.8	16.4	0.3	4.82	8.1	0.77	
BQ-1	120.3	7.2	23.5	6.6	6.0	0.3	13.2	10.5	0.8	7.8
MQ-3-1	117.2	7.0	9.7	1.1	3.0	0.1	4.95	6.2	0.78	
MQ-3-2	827.1	49.6	8.0	1.6	2.8	0.2	26.52	3.5	0.67	
MQ-3-3	386.1	23.2	16.2	4.2	6.6	0.3	20.86	1.5	0.57	
MQ-3-4	119.9	7.2	6.6	1.4	3.0	0.2	3.56	7.8	0.79	
MQ-3	118.5	7.1	8.2	1.3	3.0	0.2	4.3	7.0	0.8	1.9
NQ-1-1	453.4	27.2	2.9	6.6	43.1	2.3	9.67	12.6	0.80	
NQ-1-2	190.3	11.4	3.9	10.7	44.8	2.7	5.61	11.3	0.79	
NQ-1-3	160.3	9.6	5.5	15.9	48.9	2.9	5.98	3.8	0.71	
NQ-1-4	339.9	20.4	1.9	6.3	33.0	3.3	5.55	13.3	0.81	
NQ-1	175.3	10.5	4.7	13.3	46.8	2.8	5.8	7.6	0.8	21.2

Sample	Age [Ma]	± [Ma] 6%	U [ppm]	Th [ppm]	Sm [ppm]	Th/U	He [ncc/mg]	mass [mg]	Ft	stdev
<i>Z I R C O N</i>										
BQ-1-1	364.9	29.2	92.5	43.5	0.8	0.5	169.59	12.7	0.82	
BQ-1-2	221.6	17.7	184.4	69.4	1.5	0.4	194.10	8.6	0.80	
BQ-1-3	206.8	16.5	240.5	52.1	1.5	0.2	226.98	7.1	0.79	
BQ-1	264.4	21.2	172.5	55.0	1.3	0.4	196.9	9.5	0.8	87.3
BQ-6-1	163.8	5.1	1604.6	13.6	1.3	0.0	1041.29	9.5	0.80	
BQ-6-2	169.6	5.6	1053.2	4.3	0.2	0.0	921.15	11.9	0.81	
BQ-6-3	154.6	12.4	1369.5	30.2	1.3	0.0	917.67	8.4	0.79	
BQ-6	162.7	7.7	1342.4	16.0	0.9	0.0	960.0	9.9	0.8	7.5
MQ-3-1	187.7	15.0	106.3	46.3	1.8	0.4	91.82	5.4	0.77	
MQ-3-2	172.5	13.8	183.4	75.9	3.0	0.4	147.55	6.4	0.78	
MQ-3-3	193.2	15.5	92.5	48.9	1.4	0.5	87.49	8.7	0.80	
MQ-3	184.5	14.8	127.4	57.0	2.0	0.5	109.0	6.8	0.8	10.7
NQ-1-1	189.1	15.1	283.5	119.6	2.9	0.4	264.15	13.0	0.82	
NQ-1-2	215.4	17.2	567.3	207.6	5.4	0.4	586.57	13.2	0.81	
NQ-1-3	170.3	13.6	270.5	115.8	15.0	0.4	233.98	22.0	0.84	
NQ-1	191.6	15.3	373.8	147.7	7.7	0.4	361.6	16.1	0.8	22.6
JCQ-1-1	208.2	16.7	96.0	36.6	1.3	0.4	97.03	11.2	0.81	
JCQ-1-2	252.7	20.2	118.2	49.3	0.9	0.4	142.02	7.7	0.79	
JCQ-1-3	233.1	18.6	259.5	117.1	1.7	0.5	282.62	6.2	0.77	
JCQ-1	231.3	18.5	157.9	67.7	1.3	0.4	173.9	8.4	0.8	22.3